COMPUTATIONAL MODELING FOR DENSE GAS DISPERSION FOR VARIABLE STABILITY CLASSES

A Thesis

by

MOHAMED AMINE CHAKROUN

Submitted to the Office of Graduate and Professional Studies of
Texas A&M University
in partial fulfillment of the requirements for the degree of

MASTER OF SCIENCE

Chair of Committee,	Luc Véchot
Committee Members,	Kakosimos Konstantinos
	Mahmood Amani
Head of Department,	M. Nazmul Karim

August 2015

Major Subject: Chemical Engineering

Copyright 2015 Mohamed Amine Chakroun

ABSTRACT

The spill of many chemicals such as Liquefied Natural Gas (LNG) on land or water results in its rapid vaporization and the formation of a dense cloud. The performance of a risk assessment for the spill of flammable chemicals requires the determination of the maximum downwind distance where the Lower Flammability limit (LFL) is reached. The modeling of such spills is usually divided in two parts: source term and atmospheric dispersion. The source term describes the cryogenic liquid release rate and conditions. The atmospheric dispersion describes the increasing cloud propagation downwind after the release and the extent of the LFL distance until a steady state is reached. The focus of this work is the preparation of a model for the atmospheric dispersion after the spill of LNG on land using Computational Fluid Dynamics (CFD).

CFD is a model based on solving Navier Stokes equations (conservation equations of mass, momentum and energy) in a specific 3D domain.

The use of CFD as a tool for the prediction of dense clouds dispersion and LFL distance calculation by industry and research institutions is increasing significantly because it provides an adequate description of the phenomena of dense gas flow, dispersion and it can handle complex geometries.

The objective of this research project is to prepare a CFD scheme for vapor cloud dispersion resulting from accidental spill of cryogenic liquid on land using CFD (FLUENT) for medium scale LNG/LN_2 spill experiments to be performed at the Ras Laffan Emergency and Safety College (RLESC). The validation of the CFD (FLUENT)

model is performed using dense gas dispersion data from literature (Prairie Grass). There is a lack of dense gas dispersion modeling for the unstable class because of the complexity of velocity, temperature and turbulence equations for this class. This model should be able to predict the dense cloud vapors dispersion for different stability classes (neutral, stable and unstable).

A crucial parameter in the modelling of the dispersion of the dense gas is the choice of the turbulence model. There is currently no agreement on which model performs better for this application. This work involves a sensitivity analysis of the dispersion results to determine the choice of the turbulence model. The focus will be on three turbulence models which are the most used for this application: standard $k-\varepsilon$, realizable $k-\varepsilon$ and Reynolds Stress Model RSM.

The results from the modeling of three sets of Prairie Grass experiments suggest a good agreement between the simulation and experimental results only for the centerline concentration and for the stable and neutral classes. For the unstable class, there is a considerable overprediction of the centerline concentration. This work includes an attempt to compare model predictions with experimental concentrations at each location. Only centerline concentrations or highest concentrations were considered in previous works. Form this comparison; all three models were unable to predict the concentration measurements accurately.

The RSM model yields relatively the best results for atmospheric an dispersion modelling compared to the standard k-ε and realizable k-ε models. As a result, it is advised to use this model for this application.

DEDICATION

To my parents

ACKNOWLEDGEMENTS

I appreciate the great help and guidance I received during my masters from my supervisor Dr. Luc Véchot who encouraged and motivated me throughout this journey. I was interested in the area of process safety after my work with him since my undergraduate studies. His enthusiasm about this field and hard work inspires many students in our university.

I would like to thank my committee members Dr. Kakosimos Konstantinos and Dr. Mahmood Amani for their instruction and supervision throughout my masters. Dr. Kakosimos Konstantinos help was enormous in guiding the research to the right direction.

I would like to thank all the research staff and friends in MKOPSC-Q for their support and encouragements and I hope to see the MKOPSC as a leading institute of process safety in this region.

I would like to acknowledge BP for their generous sponsorship of the LNG safety research in Texas A&M at Qatar and also QP for their support in terms of facilities and equipment especially the use of the LNG facility TP-5 in RLESC by the MKOPSC-Q.

NOMENCLATURE

A_0 Model Constant = 4.04

A_s Model Constant = 4.6 cos ϕ

$C_{\varepsilon 1}$ Empirical FLUENT constant

$C_{\varepsilon 2}$ Empirical FLUENT constant

$C_{\varepsilon 3}$ Empirical FLUENT constant

C_p Specific heat (J/K)

C_v Specific heat (J/K)

C_μ Empirical constant

$D_{i,m}$ Mass diffusion coefficient for species in mixture (m^2/s)

$D_{T,I}$ Thermal diffusion coefficient

$D_{T,ij}$ Turbulent diffusion

$D_{L,ij}$ Molecular diffusion ($m^2/K.s$)

F_{ij} Production by system rotation

$\vec{g}$ Gravitational acceleration (m/s^2)

G_b Buoyancy from turbulent kinetic energy production (m^2/s^2)

G_k Shear stress from turbulent kinetic production (Pa)

$\vec{Ji}$ Molar flux ($moles/m^2s$)

L Monin Obukhov Length (m)

K	Von Karman Constant
k	Turbulent kinetic energy (m^2/s^2)
k_T	Thermal conductivity (W/(m.K))
LN_2	Liquid Nitrogen
M_t	Match number = ratio of fluid velocity magnitude to local speed of sound (dimensionless)
p	Pressure (Pa)
P_{ij}	Stress production
Pr_t	Turbulent Prandtl number = ratio of momentum diffusivity to thermal diffusivity (dimensionless)
q_w	Surface heat flux (W/m^2)
R_i	Rate of production of species by chemical reaction ($mole/m^3s$)
S	Total entropy (J/K)
S_i	Rate of creation and addition from dispersed phase ($mole/m^3s$)
t	Time (s)
T	Temperature (K)
T_*	Surface layer temperature (K)
T_w	Surface temperature
u	Wind velocity (m/s)
u_i	Velocity component (m/s)
$\overline{u_i}$	Mean velocity component (m/s)

$u_i^{'}$ Fluctuating velocity component (m/s)

u_{10} Wind velocity at 10 m (m/s)

u_0 Wind velocity at ground surface (m/s)

u_* Friction velocity (m/s)

$\vec{v}$ Overall velocity vector (m/s)

x_i Position component (m)

Y_i Local mass fraction of each species

Y_m Compressibility related to kinetic energy production

z Height (m)

z_0 Roughness height (m)

S_{user} User defined source term

Sc_t Schmidt number (dimensionless number)

Greek letters

A Standard adiabatic lapse rate (˚C)

β Thermal expansion coefficient (K^{-1})

ε Turbulent dissipation rate (m^2/s^3)

ρ Vapor density (kg/m^3)

Γ Shear stress (Pa)

$\bar{\bar{\Gamma}}$ Stress tensor ($kg/ (ms^2)$)

Γ_w Surface shear stress (Pa)

ϕ_m Non-dimensional wind shear function

ϕ Scalar such as pressure, energy or concentration

$\bar{\phi}$ Mean scalar value

ϕ' Fluctuating scalar component

Θ Radiation temperature (K)

ϕ_{ij} Pressure strain

μ_T Turbulent viscosity (Pa s)

σ_k Empirical FLUENT constant

σ_ε Empirical FLUENT constant

δ_{ij} Delta function (unit may vary)

η Effectiveness factor (dimensionless)

Ω_k Angular velocity (s^{-1})

S_{user} User defined source term

TABLE OF CONTENTS

Page

Page

Page

LIST OF FIGURES

Page

Page

Page

Page

LIST OF TABLES

Page

CHAPTER I

INTRODUCTION

Many severe incidents in the process industry are associated with the release of dense flammable and/or toxic gases. Such gases have a higher density than the surrounding ambient air and upon release tend to slump toward the ground under the influence of gravity. The most tragic incident was Bhopal, India where more than 40 tons of methyl isocyante (MIC) gas were released and created a dense cloud. This incident resulted in the death of 8,000 people in few days and an exposure to toxic chemicals for 20,000 which resulted in many of them suffering from cancer and birth defects.

These clouds maintain a high concentration of the chemical in question for a significant time compared to passive dispersion (light gases dispersion) [1].

A typical dense gas has a molecular weight higher than air's molecular weight (for example SO_2), or very low temperature compared to the ambient temperature which leads to an increase in the gas density.

When spilled on land or water LNG vaporizes quickly and forms a flammable vapor cloud that may cause fire and explosion hazards [2]. The assessment of the risks associated with the loss of containment of LNG and the dispersion of the dense vapor clouds are of utmost importance for the safety of LNG facilities and the protection of people.

1.1 Natural Gas and LNG

Formed by degradation of organic matter over millions of years and found in rock reservoirs in the earth crust, natural gas (NG) consists essentially of methane with smaller concentrations of heavier hydrocarbons (Table 1). Over the last years, the need for a cleaner, cheap and available energy has led NG to become a fast-growing source of energy. It is indeed considered as an environmentally friendly fuel as its combustion produces lower sulfur dioxide, nitrous oxide and carbon dioxide emissions compared to crude oil or coal [3]. It is estimated that NG will become the primary source of energy ahead of oil in 2035 with a share of 31 %. The global demand for NG is estimated to increase by 1.9% reaching 497 (Bcf/d) by 2035 [4].

Table 1: Typical composition of natural gas [3]

Component	Volume %
Methane (CH_4)	>85
Ethane (C_2H_6)	3-8
Propane (C_3H_8)	1-2
Butane (C_4H_{10})	<1
Pentane (C_5H_{12})	<1
Carbon dioxide (CO_2)	1-2
Hydrogen Sulfide (H_2S)	<1
Nitrogen (N_2)	1-5
Helium (He)	<0.5

The current largest reserves of natural gas are located in Russia, Iran and Qatar [4].In the particular case of Qatar, almost all of its natural gas production is processed into Liquefied Natural Gas (LNG) and exported overseas. Qatar has been the

largest LNG exporter to the world since 2006 with a production of more than 77 Million tons per year (MMt/y), approximately 3.7 Tcf. LNG represents the major source of income for Qatar [5].

The recent discovery of large reserves of shale gas in North America and China is expected to increase the LNG production and exportation in these countries. As a result, the US is expected to shift from being a net importer of LNG to a net exporter in 2018. Australia is expected to surpass Qatar and become the largest LNG exporter by 2018-2020 [6].

1.2 LNG Production and Transportation

After being extracted from natural reservoirs onshore and offshore, raw NG is processed in order to separate it from condensate, water and acid gases and prepare the gas according to the required specifications. The liquefaction steps consist of refrigerating the gas into its liquid state at -162˚C. The main reason behind this process is that it results in a volume reduction in the order of 620 times which makes the transport and storage much easier, practical and economically profitable [3].

LNG is then transported overseas using huge carrier vessels, called LNG supertankers. The capacity of these vessels increased from less than 30,000 m^3 in 1960 to around 250,000 m^3 in 2009. There are two main categories of LNG carriers in industry: Spherical (Moss carrier -Figure 1) and (Membrane -Figure 2) [7].

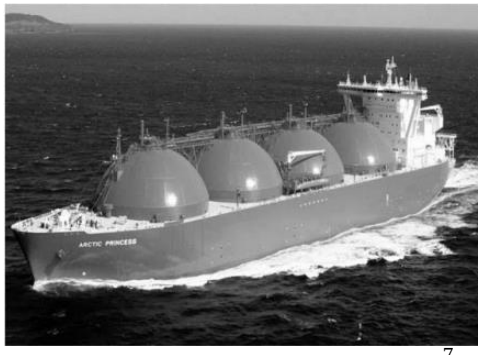

Figure 1: Moss type LNG tanker [7]

Figure 2: Membrane type LNG tanker [7]

1.3 LNG Hazards and Risk Assessment

1.3.1 Hazardous Properties of LNG and Loss of Containment Hazards

There are several hazards associated with the LNG due to its low boiling temperature and its flammability. The major hazards are structural damage of the container, pressure release due to rapid phase transitions (RPTs), tissue (skin) damage in case of a direct contact with the cryogenic liquid, fire including vapor cloud fires and pool fires, asphyxiation hazard when it displaces air especially in enclosed areas or near

the spill area and even deflagrations and detonations when the flammable mixture and the ignition source are in an enclosed space [8].

1.3.2 LNG Industry Safety Records

The safety record of the LNG industry is relatively good from a historical perspective with the exception of few major accidents which resulted in significant human and economic losses.

1.3.2.1 Cleveland, Ohio, 1944

During World War II, the East Ohio Gas Company built three new LNG tanks. The facility operated without accident for three years. After that, a large new tank was added. The stainless steel alloys were rare at that time because of the war. As a result, the material used for the new tank was 3.5 % Nickel instead of 9 % Nickel. This tank underwent brittle fracture when it was exposed to LNG. LNG was spilled on the street and reached the sewer system. A massive vapor cloud explosion erupted when the vapor cloud met an ignition source which resulting in 124 fatalities and 200-400 injuries [9].

1.3.2.2 Skikda, Algeria, 2004

On the 19th of January 2004, at the SONATRACH LNG liquefaction plant in Skikda, a leak from a refrigerant line resulted in LNG vapors travelling to the combustion air intake. This resulted in a massive explosion which devastated the facility. 27 workers were killed and 80 were injured in addition to the destruction of 3 LNG trains [10].

1.3.2.3 Collision between Hanjin Italy and Al Gharrafa Ship

Al Gharrafa tanker ship (314 m length Qatari ship) collided with Hanjin Italy cargo vessel (349 m length) on the 28th of December in 2013. This incident took place in the international waters between Batam ports and Singapore. The incident resulted in minor damages to the Gharrafa carrier bow and side of Hanjin Italy cargo. There was no loss of containment or injuries [11].

1.3.3 Risk Assessments

The risk associated with the loss of containment of LNG is measured based on the severity of an incident and its frequency. The consequence analysis or severity is based on the determination of the LNG vapor production rate and dispersion as illustrated in Figure 3. The LNG vapor production rate or source term predicts the cryogenic liquid release rate. The atmospheric dispersion describes the flammable cloud propagation downwind following the release. The focus of this work is on the severity by conducting consequence modeling of a cryogenic spill.

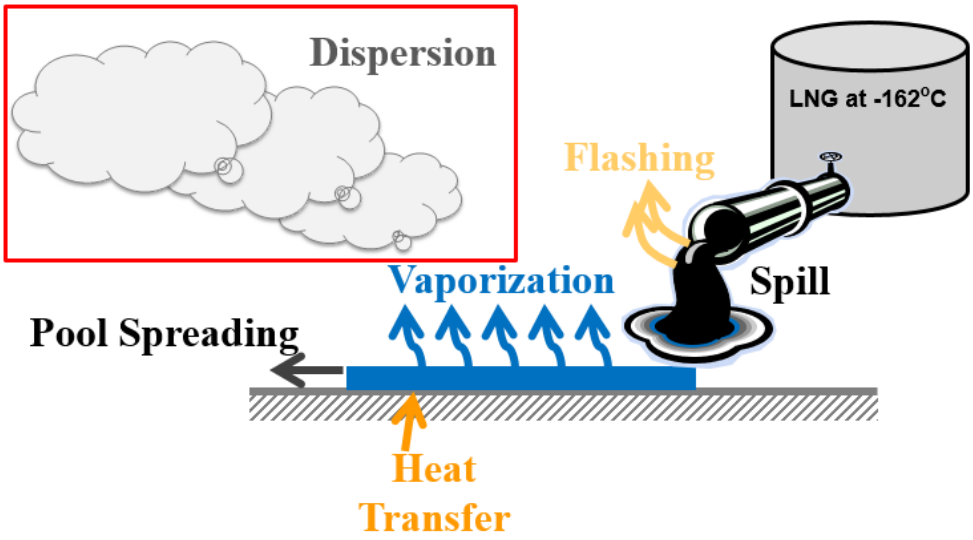

Figure 3: LNG spill modeling areas

CHAPTER II

LITERATURE REVIEW

The spill of LNG on land or water will result in a cold heavy vapor cloud. The dispersion of this cloud is affected by several factors: wind speed, atmospheric stability, ground roughness and released material initial momentum and buoyancy [10].

2.1 Atmospheric Dispersion Parameters

2.1.1 Wind Speed

The wind speed is usually defined at a height of 10-m elevation (u_{10}). The wind speed at the ground surface is equal to zero (u_0). The wind velocity drops from u_{10} to u_0 at the ground surface because of the ground roughness. Wind data are usually represented by wind roses with the wind direction determined from where it originates , for example northern wind blows from north to south [10].

A sample wind rose is presented in Figure 4. Meteorological data are required in order to carry out dispersion modeling. These data are usually obtained from nearby airports or weather stations.

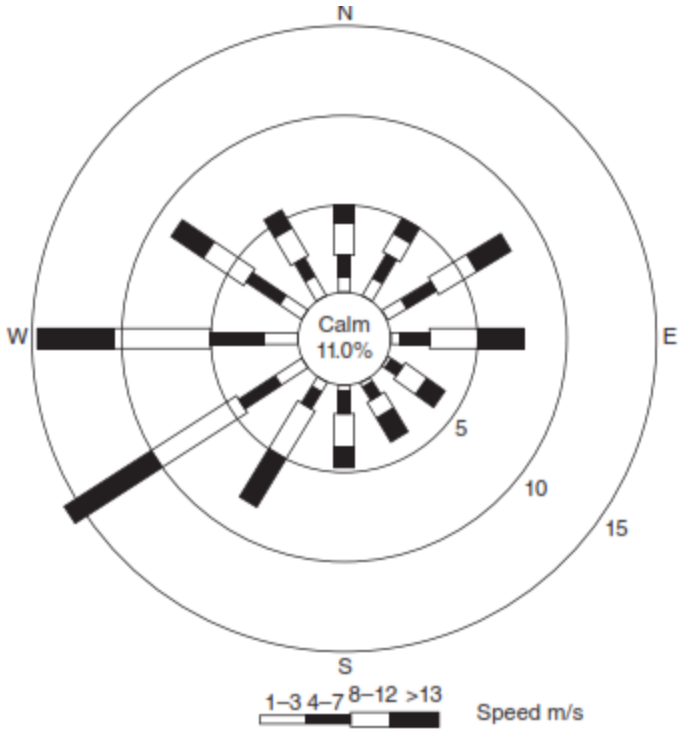

Figure 4: Wind rose [10]

2.1.2 Atmospheric Stability

Atmospheric stability is the description of air behavior corresponding to its movement downward or upward. This displacement depends on the air temperature and density. If it is less dense than surrounding air, it will move upward (positively buoyant). If it is denser than surrounding air, it will move downward (negatively buoyant).

Pasquill and Gifford developed a ranking of Atmospheric stability classes from A to F according to the incident solar radiation (insolation) in the day or cloudiness level at night and wind speed as described in Table 2.

For the unstable class, the heat transfer from the sun to the ground results in increasing the air temperature near the ground which decreases its density. This results in increasing vertical mixing in the atmosphere. Neutral stability class occurs in the evening or early morning when heat transfer from the sun to the ground is not significant. The wind speed dominates over the vertical mixing. For stable classes, the heat transfer from the sun to the ground is less than the ground cooling. This usually occurs at night. As a result, the air density near the ground is higher than the air density at higher altitudes which is a stable condition and vertical mixing is suppressed [12,2].

Table 2: Wind speed and solar radiation effect on atmospheric stability [2]

Wind Speed (m/s)	Day Time Insolation			Night time conditions	
	Strong	Moderate	Slight	Thinly Overcast >= 4/8 Low Cloud	<= 3/8 Cloud
<2	A	A-B	B	-	F
2-3	A-B	B	C	E	E
3-5	B	B-C	C	D	D
5-6	C	C-D	D	D	D
>6	C	D	D	D	D

2.1.3 Ground Roughness

Wind gradients and the resulting gas dispersion are a function of the type of terrain, whether the gas/vapor release occurs in a relatively obstructed area (buildings or trees) or on an open flat area (Figure 5). Buildings and trees increase air mixing while lakes and open areas reduce it. The surface roughness, z_0, is a calculated term depending on the type of terrain (Table 3) [10].

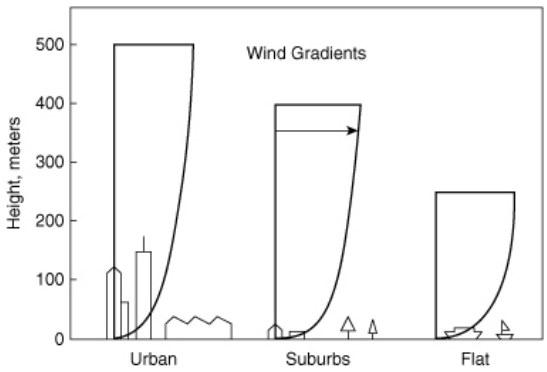

Figure 5: Wind speed variation as a function of ground condition and height [2]

Table 3: Surface roughness heights for dispersion

Terrain Classification	Terrain Description	Surface Roughness, z_0 (m)
Metropolitan area	City centers characterized with high towers or mountains.	3-10
Urban area	Town centers, average presence of woods.	1-3
Residential area	Area characterized by with condensed small buildings	1
Large plants	High equipment pieces such as distillation columns.	1
Small plants	Smaller pieces of equipment.	0.5
Agricultural land	Open area with dispersed houses.	0.3
Flat land	Plains covered with grass and a small number of trees.	0.1
Open water	Large areas of water or desert.	0.001
Sea	Calm sea, regular or snow covered land	0.0001

2.1.4 Release Height

The ground level concentrations depend on the release height. These concentrations decrease significantly as the release height increases because the dispersion is more pronounced vertically [2].

2.1.5 Released Material Initial Momentum and Buoyancy

The effective height for a release changes as a function of the initial momentum and buoyancy of the released material. The upward momentum of a high velocity flow will transport the gas higher than the release point. The material density determines if the

material will be positively buoyant or negatively buoyant. If the density of the released gas/vapor is higher than the density of air, the material will tend to sink and the generated gas/vapor cloud will be low and wide. As the cloud mixes with air, the effect of gravity is less and the ambient air velocity and turbulence will govern the dispersion of the material. If the density of the released gas/vapor is lower than the density of air , the material is positively buoyant and it will disperse vertically [2,13].

2.2 Overview of Common Dispersion Models for Dense Gas Dispersion

There are many available models for the modeling of gas dispersion. The main gas dispersion models for dense gas dispersion are Integral and CFD models. These models can address the effects associated with dense gas dispersion [10].

2.2.1 Integral Models

Integral models for gas dispersion estimate the cloud dispersion in terms of time for instantaneous releases or downwind distance in the case of continuous releases [14]. Integral models are based on solving the basic equations describing the general flow properties. For example, in the case of plume dispersion, the model solves for plume radius, height, velocity and centerline concentration. For dense gases, they are modelled as a box with the radius and volume varying as a function of time. For this reason, integral models are named box models as well. For LNG modeling using integral models, the source is usually a circular pool at a specified temperature, concentration and constant vaporization rate. However, these assumptions are not accurate because the source term is not circular and its size, shape, temperature, concentration and

vaporization rate vary with time. These models are usually fast and easy to execute However, they cannot include physical obstructions or terrains. For this reason, they provide decent results for open fields conditions only. Examples of integral models are: ALOHA, CANARY, DEGRADIS, DRIFT, SLAB, PHAST [15].

2.2.2 CFD Models

CFD models are a branch of fluid mechanics that uses numerical methods and algorithms to solve and analyze fluid flow problems. They solve the Navier Stokes equations which are three-dimensional turbulent transport equations based on the conservation of mass, species, momentum and energy balances. They are able to predict the effects of physical obstructions and terrains. However, they are more complex to use, need longer simulation time and require higher computational costs. Also, they allow the performance of full three- dimensional analysis and the accurate calculation of the velocity, temperature, turbulence and concentration at any location of the domain as function of time. Examples of CFD models include: FLUENT, CFX, FEM3A and FDS [16].

2.2.3 Shallow Layer Models

These models combine some of the advantages of CFD and integral models. They describe the flow behavior using depth averaged variables. They can model downslope buoyancy and air entrainment but they are suited for flat terrains only. They are computationally more expensive than integral models but less expensive than CFD

models [16]. An example of these models is: Safety Lagrangian Atmospheric Model (SLAM) developed by Søren Ott and Morton Nielsen from Risø National Laboratory [15].

2.3 CFD Modeling of Gas Dispersion

Computational fluid dynamics are used increasingly for the prediction of LNG vapors dispersion because of two main reasons. They are able to model complex geometries and include the effects of obstacles on dispersion. The presence of obstacles may result in reducing the LFL by providing containment to the flow or they may increase the LFL if they increase the gravity flow [16].

2.3.1 CFD Theory

CFD codes solve the Navier Stokes equations of mass (Equation 1), momentum (Equation 2), energy conservation (Equation 3), and mass transfer (Equation 4) and (Equation 5) [16]:

$$\frac{\partial \rho}{\partial t} + \nabla \cdot (\rho \vec{v}) = 0 \qquad \text{Equation 1}$$

$$\frac{\partial}{\partial t}(\rho \vec{v}) + \nabla \cdot (\rho \vec{v} \vec{v}) = -\nabla p + \nabla \cdot (\bar{\bar{\Gamma}}) + \rho \vec{g} \qquad \text{Equation 2}$$

$$\frac{\partial \rho C_v T}{\partial t} + \nabla \cdot (\rho \vec{v} C_p T) = \nabla \cdot (k_T \nabla T) \qquad \text{Equation 3}$$

$$\frac{\partial}{\partial x}(\rho Y_i) + \nabla (\rho \vec{v} Y_i) = -\nabla \cdot \vec{J}_j + R_i + S_i \qquad \text{Equation 4}$$

$$\vec{J}_j = -(\rho D_{i,m} + \frac{\mu_t}{Sc_t}) \nabla Y_i - D_{T,i} \frac{\nabla T}{T} \qquad \text{Equation 5}$$

The air flow is usually turbulent. The velocity fluctuates in turbulent flows which results in a mixing and fluctuation of other properties such as momentum, energy and concentration (Please refer to Appendix for more details).

2.4 Dense Gases Dispersion Modeling Using CFD and Experimental Validation

2.4.1 Dense Gas Dispersion Experiments

Several spill experiments were conducted in order to study the dispersion of dense gases (especially LNG), different mitigation methods (water curtains, expansion foam) and different phenomena associated with the flammability of these gases. Table 4 illustrates a summary of the main spill experiments conducted in the past which are used for models validation [8]. This table was inspired from Coldrick, Lea, & Ivings report for the validation database for the evaluation of dispersion models for safety analysis for LNG facilities [17].

Table 4: Main experiments in literature [17]

Trial Name	Trial N°	Obstructed (O) unobstructed (U)	Atmospheric Stability	Substance Released	water (W) or land (L)
Prairie Grass	13 17 33	U	A B C F D	SO_2	L
Burro, 1980	3 7 8 9	U	B D E D	LNG	L
Coyote,1981	3 5 6	U	B-C C-D D	LNG	L
Falcon, 1987	11 12 13	O	G D D-E	LNG	L
Thorney Island, 1982-4	45 47	U	E-F F	Freon 12 & Nitrogen	L
BFTF	06LNG01 07LNG01	U	D B	LNG	W

- Prairie Grass Experiments

The Prairie Grass experiments represent the reference database used for model verification for continuous releases near ground over a flat terrain. This set of experiments was conducted in July- August 1956. It consisted of a continuous release of SO_2 from a pipe at 46 cm Height. The concentration was measured at arcs of 50 m, 100 m, 200 m, 40 m and 800 m. It involved 68 runs at different meteorological conditions and stability classes [18].

- Burro Series Tests

These tests were performed by Lawrence Livermore National Laboratory (LLNL) at the Navel Weapons Center at China Lake. Eight releases of LNG on water (58 Diameter pond and 1 meter deep) were performed with volumes from 24 to 39 m^3. The spill rates ranged from 11.3 to 18.4 m^3/min and the stability classes from unstable to slightly stable. The dispersion occurred over water for 29 m and over land for 80 m. The field was irregular. Different parameters were measured during these experiments at different heights and downwind distances such as wind speed and direction, gas concentration, humidity and heat flux from ground. The phenomenon of dense gas dispersion was visible when the wind speed was low and the stability class was slightly stable. The wind flow over the cloud was similar to its flow over a solid body. The cloud was able to inhibit turbulent mixing. However, for other tests, this effect was not observed. Also, RPTs followed in these tests resulting in overpressures up to 5 kPa at 30 m downwind distance [8].

- Coyote Series Tests

Coyote series experiments were performed by the Lawrance Livermore National Laboratory (LLNL) and the Naval Weapons Center (NWC) at China Like, California in 1981. The dispersion of LNG vapor was studied for a spill on water (58 Diameter water basin at 1.5m depth). The volume ranged from 14.6 to 28 m^3. The LNG clouds were ignited in order to study the damage potential for cloud fires [19].

- Falcon Series Tests

The Falcon series tests were conducted at Frenchman Flat in Nevada by LLNL. These tests involved the release of LNG in the presence of obstacles. The efficiency of vapor fences in LNG dispersion was studied during these experiments as a mitigation method. The test was performed on a 40 m× 60 m pond surrounded by an 88 m×44 m×9.1 m vapor fence. Five tests were performed with volumes of spill rates of 8.7-30.3 m^3/min [19].

- BFTF Series Tests

Brayton Fire Training Field (BFTF) is in college station in Texas and they are affiliated with Texas Engineering Extension Service (TEEX). The main role of BFTF is firefighters training especially for LNG fires. Several medium scale LNG experiments were carried out at BFTF by Mary Kay O'Connor Process Safety Center (MKOPSC) between 2005 and 2009 in order to collect experimental data for models validation and study the main parameters of vapor dispersion. The facility has three concrete pits and one L-shape trench. These tests covered several scenarios including release on water and concrete, use of water curtain, high expansion foam and foam glass for LNG fire extinguishing.

- RLESC

The LNG facility is located at Ras Laffan Emergency and Safety College (RLESC), in Ras Laffan city, Qatar. Ras Laffan is located in the north east cost of Qatar overseeing the Arabian Gulf. Ras Laffan is 70 kilometers far from the Capital Doha. It is owned by Qatar Petroleum. It consists of different facilities used to process natural gas

reserves situated in North field. Ras Laffan Emergency & Safety College (RLESC) is the premier emergency and safety training facility in the Middle East (Figure 6). Texas Engineering Extension Service (TEEX) is the training provider for the center. This center was built similarly to BFTF with several improvements. The objective of this center is to train safety professionals in several areas: Oil, gas, petrochemical industries, marine, industrial firefighting, medical services, hazardous materials, emergency response, etc. The center's surface is 1 km^2. It includes 29 props built for firefighting training for different situations. One prop (TP-5) will be used for conducting LNG experiments in order to validate models with high quality experimental data. It consists of three different pits where the LNG spills will take place: big pit (5x6x1.2m), small pit (3x3 m) and L-shape pit (Figure 6). The experiment will be carried out in the 5x6x1.2 m large pit. This pit was well equipped by the process safety group in TAMU-Qatar to be used for research purposes. It is prepared with 100 thermocouples and 13 heat flux plates embedded in concrete in order to determine heat flux from ground to the pit (Figure 7). A weather station is also installed for meteorological data collection. There is a classroom located near the experimental site (around 80m from TP-5).The LNG tanker will be located on the North of the site at almost 56 m.

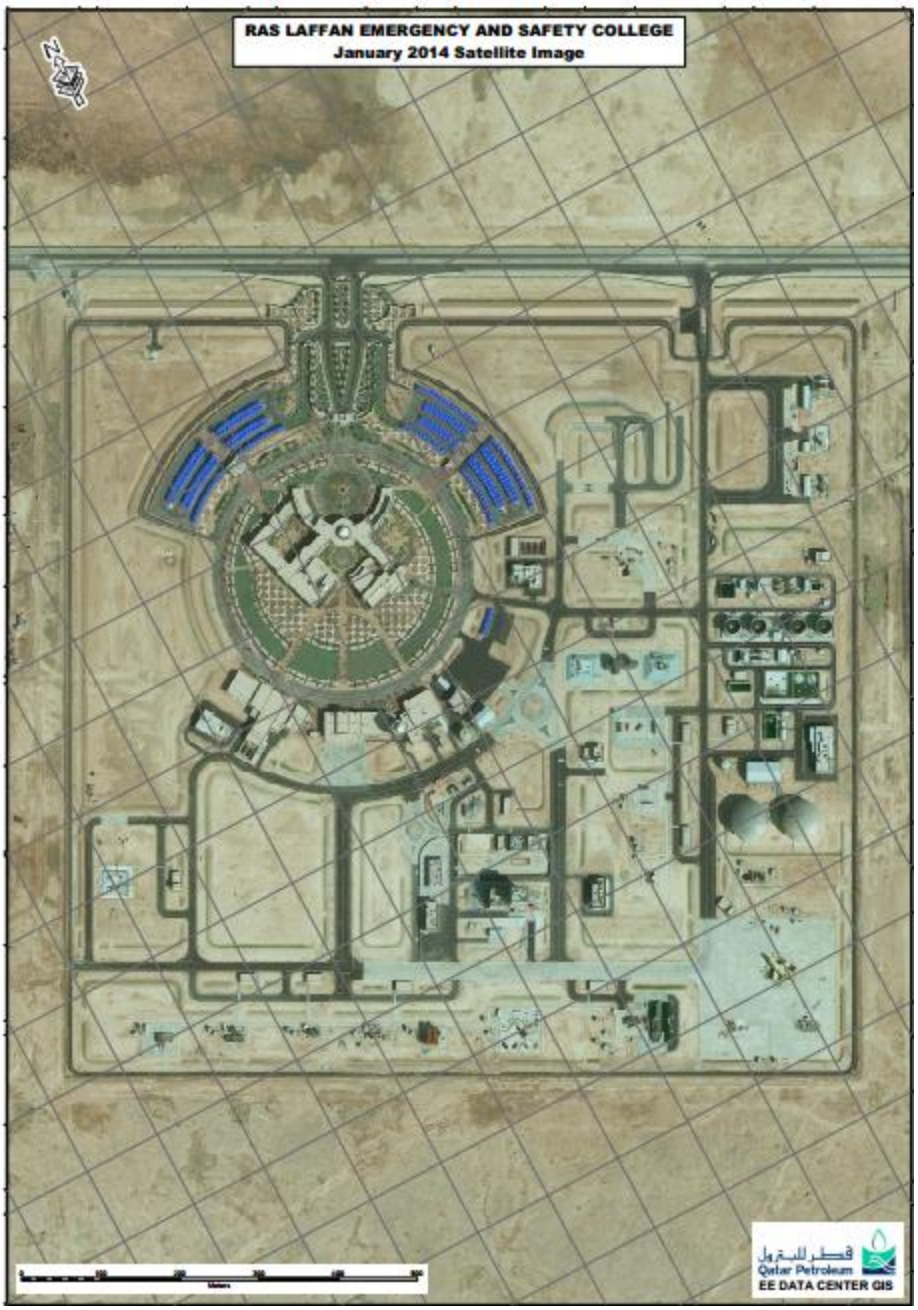

Figure 6: Ras Laffan Emergency and Safety College, Qatar

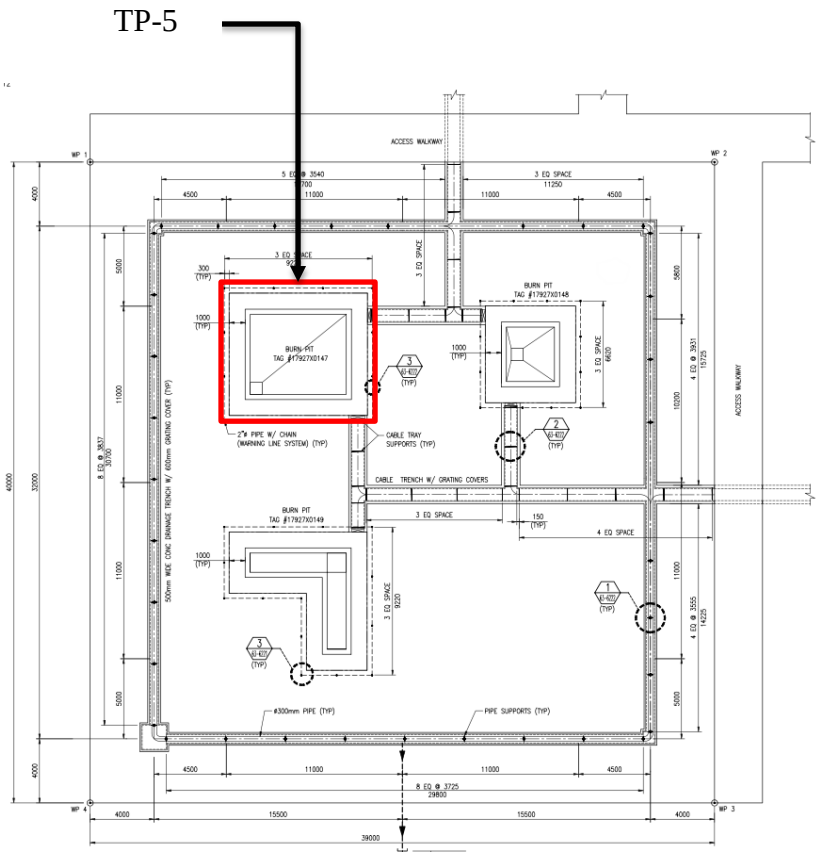

Figure 7: Layout of TP-5 (LNG prop)

2.4.2 Modeling Work using Standard Turbulence Models

The choice of the turbulence model depends on the application. Different turbulence models perform better for certain applications than others. The $k-\varepsilon$ model based on Navier-Stokes RANS is the most used for engineering applications [16]. However, this model may perform poorly for strong curvatures and stagnation points. The RNG $k-\varepsilon$ turbulence model is developed to overcome this weakness [20].

Another CFD software used for flow and dispersion modelling around buildings is FLACS, it was validated with several field experiments involving buildings and obstacles such as: Kit Fox, Must, and Prairie Grass. The results of these simulations were considerably good for dispersion modeling with 86% of the predictions within a factor of 2 of the experimental data for highest concentrations. This code is set to the standard turbulence model [21].

The simulation of Coyote series trials (LNG vapor cloud dispersion) was performed using computational fluid dynamics (CFX) successfully using the standard k-ε turbulence model [19]. The CFX code was compared to results from two box models DEGADIS and SLAB. This comparison indicated that the CFX results are more accurate than DEGADIS and SLAB results. The CFX model was able to visualize the cloud dispersion as dense cloud rather than a light gas and the cloud dimensions were predicted correctly. The overestimation of the gas concentration is common using box-models (SLAB & DEGADIS). On the other hand, CFX results are significantly accurate according to statistical performance measures [22].

Similarly, Scargiali et al used a CFD (CFX) code for the modelling of dense gas (chlorine) accidental spill. The turbulence model used was the standard $k-\varepsilon$ turbulence model. The dispersion modelling used species transport. The CFX code accounts for the additional buoyancy effects related to dense gas concentration in the momentum equations. However, it does not include the effects of concentration induced buoyancy into account [1].

In addition Giannissi performed the simulation of LNG dispersion over water surface using CFD (ADREA-HF) code based on the Falcon Series experiments. He modeled the source with two different approaches which are a vapor pool and phase jet. He concluded that the two phase jet gave better results for the downwind concentration predictions but it underestimates the concentration for most sensors. He used the standard k-ε model in his simulation [23].

Sklavounos et al used several turbulence models: $k-\varepsilon$, $k-\omega$, SST and RSM in his models to compare simulation results against experimental data from Thorney Island large scale trials. He concluded that $k-\omega$ behavior is similar to $k-\varepsilon$ but it is computationally more expensive. Also, the RSM required significant time compared to the rest of models but the accuracy improvement wasn't significant [24].

Also, Qi et al applied CFD (CFX) in order to model the LNG vapor dispersion and study key parameters governing this phenomenon. He used experimental data from November 2007 tests performed at BFTF for LNG release on water and on concrete. He compared three turbulence models $k-\varepsilon$ RNG, SSG and $k-\varepsilon$. He concluded that the differences between the models are not significant with respect to the downwind concentrations but the performances of the SSG and RNG $k-\varepsilon$ model were slightly better in the prediction of the cloud shape but this comparison wasn't based on any experimental data. The three models don't show clear differences for the available experimental results. He conducted a sensitivity analysis for source term, atmospheric conditions and turbulence equations and he concluded that the parameters involving source term are very important for the prediction of downwind distances. The CFD code

gave good results compared to experimental data. The sensitivity analysis conducted focused on release on water so for future work the focus may be for release on concrete [12].

Gavelli et al used CFD (FLUENT) for the modelling of LNG spills into geometrically complex environment. He compared simulations to data from Falcon tests because these tests addressed the effect of impoundment walls and obstructions on the dispersion of LNG vapors. He used the standard $k-\varepsilon$ turbulence model and the Reynolds Stress Model (RSM). According to Gavelli, the standard $k-\varepsilon$ turbulence model over predicts the turbulent kinetic energy. The RSM is more accurate than the $k-\varepsilon$ model but it is less stable. As a result, the $k-\varepsilon$ model was used to provide an initial guess for turbulence to the RSM model. He concluded that CFD simulations can provide good results for Falcon tests. Also, the turbulence generated by the spill is an important factor that increases mixing of the gas and its dispersion over the barrier. The velocity of the evaporated gas is required for the estimation of the spilled gas turbulence. Also, the vapor fence represents an effective barrier for the reduction of the cloud dispersion [25].

Biao Sun et al conducted the modelling of dense gas dispersion (LNG) using CFD (FLUENT) and integral model DEGADIS taking into account the effects gravity and time dependence dispersion. The work was based on the data from Burro series tests. The objective was to study the ability of impoundments to reduce the vapor dispersion of LNG. The turbulence model used was the realizable k-ε because it takes into account the slumping associated with dense gas dispersion especially in the

presence of obstacles. The main difference between the realizable $k-\varepsilon$ and the standard $k-\varepsilon$ is that the realizable computes the turbulent viscosity C_μ according to an eddy viscosity formula while the standard k-ε assumes a constant $C_\mu = 0.09$. Also, another equation for the dissipation rate is derived from transport equations. Also, species transport equations were used to model the LNG vapor dispersion.

He concluded that CFD simulations gave good results for the prediction of dense gas dispersion compared to integral model (DEGADIS).

Also, Tauseef et al performed the simulation of dense gas dispersion (Freon 12 & nitrogen) using CFD and based on Thorney Island experiment trial 26. He compared the performances of the $k-\varepsilon$ standard turbulence model and realizable $k-\varepsilon$ model. He concluded that the realizable $k-\varepsilon$ model gave better results for the prediction of concentration profiles and was able to simulate the phenomena of dispersion of a dense gas [26].

2.4.3 Modeling Work using Modifications to Standard Turbulence Models

Alinot & Masson presented a numerical method for the prediction of atmospheric boundary layer for stable, neutral and unstable stratifications. They used the $k-\varepsilon$ turbulence model with the modification of its coefficients. They demonstrated that their modifications improved the simulation for stable class and gave similar results for neutral and unstable classes to other models available in literature. Their results suggested the necessity of modifying the coefficients of the $k-\varepsilon$ turbulence model to get developed profiles of turbulent kinetic energy, turbulent dissipation rate and

temperature with accordance to Monin Obukhov Theory. However, this modified $k-\varepsilon$ model was used for atmospheric modeling only [27] .

In the same context, Richards and Hoxey suggested the modification of the C_μ and σ_k for the case of neutral stability class as follows [12,28]:

$$C_\mu = \frac{u_*^4}{k^2} \qquad \text{Equation 6}$$

$$\sigma_\varepsilon = \frac{k^3}{(C_{\varepsilon 2} - C_{\varepsilon 1})\sqrt{C_\mu}} \qquad \text{Equation 7}$$

Similar modifications were suggested by Pontiggia et all. He performed the CFD (FLUENT) modelling of SO_2 gas release based on Prairie grass experiments. He argues that the standard k-ε model cannot maintain developed profiles of velocity, temperature and turbulence along the domain. He develops a new methodology ASsM (Atmospheric Stability sub-Model) and he claims that this approach models the effect of atmospheric stratification on dense gas dispersion. This methodology is based on the standard k-ε model with the addition of source term equations for the turbulent kinetic energy and turbulent dissipation rates. For neutral stratification:

$$S_\varepsilon(z) = \frac{\rho}{z^2} u_*^4 \left[\frac{(C_{\varepsilon 2} - C_{\varepsilon 1})\sqrt{C_\mu}}{K^2} - \frac{1}{\sigma_\varepsilon}\right] - \mu \frac{u_*^3}{2Kz^3} \qquad \text{Equation 8}$$

If the term depending on viscosity is neglected, the constants proposed by Alinot and Masson are obtained [29]. For stable stratification:

$$S_k = -\frac{\partial}{\partial z}[(\mu + \frac{\mu_T}{\sigma_k})\frac{\partial k}{\partial z}]$$ Equation 9

$$S_\varepsilon(z) = \frac{\rho}{z^2}u_*^4[\frac{(C_{\varepsilon 2} - C_{\varepsilon 1})\sqrt{C_\mu}}{K^2}\phi_\varepsilon^2\sqrt{\frac{\phi_\varepsilon}{\phi_m}} - \frac{1}{\sigma_\varepsilon}(\frac{2}{\phi_m} - \frac{1}{\phi_m^2} + \frac{T_*}{KT}] - \mu\frac{u_*^3}{2Kz^3}$$ Equation 10

The obtained profiles of turbulent kinetic energy and dissipation rates were in accordance with Monin Obukov theory after the modifications according to his simulations. Also, the proposed methodology gave good results for the simulation of several tests of Prairies Grass field tests and Falcon 1 for neutral and stable stratifications. The downwind concentrations were compared for Prairie Grass experiments and the concentration as a function of time was compared with the simulation for the Falcon test [12,30].

In the same context, Parente et al suggested the addition of similar source term equations for dissipation rate and turbulent kinetic energy for stable class as recommended by Pontiggia et al for the modelling of ABL flows. The main difference between both approaches is the neglect of the viscosity term added by Pontiggia and the addition of a source term for turbulent kinetic energy for stable class. In addition, he presented a wall function for rough surfaces. He obtained good results for velocity and turbulent parameters throughout the domain [29].

Table 5: Summary of previous work for dense gas dispersion for standard and modified turbulence models

Researcher	Turbulence model	Modeling software	Modeled experiment	Results & comments
Skalvanous & Rigas [24]	Standard k-ε	CFD (CFX)	Coyote series trials	Good agreement compared to DEGADIS and SLAB results
Hanna, Hansen & Dharmavaram [21]	Standard k-ε	FLACS	Kit Fox, Must & Prairie Grass	86% of predictions within 2 factor
Scargiali et al[1]	Standard k-ε	CFD (CFX)	Chlorine Accidental spill scenario	No comparison with experimental data
Giannissi [23]	Standard k-ε	CFD (ADREA-HF)	Falcon series experiments	Two phase jet model is more accurate than vapor pool
Skavanous et al [24]	k-ε, k-ω, SST and RSM	CFD (CFX)	Thorney Island	Similar results for k-ε, k-ω and RSM with difference in computational requirements

Table 5: Continued

Researcher	Turbulence model	Modeling software	Modeled experiment	Results & comments
Reuifing Qi et al [12]	Standard k-ε, k-ε RNG, and SSG	CFD (CFX)	BFTF	Slightly better performance for RSM and k-ε RNG
Gavelli et al [31]	Standard k-ε and RSM	CFD (FLUENT)	Falcon test	RSM is more accurate
Biao Sun [32]	Realizable k-ε	CFD (FLUENT) and DEGADIS	Burro series tests	CFD results are better than DEGADIS results.
Tauseef et al [26]	Standard k-ε and realizable k-ε	CFD	Thorney Island	Better results for realizable k-ε
Alinot and Mason [27]	Modified k-ε	CFD (FLUENT)	Atmospheric modeling	Better results especially for stable class
Richard and Hoxey [28]	Modified k-ε	CFD (FLUENT)	Atmospheric modeling	Better results especially for stable class
Pontiggia et al [33]	Modified k-ε	CFD (FLUENT)	Prairie Grass	Better results than Standard k-ε
Parente et al [29]	Modified k-ε	CFD (FLUENT)	Atmospheric modeling	Better results than Standard k-ε for stable class

2.4.4 Summary of Gaps and Areas of Improvement

There are several areas of research in the LNG safety field. The main ones are:

- Factors leading to boiling liquid expanding vapor explosions (BLEVEs).
- Inaccurate handover of the source term model to the dispersion model (especially for integral models) which leads to errors in consequence modeling.
- Uncertainty in consequence modeling due to the variation of atmospheric data during experiments (wind speed, direction and atmospheric stability).
- Test the effectiveness of LNG containment systems (carriers, storage tanks, etc.) including modeling of ship collision or a terrorist attack on the ship to determine and improve hull strength.
- Test mitigation techniques such as foams, water sprinklers, and gas detectors in order to determine their effectiveness in the case of incidents.
- Advance CFD models of source term and vapor dispersion.

In order to illuminate these areas, there is a need to perform large scale LNG spills and pool fire tests and validate current models against experimental data in order to determine their accuracy and develop better models. The focus should be on source term modeling because it received less attention compared to dispersion modeling. Experimental data are needed in many aspects related to source term modeling including: flow rate, high momentum, jet releases, rainout, liquid pool spreading and vaporization rate [34,35].

The focus of this work will be the uncertainty in consequence modeling due to the variation of experimental data mainly different stability classes and the development

of better CFD models for vapor dispersion. The modelling of dense gas dispersion was done for two main stability classes: Neutral and Stable. The released gas is diluted more effectively for the unstable atmospheric class which results in a decrease in the downwind concentration of the hazardous gas. The stable and neutral conditions are the most used for risk assessments because typically the objective is worst case scenarios [33,23,32]. The CFD modelling of the unstable class is more demanding because of the complexity of the velocity and turbulence profiles for this class compared to the stable and neutral conditions. Also, it's hard to get a converged solution for this class. However, the dominating atmospheric stability class (during the day) is usually the unstable class especially for Qatar. As a result, the performance of accurate risk assessments requires the simulation in these unstable atmospheric conditions.

The main challenge for this task is that the CFD code must provide an acceptable representation of the atmospheric boundary layer in order to provide accurate dispersion results. The wind, temperature and turbulence profiles should be in accordance with the Monin Obukhov theory for the three stability classes [33]. The modeling of the atmospheric boundary layer for the unstable class using CFD is an ongoing research topic in the atmospheric and meteorology fields.

In addition, the choice of turbulence model is clearly very important for the dispersion modelling. There is no agreement on which model performs better for this application. There are several turbulence models which are tested and suggested to give accurate results for dense gas dispersion modelling. However, from the literature review done in previous sections, the best results for dispersion modelling were performed using

three main models: standard $k-\varepsilon$, realizable $k-\varepsilon$ and RSM models. The comparison of these three models is one main part of this work and was done in order to check which model performs better for dense gas dispersion.

CHAPTER III

SCOPE OF WORK

3.1 Problem Statement

The use of CFD in risk assessments for LNG facilities is increasing considerably because of its ability to build or import complex geometries and describe the phenomena of dense gas dispersion properly. As a result, the accuracy and reliability of its results are higher than integral models.

However, there is a lack of modeling of dense gas dispersion in the unstable class even though this class represents the dominating stability class during the day in Qatar and in many places in the world. A complete risk assessment must consider worst case scenario which is a spill when the stability class is stable or neutral and also the dominating stability class. Several issues are related to the simulation of LNG dispersion for this class. The wind, temperature and turbulence profiles are much more complex which means that modeling the atmospheric conditions at this class is more demanding computationally. Also, the solution is harder to converge which means that the accuracy of the results is uncertain.

Besides, there is a disagreement about the appropriate turbulence model to be used for the prediction of dense gas dispersion (Please refer to appendix for more details about turbulence models). A considerable work was done comparing the performance of different turbulence models which helps to identify the main ones to be considered for

this work. Among all turbulence models, the RANS models are widely used for engineering applications. They represent an excellent compromise between computational requirements and results accurateness.

Figure 8 represents the results of a survey done by ANSYS on the turbulence model choice for fluid applications by a considerable number of users. It was found that the main turbulence models used for fluid flow applications are the standard k-ε model, realizable k-ε model and SST turbulence models. However, different turbulence models performances depend on the application. Figure 9 illustrates most used turbulence models for dense gas dispersion modelling using CFD. This figure was generated after a literature review of several papers of this topic during this work. These models are: standard k-ε model, realizable k-ε and RSM models. Previous work on CFD modeling of dense gas dispersion for the Prairie Grass tests was done by Pontiggia. It focused on the comparison between CFD and experimental data for centerline concentration only for neutral and stable classes. The conclusion was that the model (modified k-ε) provides good agreement with experimental data [33]. Similarly, for the same tests, Hanna compared the highest model and experimental concentrations across the different arcs (which is usually centerline concentration as well) and concluded that the model (standard k-ε) provides a good estimation for dense gas dispersion [21]. In this work, an attempt was made to compare models predictions and experimental concentrations at each location to get a realistic idea about models performances.

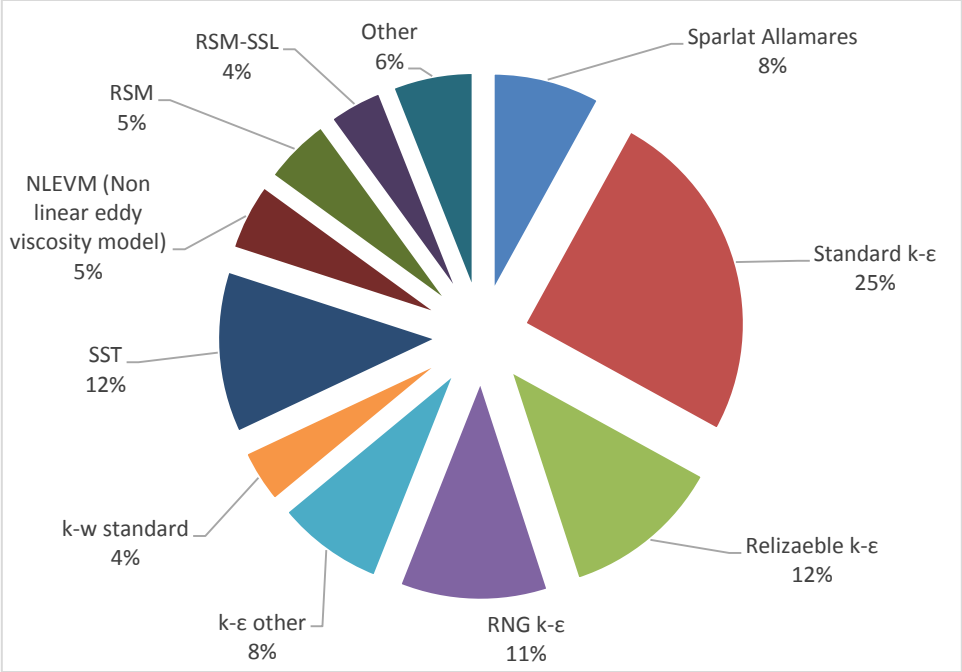

Figure 8: RANS turbulence models reported in ASME journal of Fluids Engineering [36]

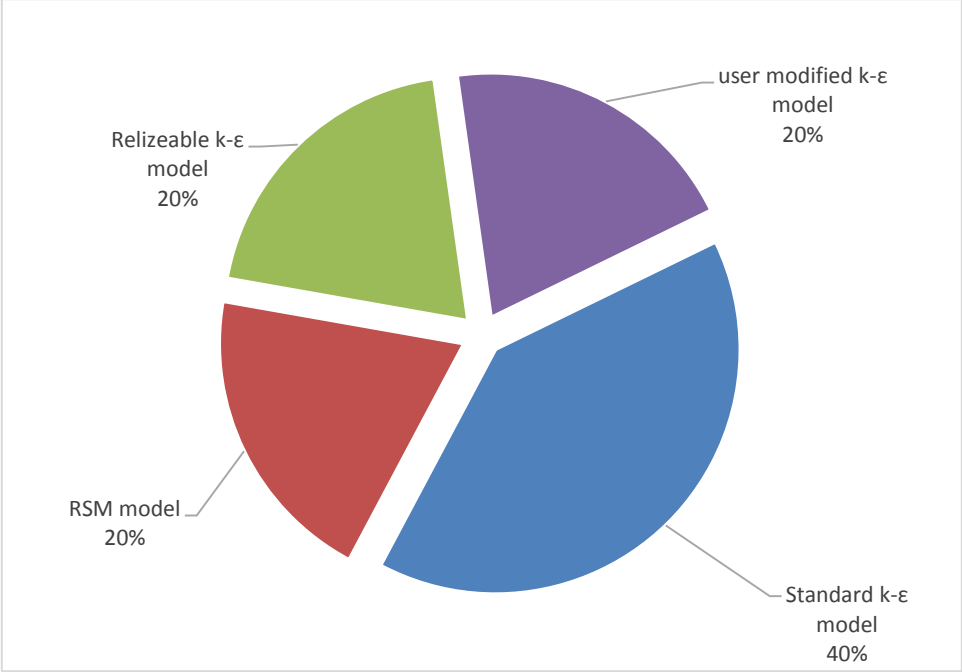

Figure 9: Most used turbulence models for dense gas dispersion simulations using CFD

3.2 Objectives

The objectives of this research are:

- Develop a CFD tool able to predict the dispersion of a cryogenic liquid (LNG/LN2) spill for the experiments to be performed at TP-5 in RLESC.

- Validation of this model with Prairie Grass tests for different stability classes.

- A comparison between three main turbulence models: standard k-ε, realizable k-ε and RSM models to identify the best model for this application.

The results of the dispersion model will be used in conducting a risk assessment for LNG facilities. However, the dispersion models are only good if they are successfully validated with experimental data. In Qatar, it is possible to conduct LNG spill experiments in RLESC in TP-5 in order to provide high quality data for models validation. These steps are described in Figure 10.

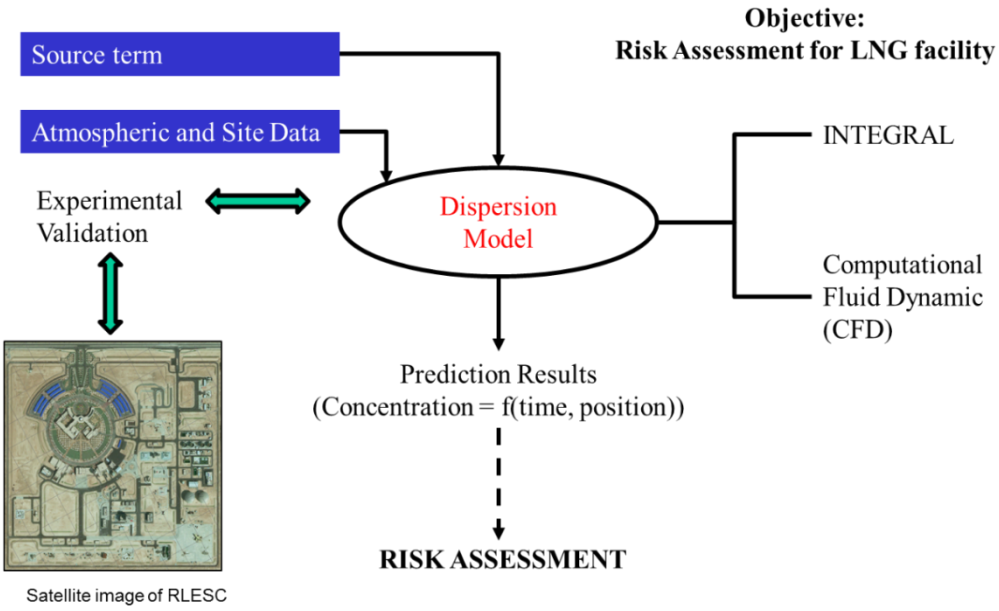

Figure 10: Elements of risk assessment for LNG facilities

CHAPTER IV

METHODOLOGY AND SPECIFICATION OF THE CFD MODEL

4.1 Methodology

A framework was developed as in Figure 11 below in order to achieve the objectives of the research. The first setup of the work is to test the influence of height on the profiles of velocity and turbulence in order to choose the appropriate domain height. After that, the CFD profiles of velocity, temperature and turbulence are checked with the vertical Monin Obukhov similarity theory profiles along the domain for each stability class. An accurate description of the atmosphere is required for precise dispersion results. Three Prairie Grass tests corresponding to three different stability classes: neutral, stable and unstable were chosen in order to validate the CFD model. Prairie Grass set of tests was chosen because they became the standard database for model assessment for continuous releases near ground over flat terrain [18].These conditions are similar to the release experiments planned for TP-5 at RLESC.

User defined functions (UDFs) for velocity, temperature and turbulence were coded from the Monin Obukov theory according to the corresponding stability class (Please refer to appendix for more details about used UDFs). A 3D simulation in an empty domain using UDF functions for turbulence, velocity and temperature was

conducted for three different heights (30, 60, 90 m). After that, the velocity, temperature and turbulence profiles were compared to Monin Obukhov theory and verified to be developed along the domain for three turbulence models: standard k-ε, realizable k-ε and RSM models. Next the source term was added to the setup. The mesh was refined after that in order to obtain a mesh independent solution. The downwind concentration is determined after that and it is compared to the experimental data. A sensitivity analysis of the turbulence model was conducted in order to determine the performance of three main turbulence models: standard $k-\varepsilon$, realizable $k-\varepsilon$ and RSM models and the best model for this application. The comparison was done with experimental results for concentration. After that, the geometry of TP-5 was built in Solid works and imported to ANSYS. The simulation of the spill experiment for neutral stability class to be conducted in TP-5 was performed.

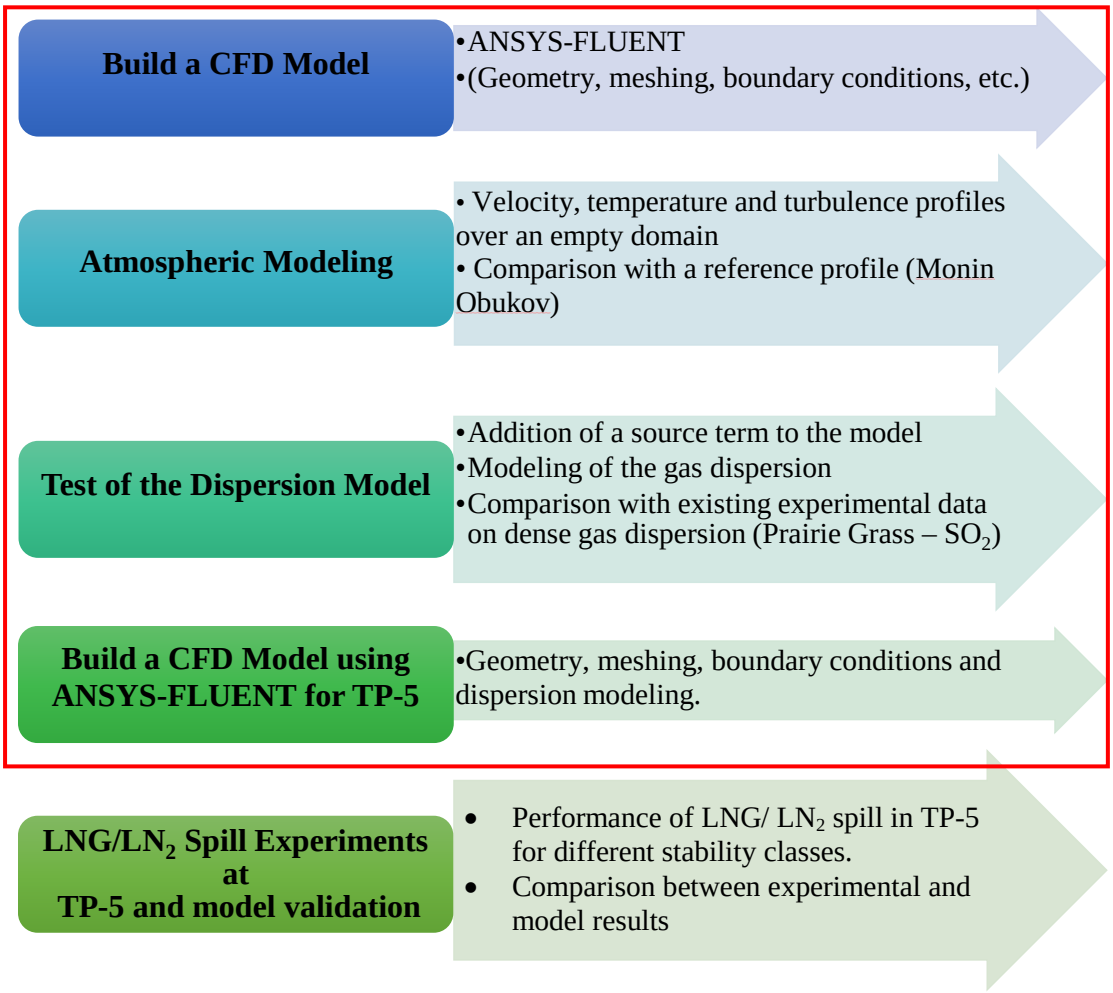

Figure 11: CFD modelling methodology

4.2 Specification of the CFD Model under ANSYS (FLUENT)

4.2.1 Atmospheric Modeling

Accurate modeling of the atmospheric boundary layer is required in order to obtain precise predictions for gas dispersion [37].

The atmospheric boundary layer is defined as the height where the earth surface affects the atmosphere through heat and momentum transfers. The height of the planetary

boundary layer (PBL) is approximately 10% of the atmospheric boundary layer. It varies between 250 m to 5 km depending on several factors especially solar radiation [16]. The PBL is the region of interest for LNG dispersion because of the height of the cloud even for a spill of 200,000- 300,000 m^3.

The vertical profiles of wind velocity (U), temperature (T_{air}) and turbulence in the atmospheric surface layer can be described by the Monin Obukhov theory [12].

The wind velocity is expressed as a function of the altitude (z), the friction velocity (u_*), the Monin Obukhov Length (L), non-dimensional wind shear function (ϕ_m):

$$\frac{\partial U}{\partial z} = \frac{u_*}{z} f\left(\frac{z}{L}\right) \qquad \text{Equation 11}$$

$$u_* = \sqrt{\frac{\Gamma_w}{\rho}} \qquad \text{Equation 12}$$

The Monin Obukhov Length (L) is a function of the surface layer temperature (ground temperate T_w), T_*, the Von Karman constant (K) and the gravitational acceleration constant (g):

$$L = \frac{u_*^2 T_w}{KgT_*} \qquad \text{Equation 13}$$

With $T_{*\,a}$ a function of the surface heat flux (q_w) as follows:

$$T_* = \frac{-q_w}{C_p u_* \rho} \qquad \text{Equation 14}$$

ϕ_m is a non-dimensional wind shear function [27]. Assuming constant heat flux and shear stress over the ground surface layer, the profiles of velocity and temperature are as follows:

- For $L < 0$,

$$\varphi_m\left(\frac{z}{L}\right)=\left(1-16\frac{z}{L}\right)^{-\frac{1}{4}} \quad \text{Equation 15}$$

$$u_{0(z)^*}=\frac{u_*}{K}\left[\ln\left(\frac{z}{z_0}\right)+\ln\left(\frac{8\varphi^4{}_m\left(\frac{z}{L}\right)}{\left(\varphi_m\left(\frac{z}{L}\right)+1\right)^2\left(\varphi_m^2(\frac{z}{L})+1\right)}\right)-\frac{\pi}{2}+2\arctan\left(\frac{1}{\varphi_m\left(\frac{z}{L}\right)}\right)\right] \quad \text{Equation 16}$$

$$T_0(z)-T_{w^*}=\frac{T_*}{K}\left[\ln\left(\frac{z}{z_0}\right)-2\ln\left(\frac{1}{2}\left[1+\varphi^{-2}{}_m\left(\frac{z}{L}\right)\right]\right)\right]-\frac{g}{C_p}(z-z_0) \quad \text{Equation 17}$$

- For $L > 0$:

$$\varphi_m\left(\frac{z}{L}\right)=1+5\frac{z}{L} \quad \text{Equation 18}$$

$$u_0(z)=\frac{u_*}{K}\left[\ln\left(\frac{z}{z_0}\right)+\varphi_m\left(\frac{z}{L}\right)-1\right] \quad \text{Equation 19}$$

$$T_0(z)-T_{w^*}=\frac{T_*}{K}\left[\ln\left(\frac{z}{z_0}\right)-\phi_m\left(\frac{z}{L}\right)-1\right]-\frac{g}{C_p}(z-z_0) \quad \text{Equation 20}$$

In addition to velocity and temperature profiles, turbulence in the atmosphere (irregularity and randomness of a flow) needs to be described for atmospheric modelling

using the following parameters and their expression according to Monin Obukhov theory [27]:

- Turbulent kinetic energy, k_0 (measure of turbulence intensity)

$$k_0(\mathrm{z}) = \sqrt{\frac{\mu_{T0}\varepsilon_0}{\rho C_\mu}} \qquad \text{Equation 21}$$

- Turbulent dissipation rate, ε_0, (measure of the reduction of turbulence):

$$\varepsilon_{0(z)} = \frac{\mathrm{u}_*^3}{Kz}\varphi_\varepsilon \qquad \text{Equation 22}$$

Where

$$\phi_\varepsilon(\frac{\mathrm{z}}{\mathrm{L}}) = 1 - \frac{\mathrm{z}}{\mathrm{L}} \quad \text{for} \quad L < 0 \qquad \text{Equation 23}$$

$$\phi_\varepsilon(\frac{\mathrm{z}}{\mathrm{L}}) = \phi_\mathrm{m}(\frac{\mathrm{z}}{\mathrm{L}}) - \frac{z}{L} \quad \text{for} \quad L > 0 \qquad \text{Equation 24}$$

- Turbulent viscosity, $\mu_{T(z)}$ (momentum transfer by turbulent eddies or circular air movements).

$$\mu_{T(z)} = \frac{\rho K u_* z}{\varphi_m\left(\frac{z}{L}\right)} \qquad \text{Equation 25}$$

4.2.2 FLUENT Solver

The CFD (FLUENT) software solves the Navier-Stokes equations for gas flow simultaneously with the diffusion and energy equations. The incompressible ideal gas approach (constant density) was assumed in this simulation. This means that the gas

density varies as a function of the local temperature and chemical composition neglecting the pressure effects [31].

4.2.3 Boundary Conditions

Before running the simulation, the CFD user needs to choose the appropriate boundary conditions. The choice of boundary conditions in this section was based on literature review about LNG vapor modeling setup using CFD and is illustrated in Figure 12 [16,33] :

The inlet boundary condition corresponds to the inlet profiles using user defined functions (UDFs) for velocity, temperature and turbulence. The Monin Obukhov equations were coded for the neutral and stable classes. For the unstable class, the trendline equations (using Excel) of the Monin Obukhov theory were used instead because of the complexity of the original Monin Obukhov equations. The UDFs for velocity, temperature and turbulence used for the three stability classes are available in the appendix. Their direction was specified normal to the inlet boundary and in the flow direction.

The outlet boundary was set as pressure outlet at the atmospheric pressure and zero gradients for the other variables.

The top boundary condition is specified as velocity inlet boundary similarly to the inlet boundary with the direction changed to match the flow direction.

The side boundary conditions are specified as velocity inlet boundary similarly to the inlet boundary with the direction changed to tangent to the surface.

The ground is specified as a wall boundary and the appropriate roughness value is given along with the ground temperature for neutral stability class or heat flux for stable and unstable classes. The roughness value in FLUENT was specified with accordance to Blocken constraints according to the following equation:

$$K_{S,ABL} = \frac{9.793 y_0}{C_S} \qquad \text{Equation 26}$$

The gas inlet boundary condition was specified as mass flow inlet boundary condition with the appropriate mass flow rate, temperature and turbulence.

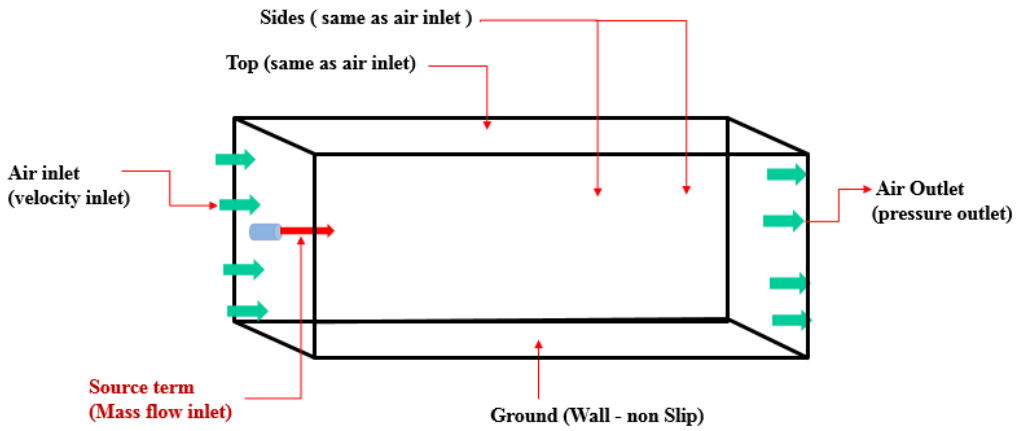

Figure 12: Model boundary conditions for Prairie Grass tests

4.2.4 Initial Conditions

The flow initialization was done using the Hybrid method. This method consists of conducting a basic flow simulation using Laplace equations. The equations of

pressure and momentum are solved in order to determine the overall flow field. This method converges faster than the standard initialization which provides constant values.

4.2.5 Domain and Grid

The simulation results must be tested to be mesh independent. This can be done by performing different simulations with varying mesh sizes from a coarse to fine meshes. When the change in concentration contours is not significant, the solution is mesh independent. The change in mesh size is usually done by a factor of 2 [16].

4.2.6 Critical Parameters

The gas released to the atmosphere is considered to be dense in the following circumstances:

- They are released at a low temperature.
- Their molecular weight is higher than the molecular weight of air.

The dispersion of dense gases is different from passive gases dispersion in the following aspects:

- The stable stratification and gravity flow.
- The gravity spreading is driven by density difference between the cloud and ambient conditions.

The fluid motion is usually horizontal except the front cloud where there is a recirculating vortex. The dense gas changes the ambient turbulence mixing. The formation of aerosols after the spill contribute to cooling the cloud and keeping it dense for long distances downwind which decreases mixing with air [16].

The CFD code must model the turbulent mixing of the cloud with the atmosphere (buoyancy, shear or other mechanisms), the heat transfer between the lower cloud surface and the ground, the density change as function of temperature and the developed profiles of velocity and also temperature and turbulence with accordance to Monin Obukhov theory in order to represent the phenomena of dense gas dispersion correctly. The conservation of the profiles of velocity, temperature and turbulence throughout the domain is essential before performing any modeling in order to obtain accurate dispersion results. The temperature is an important factor to take into account in the simulation since it results in a change in density, in buoyancy and the LNG vapor cloud behavior as a consequence [21, 24, 28].

CHAPTER V

RESULTS AND DISCUSSION

5.1 Modeling of Empty Domain for Different Heights

There are no guidelines for choosing the appropriate height of the computational domain in literature if there are no obstacles. From the work done previously in dispersion modelling using computational fluid dynamics, the domain height varied between 30 and 100m. The reasons behind this choice were not specified. The profiles of velocity, turbulent kinetic energy, turbulent dissipation rate and turbulent viscosity were compared for three simulations at 3 different heights: 30m, 60m, and 90m using standard k-ε model and Monin Obukhov theory in order to determine the required height representing the velocity and turbulence profiles according to Monin Obukhov theory.

5.1.1 Neutral Stability Class

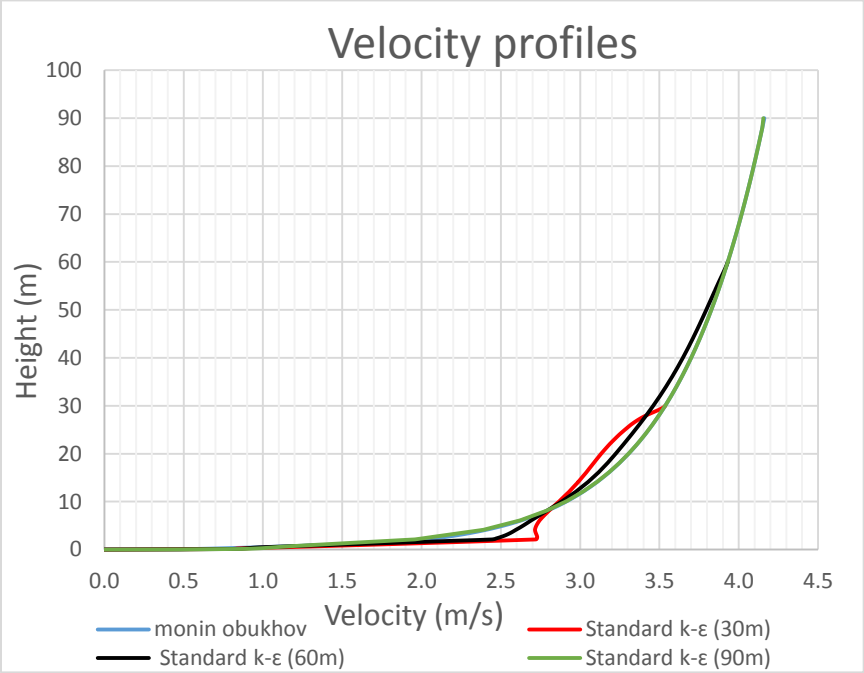

Figure 13: Velocity profile as a function of height

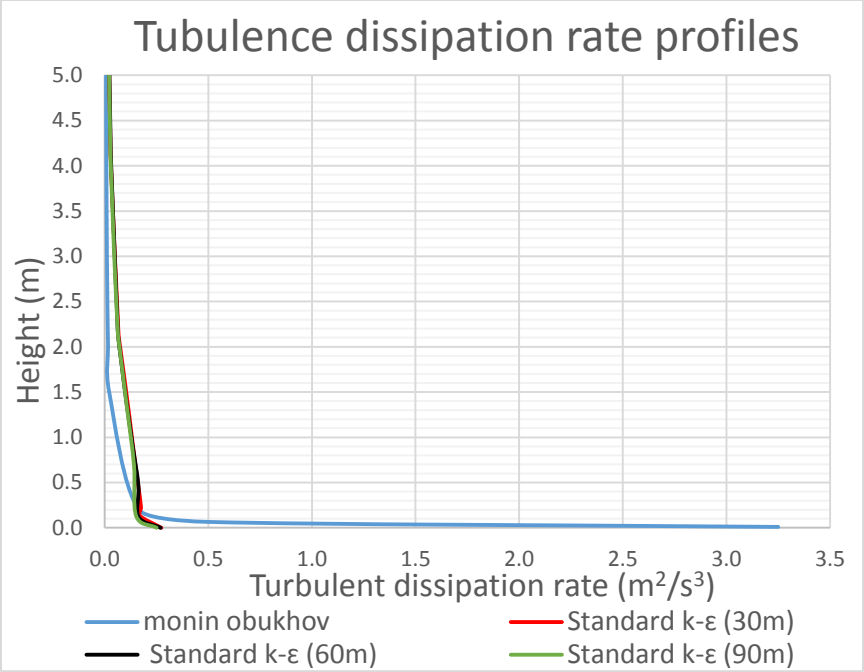

Figure 14: Turbulent dissipation rate profiles as function of height

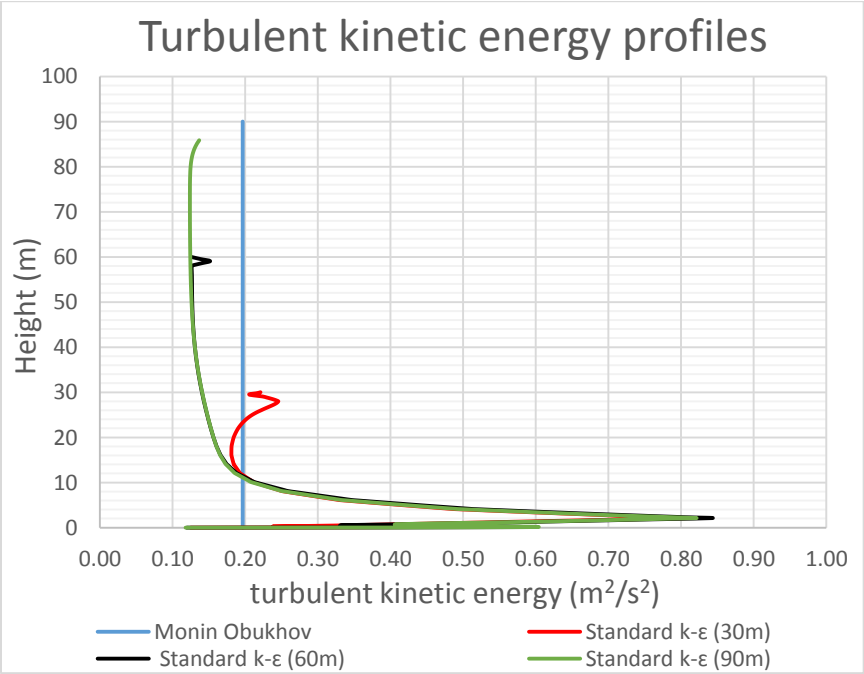

Figure 15: Turbulent kinetic energy as a function of height

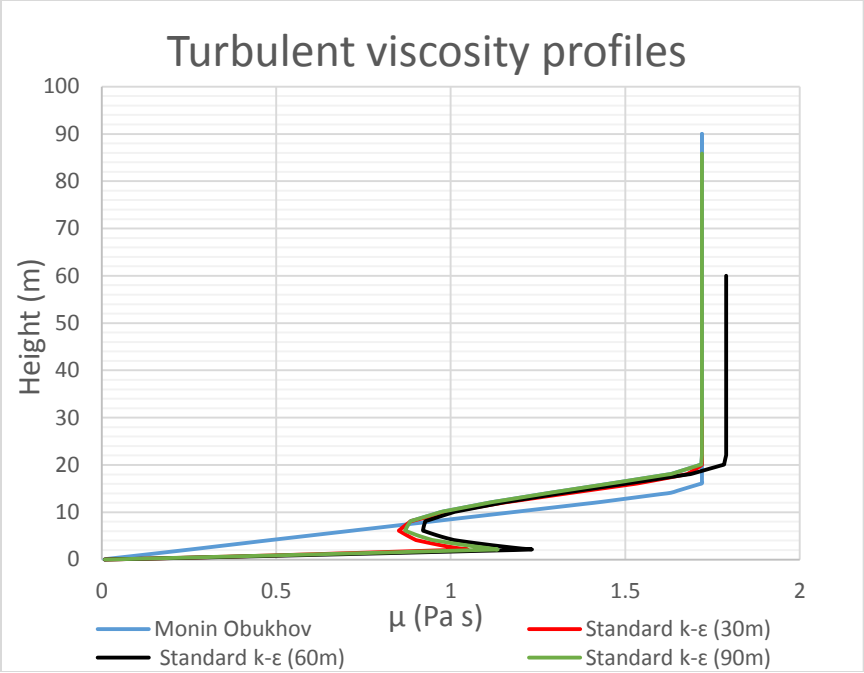

Figure 16: Turbulent viscosity profiles as a function of height

For the neutral class, there is a good agreement for the velocity profiles for the three heights (30m, 60 m, and 90 m) for the standard k-ε turbulence models especially at 60m and 90m. For the turbulent dissipation rate, the profiles for all heights show a considerable deviation from the Monin Obukhov profile near the ground which is a reported limitation for this turbulence model (Please refer to section 2.4.3 for more details). For the turbulent kinetic energy there is a considerable deviation for all the heights from the Monin Obukhov theory. This deviation is due to the fact that the standard k-ε model underestimates the turbulent kinetic energy. The profiles for all the heights are similar which means that this deviation does not depend on the height. For the turbulent viscosity profiles, there is an important deviation especially in the first

10 m. This deviation may be due to the deviation in turbulent kinetic energy since turbulent viscosity depends on turbulent kinetic energy.

5.1.2 Stable Class

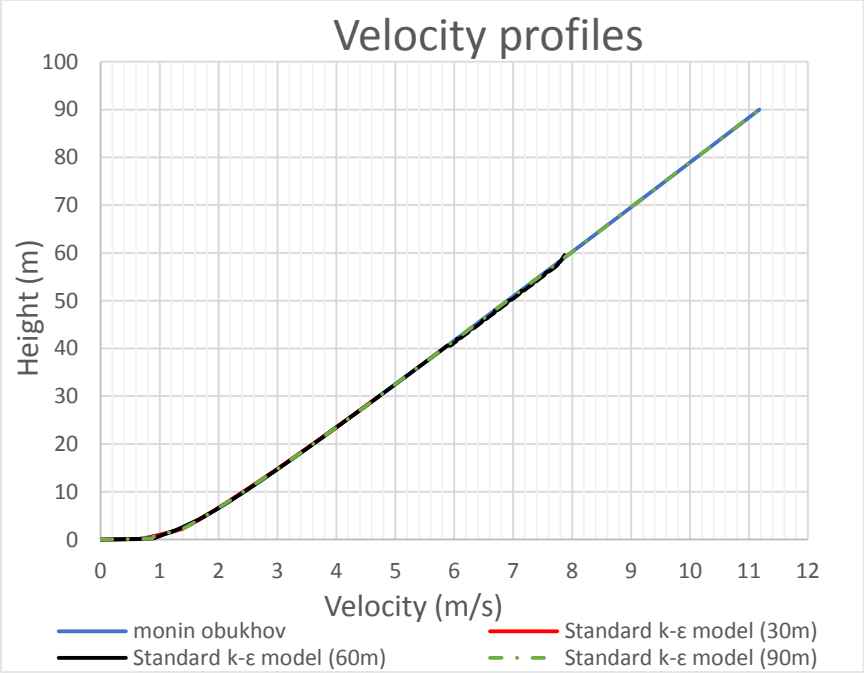

Figure 17: Velocity profile as a function of height

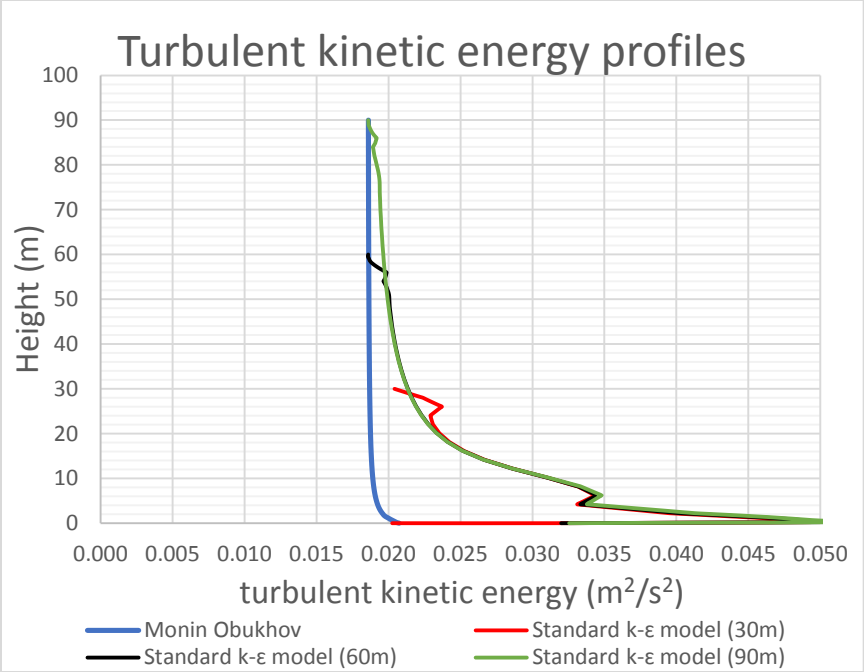

Figure 18: Turbulent kinetic energy as a function of height

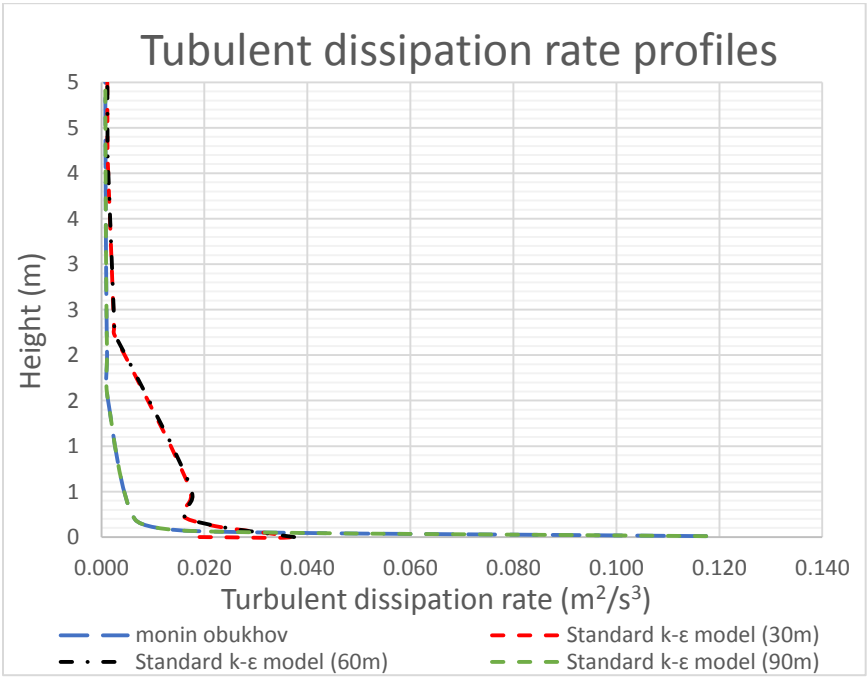

Figure 19: Turbulent dissipation rate as function of height

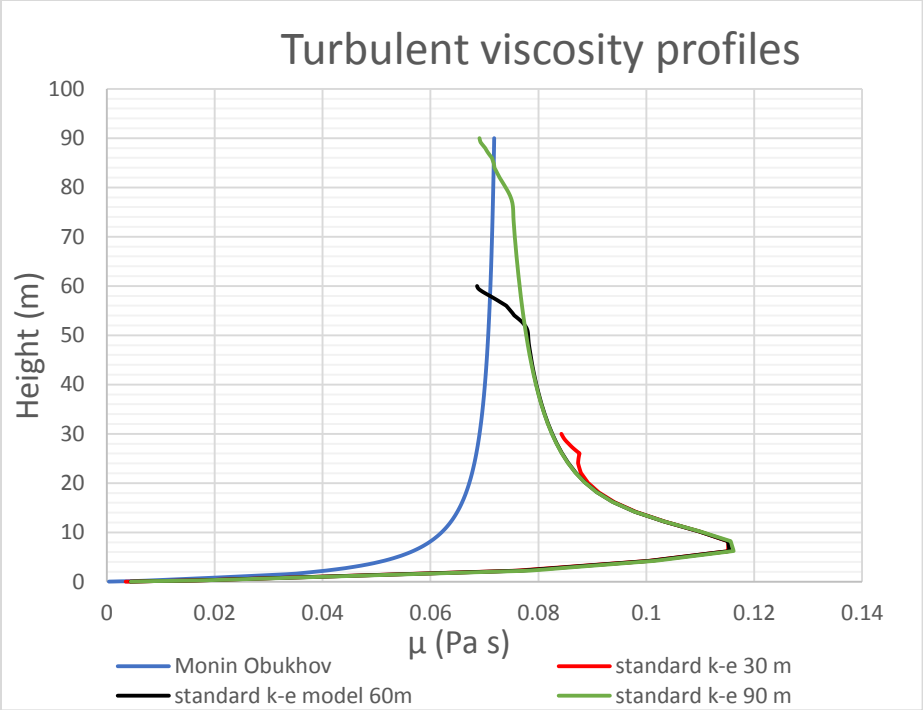

Figure 20: Turbulent viscosity profile as a function of height

For the stable class, there is a good agreement for the velocity profiles for the three heights (30m, 60 m, and 90 m) for the standard k-ε turbulence models. For the turbulent dissipation rate, the profile for 30 m is identical to Monin Obukhov profile but there is deviation for 60 and 90 m in the first 5 m. However, for the turbulent kinetic energy, there is a considerable deviation for all the heights with the Monin Obukhov theory near the ground. This deviation is known as function wall effect. The profiles for all the heights are similar which means that this deviation does not depend on the height. For the turbulent viscosity profiles, there is an important deviation especially in the first 10 m. This deviation may be due to the deviation in turbulent kinetic energy since turbulent viscosity depends on turbulent kinetic energy.

5.1.3 Unstable Class

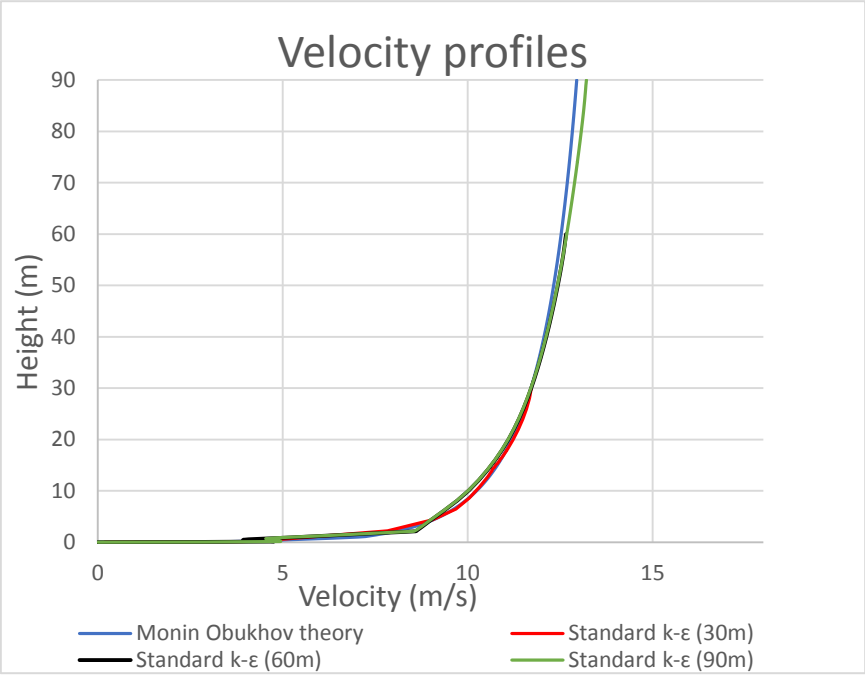

Figure 21: Velocity profile as a function of height

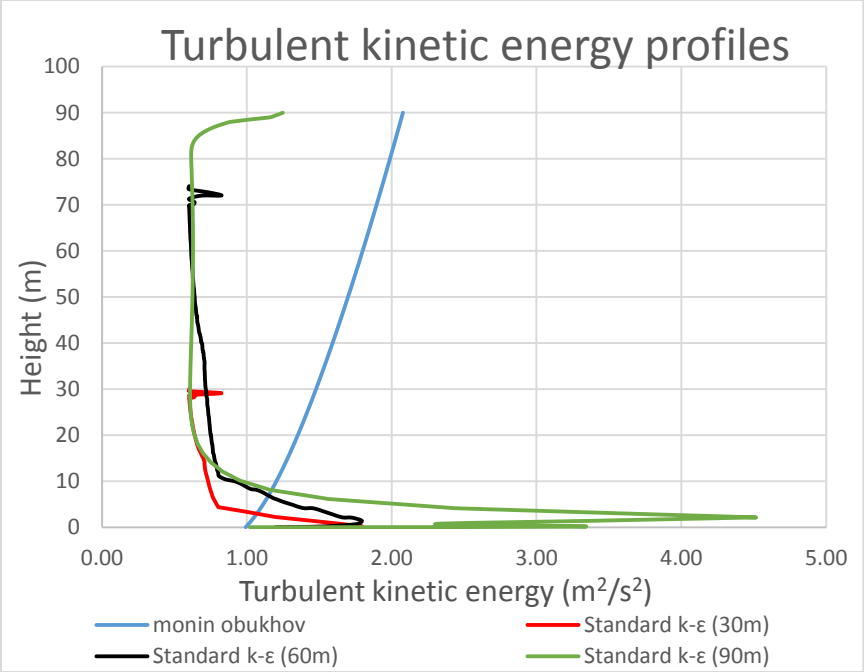

Figure 22: Turbulent kinetic energy as a function of height

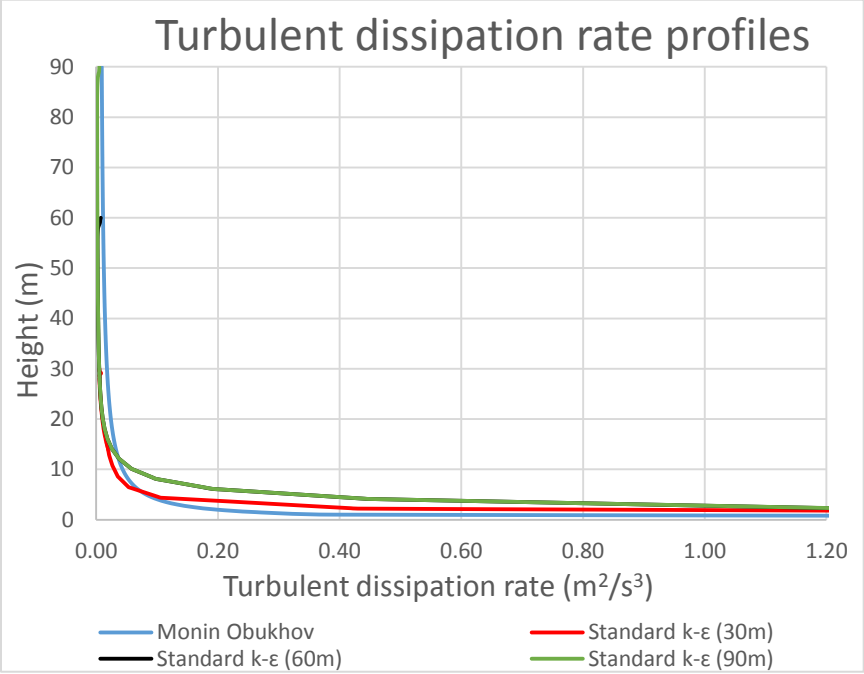

Figure 23: Turbulent dissipation rate as function of height

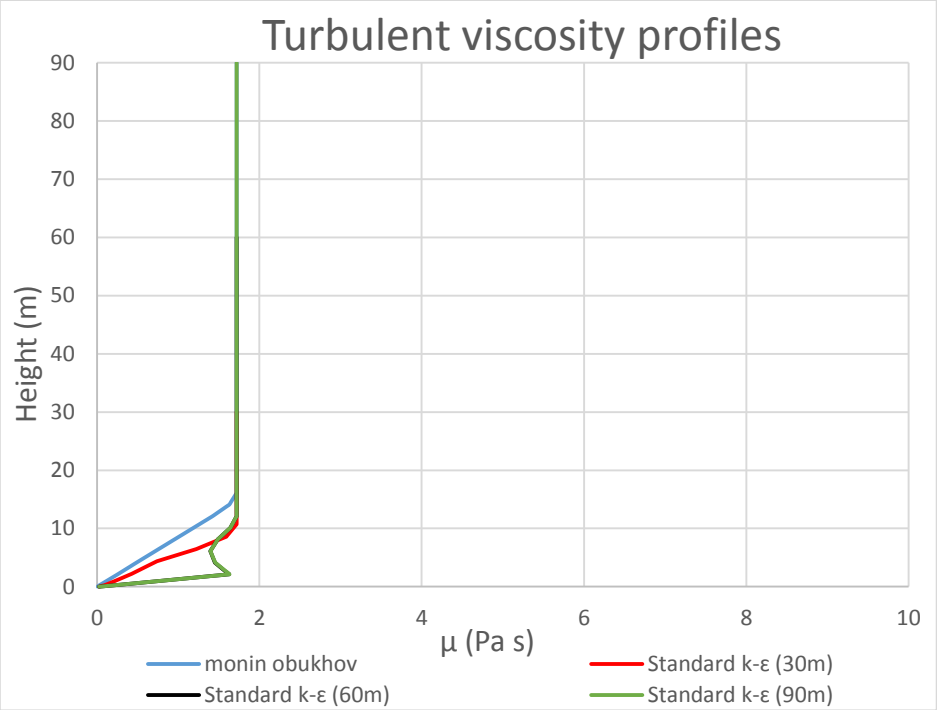

Figure 24: Turbulent viscosity profiles as a function of height

For the unstable class, there is a good agreement for the velocity profiles for the three heights (30m, 60 m, and 90 m) for the standard k-ε turbulence models. For the turbulent dissipation rate, the profile for 30 m is close to Monin Obukhov profile but the deviation increases for 60 m and 90 m in the first 5 m. However, for the turbulent kinetic energy there is a considerable deviation for all the heights with the Monin Obukhov theory especially for the 90 m profile. This deviation is due to the fact that the standard k-ε model underestimates the turbulent kinetic energy .The deviation is higher for the 90 m profile which means that it may depend on height. For the turbulent viscosity profiles, there is an important deviation after few meters altitude. This deviation may be due to the deviation in turbulent kinetic energy since turbulent viscosity depends on turbulent kinetic energy.

From the previous simulations, the velocity and turbulence profiles do not depend on the height. As a result, the minimum height will be chosen for the modelling of Prairie grass tests which is 30m.

5.2 Modeling of Prairie Grass Experiments

The Prairie Grass experiments involved 68 runs from the months of July and August for different stability classes. These runs consist of a continuous release of SO_2 from a pipe at 46 cm height over a flat Prairie in Nebraska in the United States. The SO_2 concentrations were measured at several arcs: 50m, 100m, 200m, 400m and 800m and Heights : 17.5,13.5,10.5,7.7,4.5,2.5,1,0.5m at 100m downwind distance [18]. Three Prairie grass tests were chosen corresponding to three different stability classes:

- PG 17 for neutral stability class
- PG 13 for stable class
- PG 33 for unstable class

Also, for each run, three turbulence models were used:

- Standard $k-\varepsilon$ model
- Realizable $k-\varepsilon$ model
- RSM model

5.2.1 Geometry and Meshing

The computational domain is parallelepiped of 1000 m length, 260m width and 30 m height. This large volume was chosen in order to get results corresponding to the locations of different experimental concentration measurements. The source term of SO_2

is a horizontal pipe at a height of 0.46 m and a diameter of 0.0508 m and its length is 0.2m. This pipe was modeled as a cylinder at the center of the inlet face of the parallelepiped as shown in Figure 25.

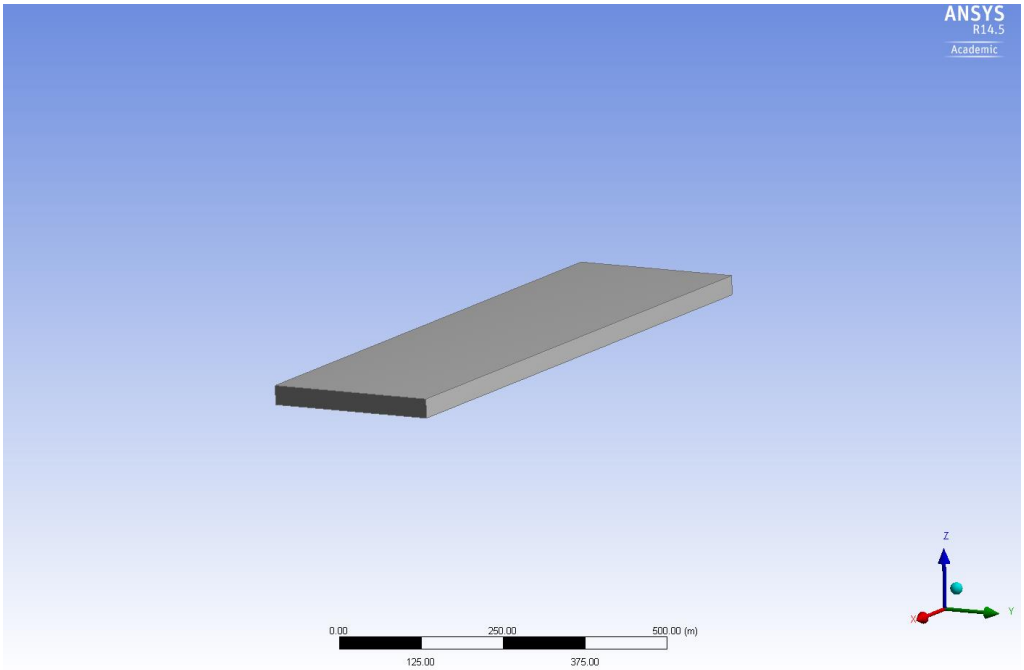

Figure 25: Model domain and source term

A first model counted for 405,533 elements. A hexahedral mesh was used and the meshing method was multizone in order to have a fine mesh near the source. An inflation layer was used to have a height of 0.12m for the first cell near the ground which is double the ground roughness in order to comply with Blocken conditions [37]. A more fined mesh counted 1,548,533 elements. The element size ranged from 1 mm near the source to 2 m far from it. Figure 26 and Figure 27 show the domain meshing for Prairie

grass domain. This geometry and meshing were used for all the simulations. It was found that the results were mesh independent for all the runs.

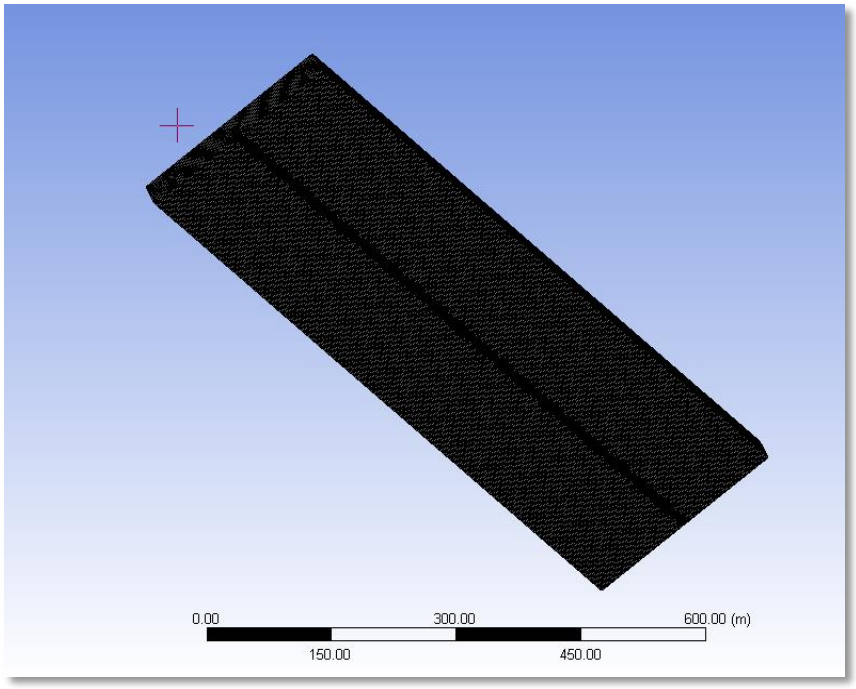

Figure 26: Bottom view of Prairie Grass domain mesh

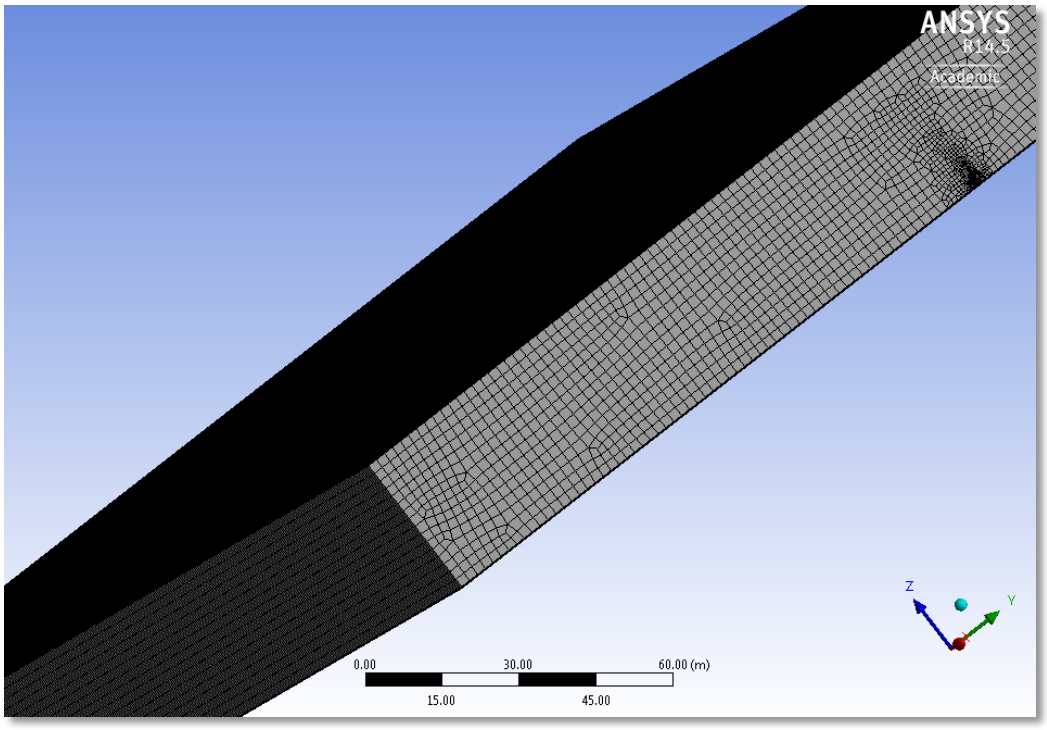

Figure 27: Side view of Prairie Grass model mesh

5.2.2 PG 17 Modeling

This run was chosen because it was performed at neutral stability class. In these ideal conditions, the heat flux from ground is equal to zero which simplifies the equations for Monin Obukhov length, velocity and turbulence. The conditions of this run are summarized in Table 6.

Table 6: PG 17 run details

Release rate (kgs^{-1})	0.0565
Release velocity (ms^{-1})	10.5
Stability class	D
Wind Speed (z=2)ms^{-1}	3.3
Ambient Temperature (K)	300.15
Monin Obhukov length (m)	∞
U*	0.239
T*	-
Z_0 (m)	0.006
Wind direction from North (degrees)	180

User defined functions (UDF) for velocity, temperature and turbulence were coded from the Monin Obukov theory according to the corresponding stability class. A 3D simulation using UDF functions for turbulence, velocity, temperature was conducted. A constant value for the source term or SO_2 release rate was specified in the model. For all runs, the roughness value specified in the model was calculated using Blocken Constraints as described in 4.2.3 and found to be equal to 0.06 m. Velocity, temperature and turbulence profiles were compared to Monin Obukhov theory and verified to be developed along the domain. A sensitivity analysis of the turbulence model was conducted in order to determine the performance of three main turbulence models: standard $k-\varepsilon$, realizable $k-\varepsilon$ and RSM models for the velocity, turbulent

kinetic energy, turbulent dissipation rate and turbulent viscosity profiles compared to Monin Obukhov theory. After that, the model concentration results were compared against experimental measurements of Prairie Grass tests.

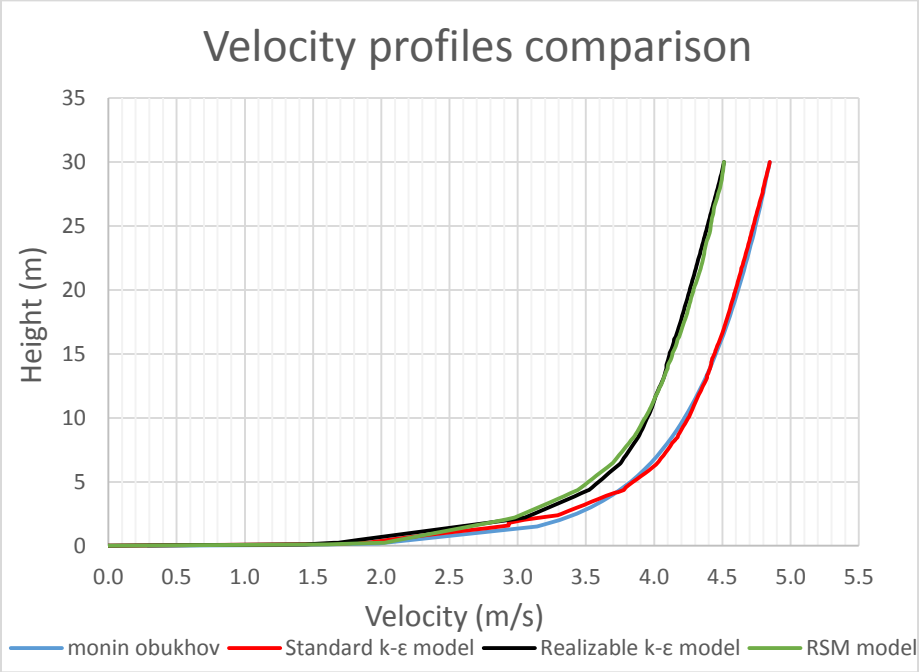

Figure 28: Comparison of velocity profiles for different turbulence models for PG 17

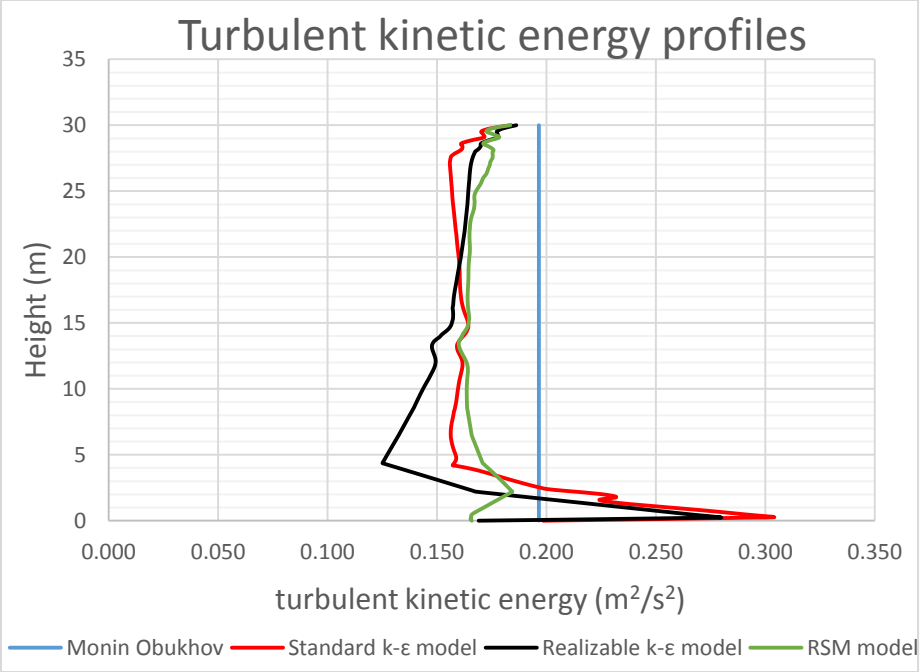

Figure 29: Comparison of turbulent kinetic energy profiles for different turbulence models for PG 17

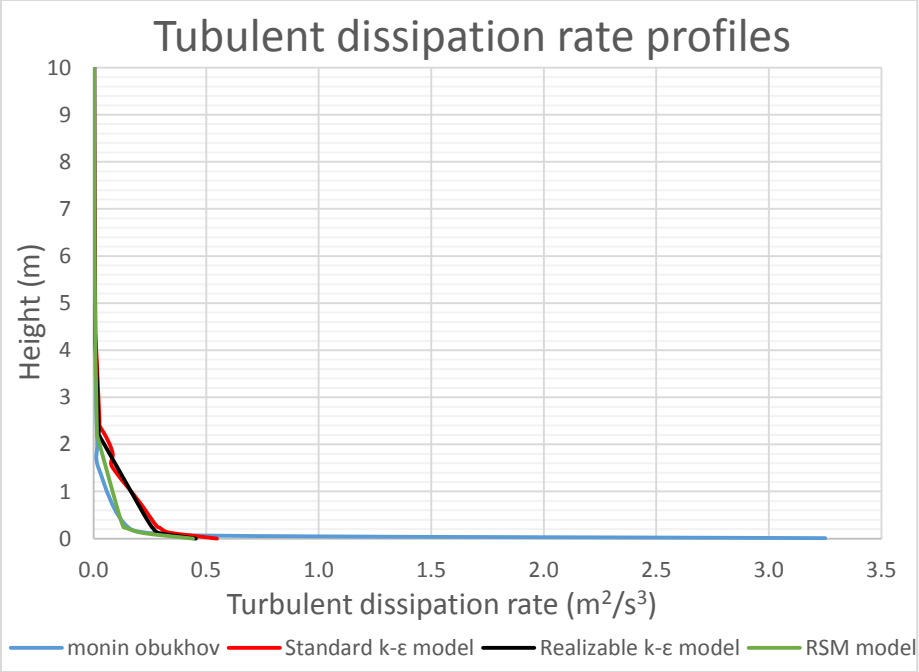

Figure 30: Comparison of turbulent dissipation rate profiles for different turbulence models for PG 17

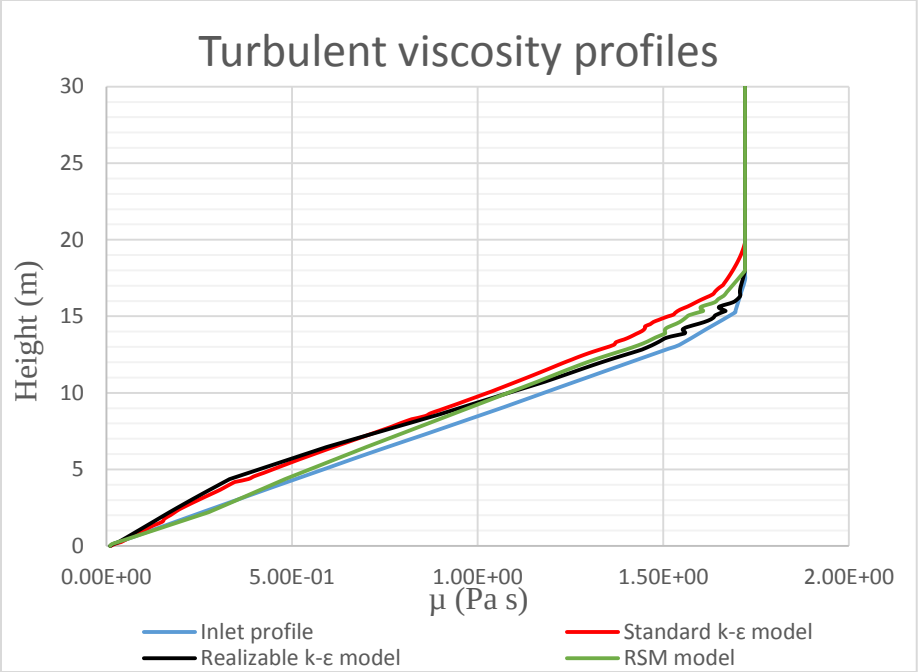

Figure 31: Comparison of turbulent viscosity profiles for different turbulence models for PG 17

Figure 28 shows the velocity profiles for different turbulence models compared to the profile from Monin Obukhov theory. The standard k-ε model shows an agreement with the Monin Obukhov theory. The realizable k-ε and RSM models show an equal deviation from the Monin Obukhov theory.

Figure 29 illustrates the turbulent kinetic energy for different turbulence models. There is a reduction of the turbulent kinetic energy with respect to Monin Obukhov theory for all the turbulence models. However, the RSM model provides the best results. Figure 30 shows that the RSM model provides a good description for the turbulent dissipation rate and other models show a small deviation at low heights.

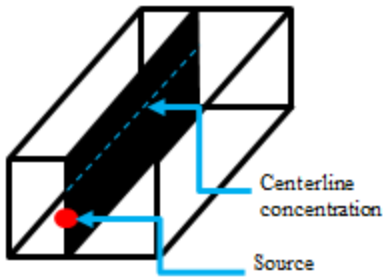

Figure 32: Location of centerline concentration

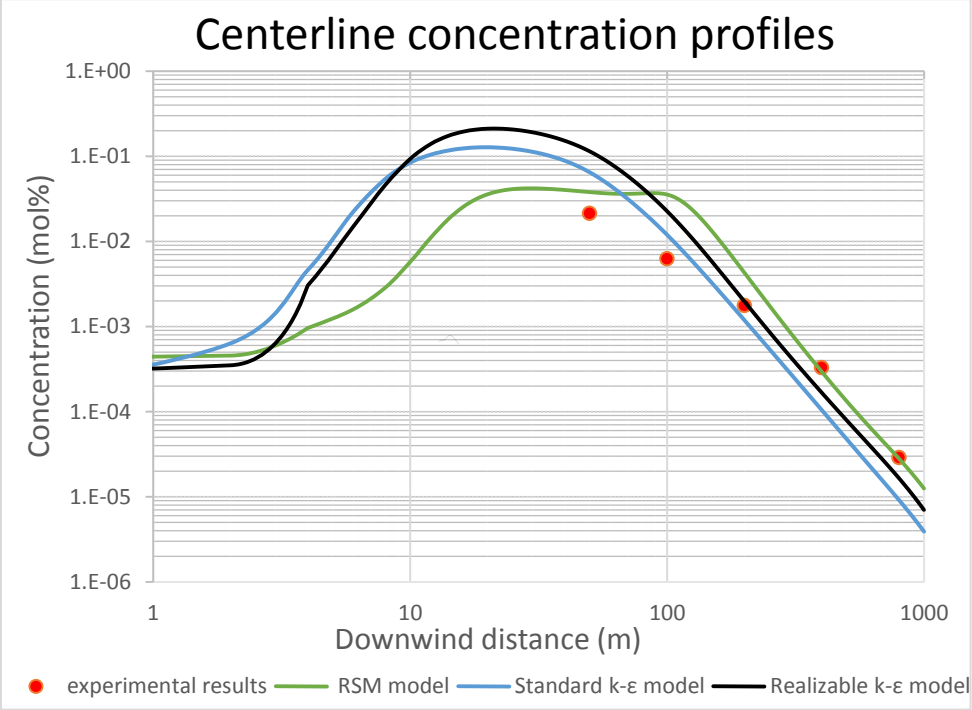

Figure 33: Comparison between centerline concentration results for the three turbulence models and experimental results

Note: Please refer to appendix for residual graphs for simulations of PG-17, 13 and 33 for the three turbulence models. The convergence criterion is 10^{-6} for continuity, velocity, energy, turbulence and mass fraction residuals.

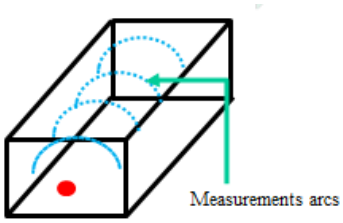

Figure 34: Concentration measurement arcs for all points

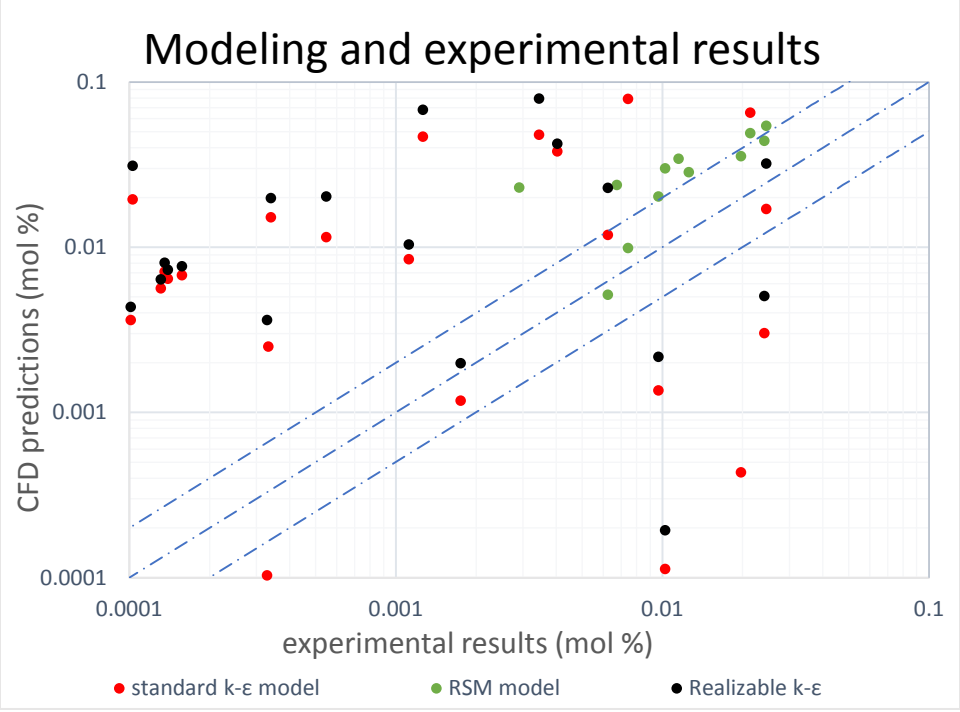

Figure 35: Comparison between experimental and modelling results using 2-factor method for three turbulence models

Table 7: PG-17 results summary

	Turbulence model	Centerline concentration	All points
Fractional Bias (FB)	Standard k-ε	-0.894	0.44
% points where error is lower than factor of 2	Standard k-ε	50	13.04
Fractional Bias (FB)	Realizable k-ε	-1.3	1.40
% points where error is lower than factor of 2	Realizable k-ε	60	8.7
Fractional Bias (FB)	RSM	-0.89	1.27
% points where error is lower than factor of 2	RSM	75	20.83

The comparison of turbulence models was summarized in Table 7 according to the fractional bias and percentage of points where the error is lower than a factor of 2. Fractional Bias values range between -2.0 for extreme underprediction to +2 for extreme overprediction. Values of FB equal to -0.67 are equivalent to underprediction by a factor of 2.Values of FB equal to +0.67 are equivalent to overprediction by a factor of 2. According to Table 7 and Figure 33 which shows simulations for centerline concentration of different turbulence models compared to experimental results, the RSM model provides the best results for the centerline concentration with a fractional bias value of -0.89 and 75%. When considering all concentration measurements in Figure 35, all models fail to predict the concentration accurately because the majority of points are outside the 2 factor range. This may be due to the randomness of atmospheric processes

especially wind speed and direction. These variations should be modeled in order to be able to make this comparison.

Relatively, the RSM model provides the best results for the number of points where the error is lower than factor of 2 compared to the standard k-ε and realizable k-ε models with 20% of points within the 2 factor range.

5.2.3 PG 13 Modeling

This run was chosen because it was performed for stable class stratification. In these conditions, the heat flux from air to ground is positive which makes the equations for Monin Obukhov length, velocity and turbulence more complex compared to neutral conditions. The conditions of this run are summarized in Table 8.

Table 8: PG-13 run details

Release rate (kgs^{-1})	0.0611
Release velocity (ms^{-1})	11.1
Stability class	F
Wind Speed (z=2)ms^{-1}	1.3
Ambient Temperature (K)	293.15
Monin Obhukov length (m)	9
U*	0.0789
T*	0.0491
Z_0 (m)	0.006
Wind direction from North (degrees)	190
Ground heat flux q_w (J/m^2s)	-4.76

The same approach for modelling used for PG-17 was done for PG-13. A sensitivity analysis of the turbulence model was conducted in order to determine the performance of three main turbulence models: standard k-ε, realizable k-ε and RSM models for the velocity, temperature, turbulent kinetic energy and dissipation rate profiles compared with Monin Obukhov theory. After that, the model concentration results were compared against experimental measurements during the Prairie Grass test.

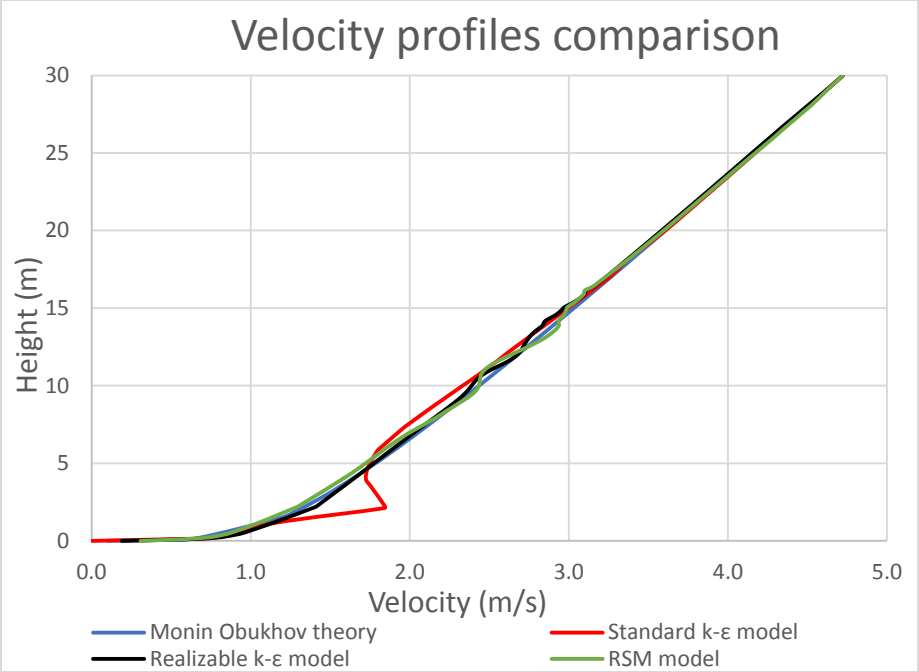

Figure 36: Comparison between velocity profiles using different turbulence models for PG-13

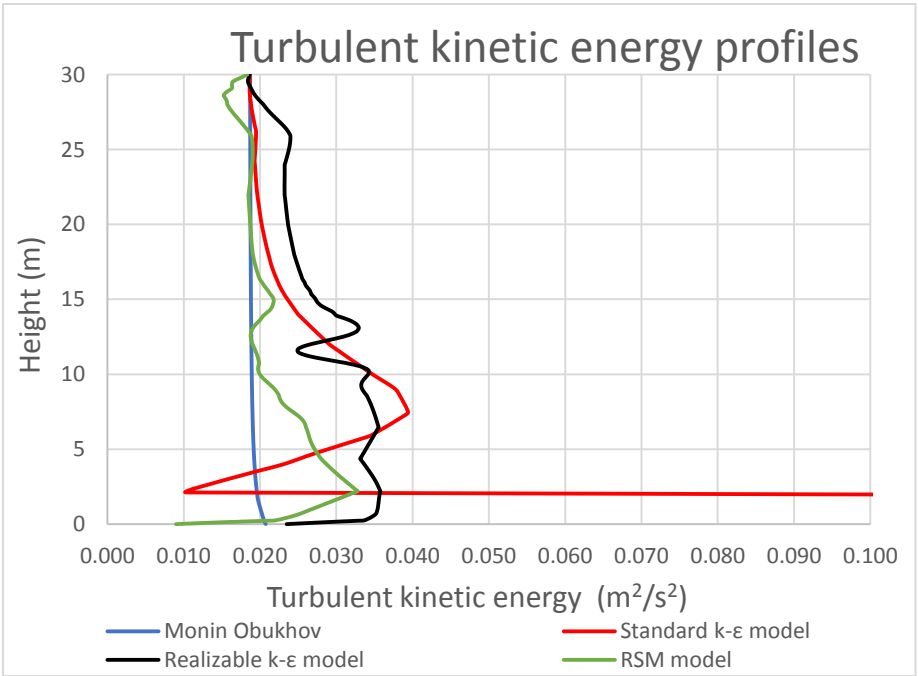

Figure 37: Comparison between turbulent kinetic energy profiles using different turbulence models for PG-13

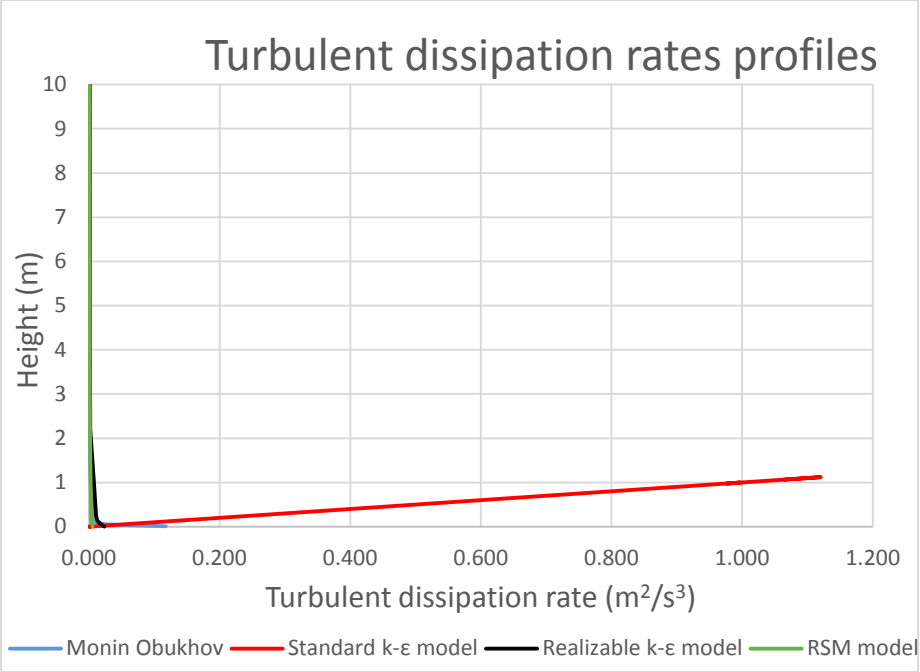

Figure 38: Comparison between turbulent dissipation rate profiles using different turbulence models for PG-13Standard k-ε model results

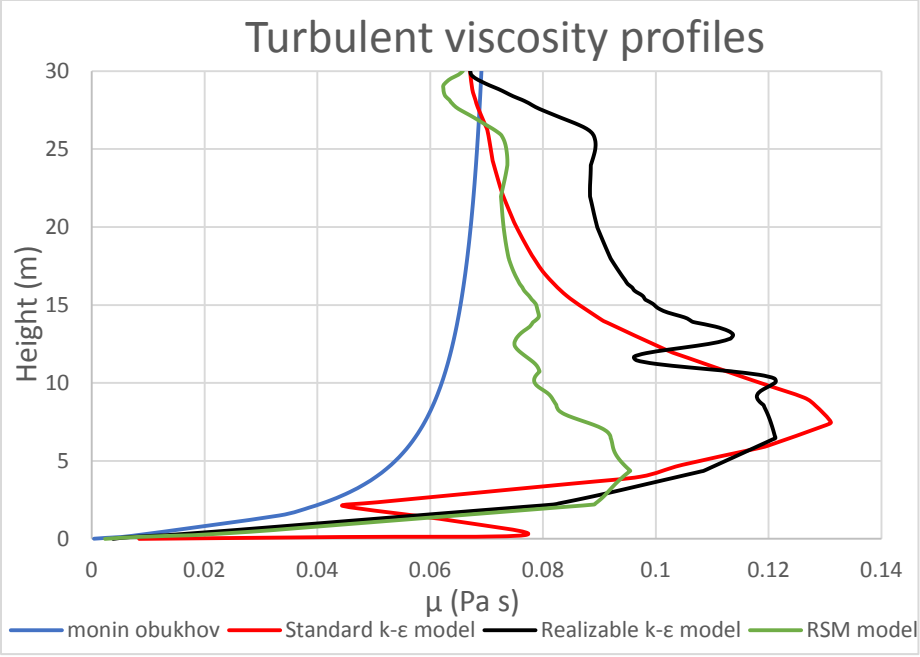

Figure 39: Comparison between turbulent viscosity profiles for different turbulence models

Figure 36 shows the velocity profiles for different turbulence models compared to the profile from Monin Obukhov theory. They show a good agreement with Monin Obukhov theory for different turbulence models. Figure 37 illustrates the turbulent kinetic energy for different turbulence models. The standard k-ε model shows a peak near the ground which may be attributed to the function wall effect. For the other models, the deviation from Monin Obukhov theory is reduced especially for the RSM model. There is a peak of turbulent kinetic energy for the all models but the highest deviation is observed for the standard k-ε model while the closest profile to Monin Obukhov theory is obtained using the RSM model. Figure 38 shows that all turbulence models provide a good description of the turbulent dissipation rate with respect to Monin Obukhov theory except for the standard k-ε where the turbulent dissipation rate is different from zero for heights less than 1 meter which is clearly not in accordance with the Monin Obukhov theory . According to Figure 39, all turbulence models show a deviation from the Monin Obukhov profile for turbulent viscosity especially in the first 10 m. This deviation is more pronounced for the standard k-ε model and the closest profile to the Monin Obukhov theory is the RSM model profile.

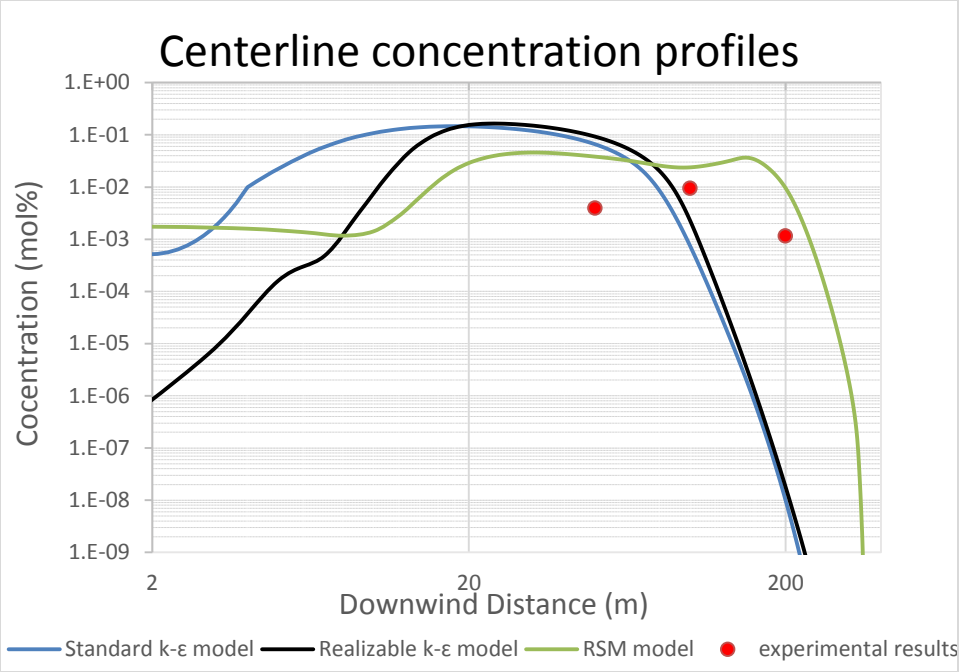

Figure 40: Comparison between centerline concentrations for three turbulence models and experimental data

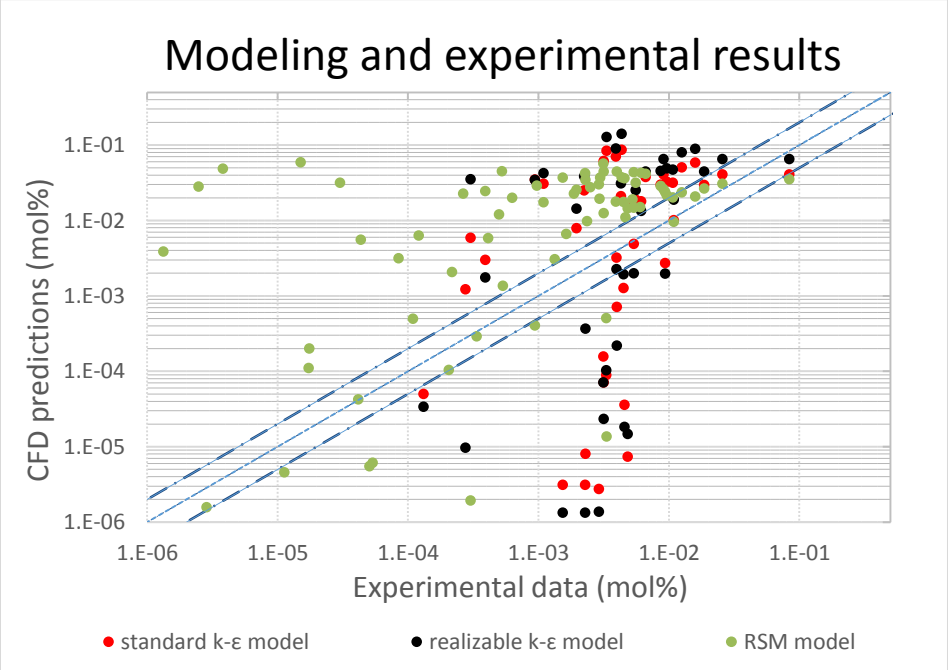

Figure 41: Comparison between turbulence models performances using a factor of 2 method for concentration modeling results as a function of experimental data

Table 9: PG-13 results summary

	Turbulence model	Centerline concentration	All points
Fractional Bias (FB)	Standard k-ε	1.48	0.85
% points where error is lower than factor of 2	Standard k-ε	33.33	18.18
Fractional Bias (FB)	Realizable k-ε	1.48	1.99
% points where error is lower than factor of 2	Realizable k-ε	33.33	12.5
Fractional Bias (FB)	RSM	1.33	-1.25
% points where error is lower than factor of 2	RSM	100	14.5

According to Figure 40 which shows the centerline concentration of different turbulence models compared to experimental data, the RSM model provides the best results for the centerline concentration. However, when considering all points where concentration measurements are available, as shown in Figure 41, all models don't provide accurate results for concentration predictions compared to experimental data. This may be due to the randomness of atmospheric processes especially wind speed and direction. These variations should be modeled in order to be able to make this comparison. In most cases, there is an overprediction of the experimental data measurements.

5.2.4 PG 33 Modeling

This run was chosen because it was performed at an unstable class. In this class, the heat flux from ground to air is positive which makes the equations for Monin Obukhov length, velocity and turbulence more complex compared to neutral and stable conditions. The conditions of this run are summarized in Table 10.

Table 10: PG-33 run details

Release rate (kgs^{-1})	0.0947
Release velocity (ms^{-1})	18.42
Stability class	C
Wind speed (z=2)ms^{-1}	6.9
Ambient temperature (K)	302.25
Monin Obhukov length (m)	-81
U*	0.5453
T*	-0.269
Z_0 (m)	0.006
Wind direction from North (degrees)	181
Ground heat flux q_w (J/m^2s)	180.74

The same approach used for PG-17 and 13 was done for PG-33. For simplification purposes, the equations of velocity, turbulence and temperature were entered as UDFs using the trend line function in Excel from the Monin Obukhov equations. The profiles were almost identical to Monin Obukhov equations. A sensitivity analysis of the turbulence model was conducted in order to determine the performance of three main turbulence models: standard $k-\varepsilon$, realizable $k-\varepsilon$ and RSM models for the velocity, temperature, turbulent kinetic energy and turbulent dissipation rate profiles

compared with Monin Obukhov theory. After that, the model concentration results were compared against experimental measurements during the Prairie Grass test.

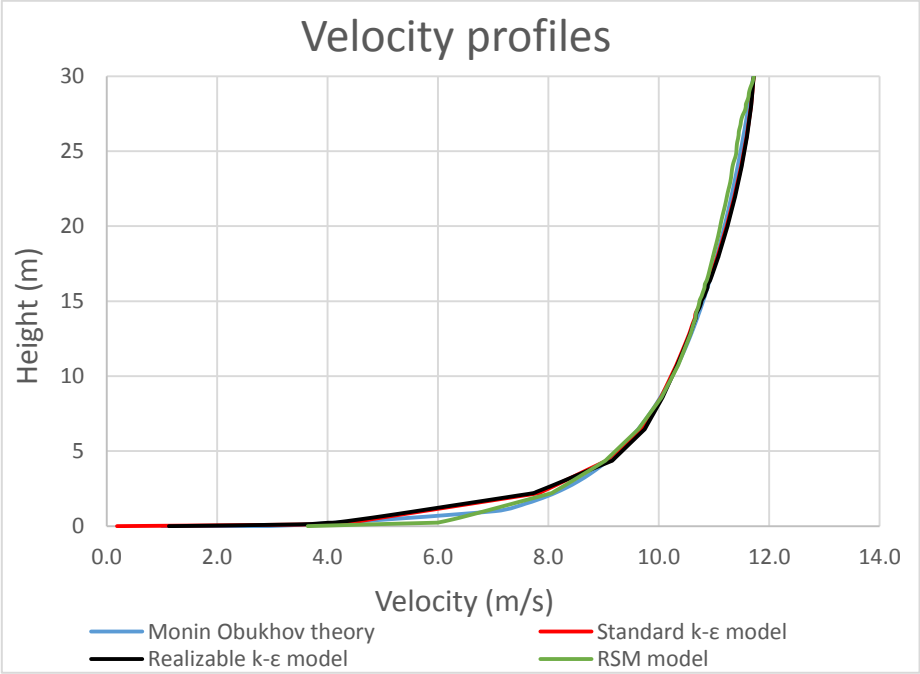

Figure 42: Comparison between velocity profiles using different turbulence models for PG-33

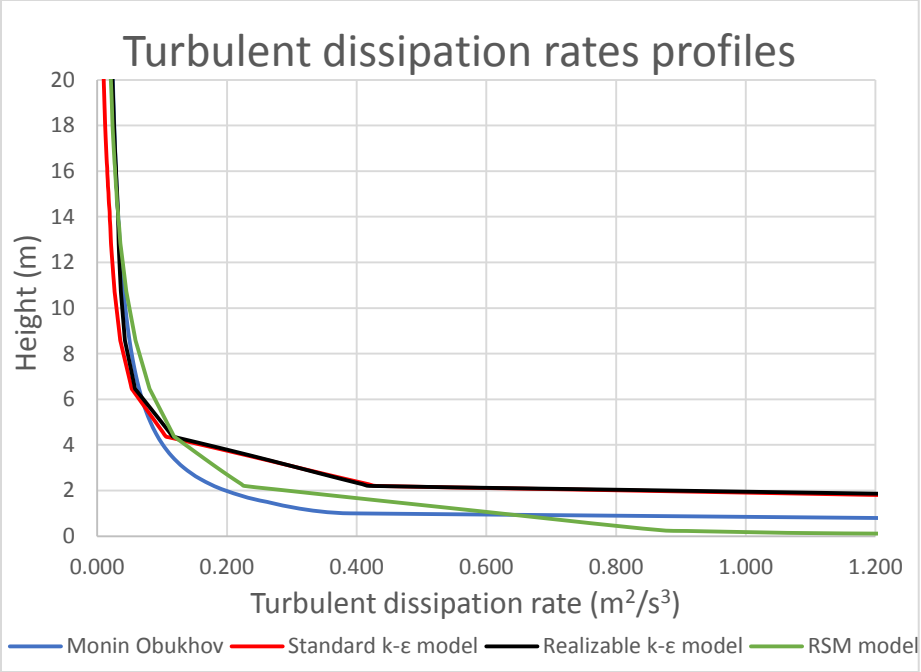

Figure 43: Comparison between turbulent dissipation profiles using different turbulence models for PG-33

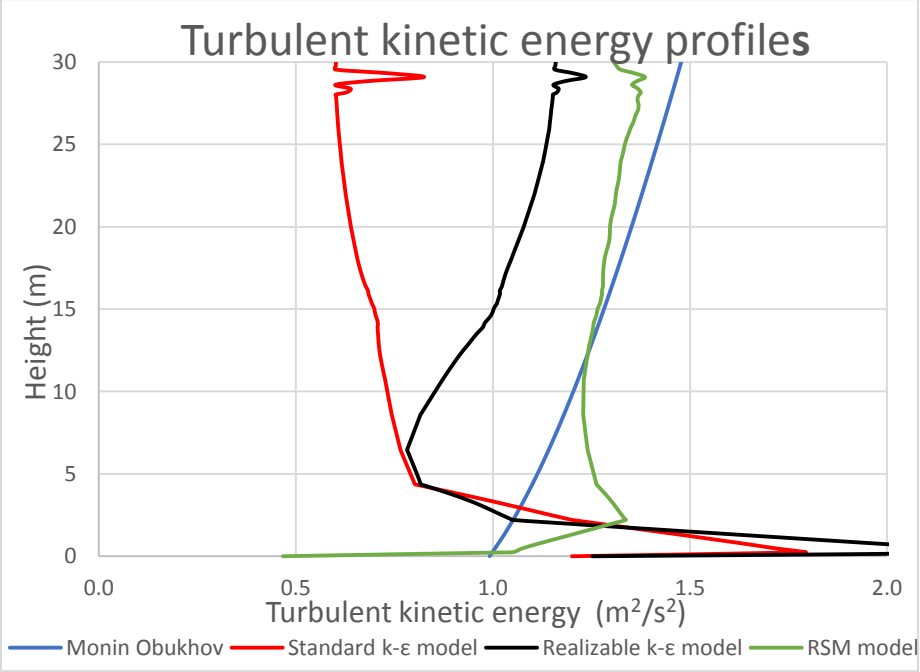

Figure 44: Comparison between velocity turbulent kinetic energy profiles using different turbulence models for PG-33

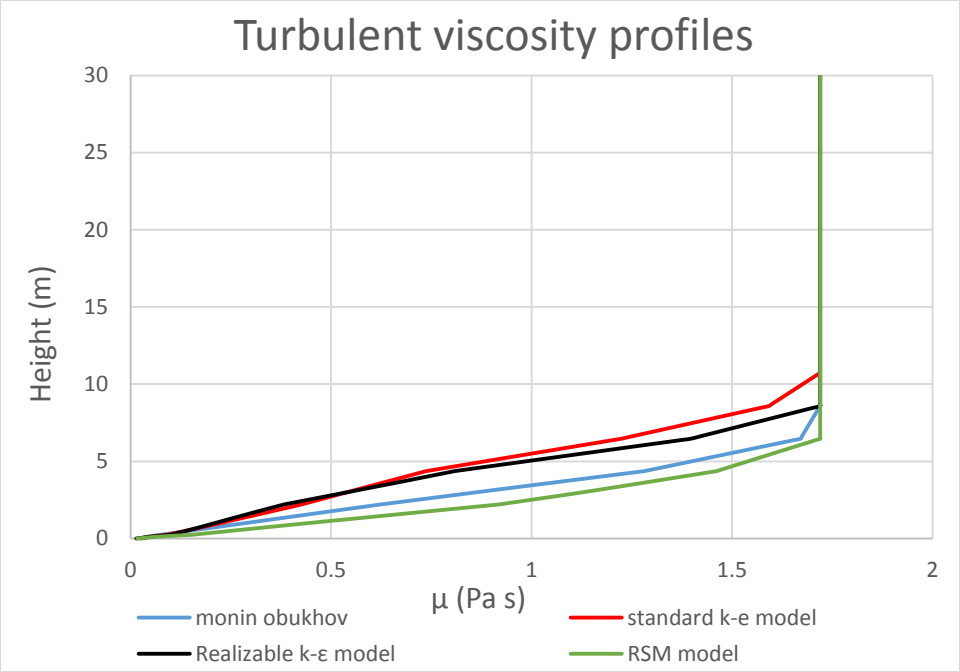

Figure 45: Comparison between turbulent viscosity profiles using different turbulence models for PG-33

Figure 42 shows the velocity profiles for different turbulence models compared to the profile from Monin Obukhov theory. The profiles show a good agreement with Monin Obukhov theory for different turbulence models.

Figure 44 illustrates the turbulent kinetic energy profiles of different turbulence models. There is a considerable underestimation of the turbulent kinetic energy for the standard and realizable k-ε models while the RSM model shows the closest profile to Monin Obukhov theory. Figure 43 shows that there is a deviation of turbulent dissipation rate at low heights for standard and realizable k-ε turbulence models at low heights and the RSM model's profile is the closest profile to Monin Obukhov theory. For the

turbulent viscosity, the profiles for the three turbulence models are similar and in accordance with Monin Obukhov profile as illustrated in Figure 45.

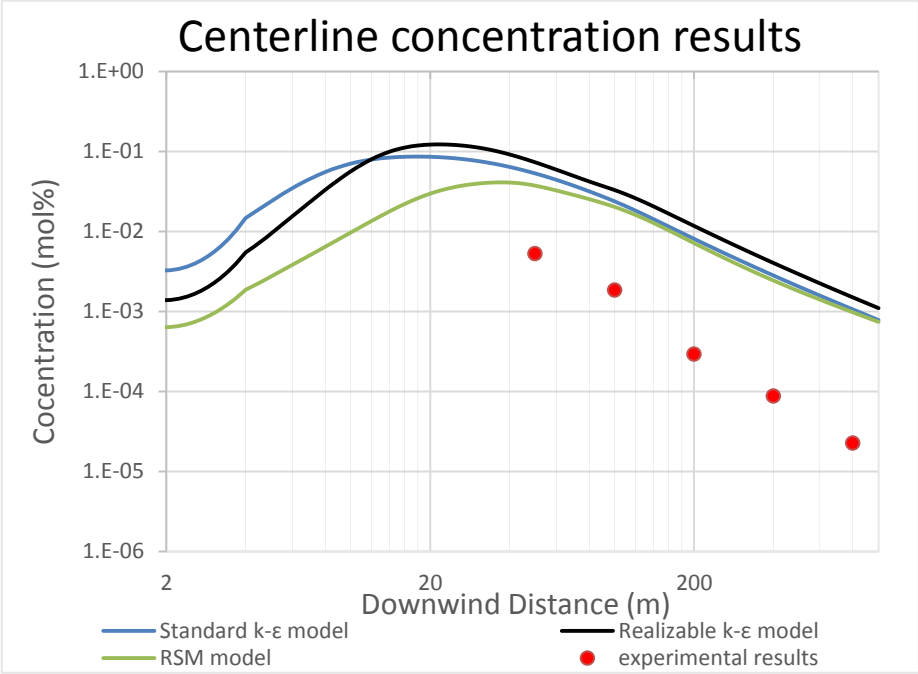

Figure 46: Comparison between centerline concentration using the three turbulence models and experimental data

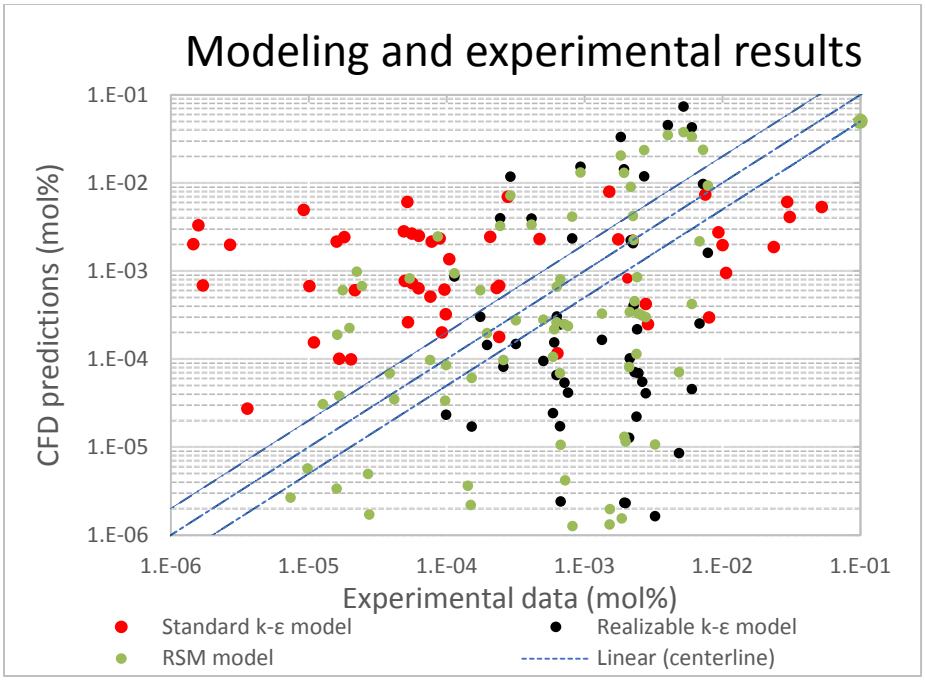

Figure 47: Comparison between the turbulence models performances as a function of experimental data using a factor of 2 method

Table 11: Summary of PG: 33 modeling results

	Turbulence model	Centerline concentration	All points
Fractional Bias (FB)	Standard k-ε	1.68	0.54
% points where error is lower than factor of 2	Standard k-ε	20	17.4
Fractional Bias (FB)	Realizable k-ε	1.77	0.82
% points where error is lower than factor of 2	Realizable k-ε	0	12.5
Fractional Bias (FB)	RSM	-1.59	0.75
% points where error is lower than factor of 2	RSM	40	26

According to Figure 46, all models show a similar overprediction of the centerline concentration. The used turbulence models doesn't account for eddies which are generated as a result of wind speed and direction variations with time. Their effect is more pronounced in the unstable classes. This results in underestimation of turbulence and as a result overprediction of downwind concentration.

When considering all points where concentration measurements are available, as shown in Figure 47, all models fail to predict the concentration accurately. This may be due to the randomness of atmospheric processes especially wind speed and direction. These variations should be modeled in order to be able to make this comparison.

5.2.5 TP-5 Modeling for Neutral Stability Class

After modeling of Prairie Grass tests, the modeling of the future LNG spill experiment in the LNG prop (TP-5) in RLESC was performed for neutral stability class. These experiments will be conducted by MKOPSC- Qatar in order to provide good quality data for validation for LNG dispersion and source term models.

The geometry consists of a small LNG pool (5m×6m×1.2m), trenches for water conduction and a building (classrooms). The model size in ANSYS was 131 m×132 m ×50 m as described in Figure 48. An automatic mesh was generated for the model as described in Figure 49. This mesh generated tetrahedral mesh for the whole domain. A sweep method and face sizing was done for the pool in order to have hexahedral fine mesh near the source. The roughness was estimated to be 0.01 m for plains covered with concrete. The model value for roughness was found to be 0.1 m. An inflation layer of 0.2 m was inserted so the first cell height is double roughness value in

order to fulfill Blocken requirements [32]. The mesh counted 1,575,847 elements. The atmospheric data for TP-5 are identical to PG-17 (neutral stability class) because wind data are not available yet. The used turbulence model is RSM. The release rate was estimated using PHAST assuming a steady state spill of 40 m^3 of LNG in the pit.

Table 12: Run details for TP-5

Release rate (kgs^{-1})	0.87
Release velocity (ms^{-1})	10.5
Stability class	D
Wind Speed (z=2)ms^{-1}	3.3
Ambient Temperature (K)	300.15
Monin Obhukov length (m)	∞
U*	0.239
T*	-
Z_0 (m)	0.1
Wind direction from North (degrees)	180

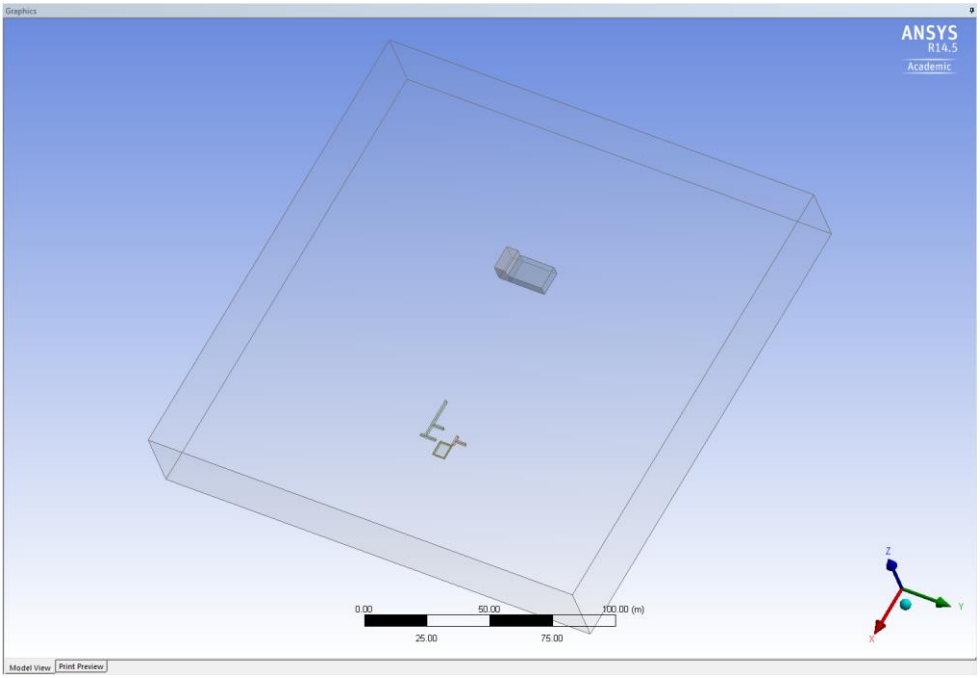

Figure 48: TP-5 geometry model in ANSYS

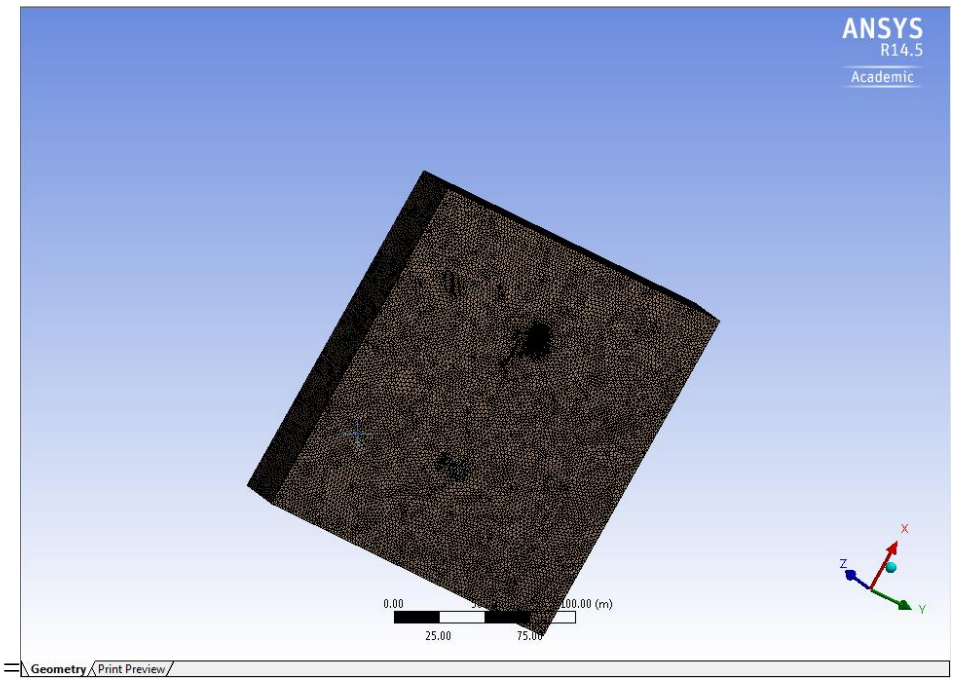

Figure 49: TP-5 meshed geometry in ANSYS

The results of the simulation for centerline concentration and concentration contour are illustrated in Figure 50 and Figure 51. These data will be used in order to prepare the LNG spill experiments. Figure 50 illustrates the Methane concentration contours corresponding to the ½ LFL (methane volumetric concentration of 2.5%). The flammable cloud generated from this spill will be close to the pool and its width will be only few meters.

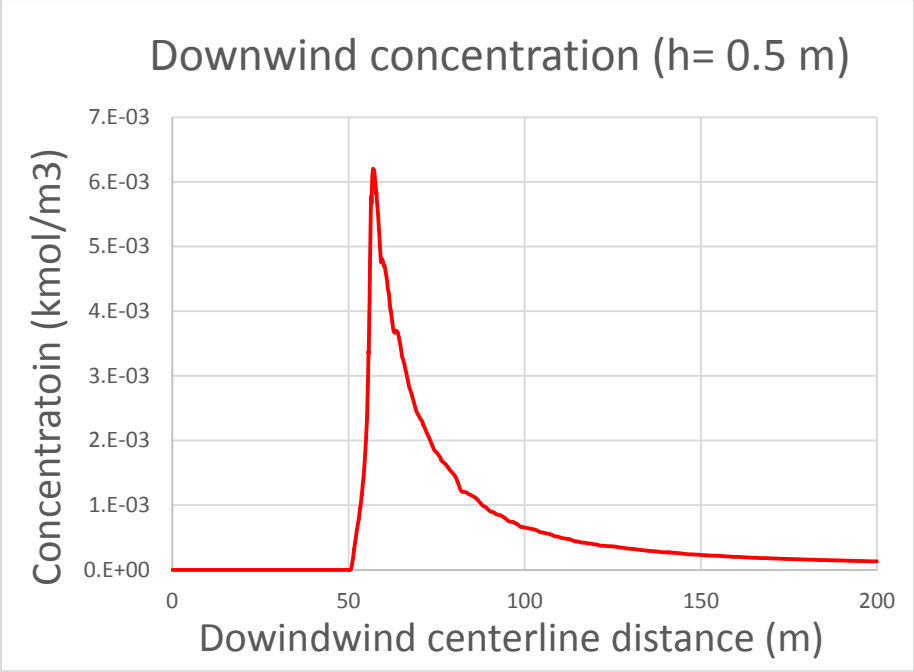

Figure 50: Downwind concentration for TP-5 model

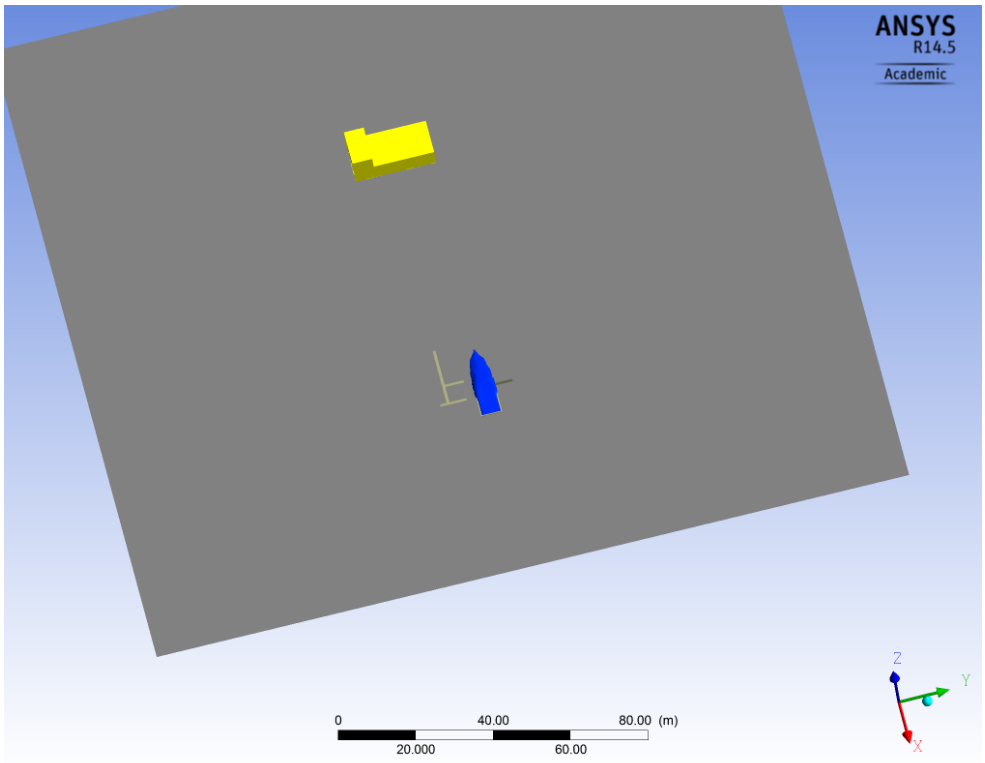

Figure 51: Methane concentration contours for TP-5 simulation

CHAPTER VI

CONCLUSION AND FUTURE WORK

Risk assessments of dense gas dispersion received a lot of attention in process safety because many severe incidents are associated with these releases.

A CFD model for atmospheric dispersion of dense gases for different stability classes was tested and compared against experimental data from three Prairie Grass tests (PG 13, 17 and 33). The comparison of the standard k-ε model performance for atmospheric modeling for three heights (30, 60 and 90 m) was performed in order to choose the domain size. After that, the model compared the performances of three turbulence models: standard k-ε, realizable k-ε and RSM models for atmospheric modeling with Monin Obukhov theory, centerline concentration and concentration measurements in different locations with experimental data. The last part consisted of modeling an LNG spill experiment which will be performed in TP-5 (LNG prop) in RLESC.

The comparison of the profiles of velocity, turbulent kinetic energy, turbulent dissipation rate and turbulent viscosity for the three stability classes at 3 different heights: 30m, 60m, 90m using standard k-ε model and Monin Obukhov theory suggests that the velocity and turbulence profiles do not depend on height. As a result, a minimum height of 30 m of all models will be sufficient and there is no need for larger computational domain if the objective is to focus on dense gas dispersion at low heights.

The comparison between the three turbulence models standard k-ε, realizable k-ε and RSM models with Monin Obukhov theory for atmospheric modelling suggests that the RSM model provides the closest results with respect to the Monin Obukhov theory. However, these results show a deviation for the Monin Obukhov theory especially for the turbulent kinetic energy. A possible solution of this deviation which was not considered in this work is the use of modified equations for turbulence. This needs a lot of effort and knowledge in ANSYS.

The results from the modeling of three sets of Prairie Grass experiments corresponding to neutral, stable and unstable classes suggest only a good agreement between the simulation and experimental results for the centerline concentration for the stable and neutral classes especially for the RSM model. For the unstable class (PG-33), the centerline concentration was over predicted mainly after 200 m downwind distance by all models. The modeling of dense gas dispersion for unstable classes should be investigated further in order to get better results. The used turbulence models don't account for eddies which are the result of wind speed and direction variations with time. This results in underestimation of turbulence and as a result overprediction of downwind concentration [21]. For the unstable class, a more sophisticated turbulence model such as Large Eddies Simulation (LES) which models larges eddies only using a filter approach may yield better results. However, this model may need much more execution time since it's computationally one order of magnitude higher than RANS models.

From the investigated models, it is advised to use the RSM model to obtain the best results. However, since the RSM model is less stable and requires initial guesses.

It's better to use the standard k-ε to get quick results with reasonable accuracy and from there use the RSM model to get the best results. This approach was suggested by Gavelli as well [25].

In this work, an attempt was made to compare model predictions with experimental concentrations at each location. Only centerline centration or highest concentrations was considered in literature for these experiments [21, 33].
Form this comparison, all three models were unable to predict the concentration measurements accurately which suggests that the error is not related to the choice of turbulence model. This may be due to several causes: The randomness of atmospheric processes. In fact, the wind direction variation during the experiment was not measured. The error was more pronounced for concentration measurements outside the release centerline which suggests that an uncertainty may be associated with the wind direction measurements. One CFD Software (FLACS) may provide better results because it models wind variation according to a sinusoidal function.

Also, concentration measurements during Prairie Grass experiments were performed using Midget Impingers. The error of this technique is quite high and may reach 10% according Prairie Grass data report [38]. Also, the source release rate was constant according to data but the report indicates that it may vary during the experiment [38].

Consequently, this model should be tested with other recent spill tests of cryogenic liquids such as Falcon and Burro which data should be more accurate than Prairie Grass tests or tests in TP-5 in RLESC which will be performed in future by

MKOPSC-Q. These tests will provide high quality data for model validation and will consist of spills of LN2 and LNG for different stability classes. The choice of Prairie Grass tests was done because it's one main experiment for model validations of dense gas dispersion for different stability classes. Also, previous work on atmospheric modeling and dispersion for few tests was done by Pontiggia and served for comparison between models. For a comprehensive model validation, different tests should be considered as well. However, this is beyond the scope of this work.

In addition, most of the work done on modeling of dense gas dispersion using CFD focused on comparing centerline concentration with experimental data. However, the obtained results indicate that the CFD model may describe only the centerline concentration accurately and it may give inaccurate results elsewhere. As a result, the CFD model should be able to predict the concentration in different locations accurately and not only the centerline concentration.

In the last part, the modeling of TP-5 spill test for neutral stability class was performed for the spill experiment which will be performed in the future. Only a comparison with the experimental data will indicate the performance of this model. During these experiments, it's advised to measure the wind variation and gas concentrations accurately to get high quality data. Also, the gas concentration should be measured in different locations and not only the release centerline. These experiments should be done for different stability classes in order to provide a benchmark for models validation.

REFERENCES

1. Scargiali F, Di Rienzo E, Ciofalo M, Grisafi F, Brucato A. Heavy Gas Dispersion Modelling Over a Topographically Complex Mesoscale. Process Saf. Environ. Prot. 2005;83(3):242-256. doi:10.1205/psep.04073.

2. Crowl D. Chemical Process Safety. (Goodwin B, ed.). Paul Boger Available at: http://ptgmedia.pearsoncmg.com/images/9780131382268/samplepages/0131382268.pdf.

3. Mokhatab S, Poe A, James G. Handbook of Natural Gas Transmission and Processing.; :1-28. Available at: http://www.sciencedirect.com/science/book/9780750677769.

4. BP Statistical Review of World Energy June 2011.; 2011:45. Available at: www.bp.com/statisticalreview.

5. Qatar. www.eia.gov/. U.S. Energy Information Admninstration, 30 Jan. 2014. Web. 1 Jan. 2015. Available at: http://www.eia.gov/countries/cab.cfm?fips=qa.

6. Obeid J. Bursting the Bubble: Shale Gas Impact on Natural Gas Exports in GCC. energy Collect. Available at: http://theenergycollective.com/jessica-obeid/2155081/bursting-bubble-shale-gas-impact-natural-gas-exports-gcc.

7. Qi R. Liquified Natural Gas (LNG) Vapor Dispersion Modeling with Computational Fluid Dynamics Codes. 2011;(August). Available at: http://pscfiles.tamu.edu/library/center-publications/theses-and-dissertations/QI-DISSERTATION.pdf.

8. Luketa-Hanlin A. A review of large-scale LNG spills: Experiments and modeling. J. Hazard. Mater. 2006;132(2-3):119-140. doi:10.1016/j.jhazmat.2005.10.008.

9. Mokhatab S, Mak J, Jaleel V. Handbook of Liquefied Natural Gas. USA Gulf Publ. Company, 2013. 2015;(January):2013-2016.

10. Pitblado R, Baik J, Hughes G, Ferro C, Shaw S. Consequences of liquefied natural gas marine incidents. Process Saf. Prog. 2005;24(2):108-114. doi:10.1002/prs.10073.

11. Stansfield J. Video of collision between Hanjin Italy and Al-Gharrafa. 2014. Available at: http://www.vesselfinder.com/news/1737-VIDEO-of-Collision-between-Hanjin-Italy-and-Al-Gharrafa. Accessed September 17, 2014.

12. Cormier B, Qi R, Yun G, Zhang Y, Mannan S. Application of computational fluid dynamics for LNG vapor dispersion modeling: A study of key parameters. J. Loss Prev. Process Ind. 2009;22(3):332-352. doi:10.1016/j.jlp.2008.12.004.

13. Koopman R, Ermak D. Lessons learned from LNG safety research. J. Hazard. Mater. 2007;140(3):412-428. doi:10.1016/j.jhazmat.2006.10.042.

14. Hankin R. Heavy gas dispersion: integral models and shallow layer models. J. Hazard. Mater. 2003;103(1-2):1-10. doi:10.1016/S0304-3894(03)00219-X.

15. Ivings M, Jagger S, Lea C. Evaluating Vapor Dispersion Models for Safety Analysis of LNG Facilities. (April 2007). Available at: http://www.nfpa.org/~/media/Files/Research/Research Foundation/Research Foundation reports/Hazardous materials/lngvapordispersionmodel.pdf.

16. Luketa-Hanlin A, Koopman R, Ermak D. On the application of computational fluid dynamics codes for liquefied natural gas dispersion. J. Hazard. Mater. 2007;140(3):504-17. doi:10.1016/j.jhazmat.2006.10.023.

17. Coldrick S, Lea C, Ivings M. Validation Database for Evaluating Vapor Dispersion Models for Safety Analysis of LNG Facilities.; 2009:35. Available at: http://www.nfpa.org/foundation.

18. Hanna S, Hansen O, Dharmavaram S. FLACS CFD air quality model performance evaluation with Kit Fox, MUST, Prairie Grass, and EMU observations. Atmos. Environ. 2004;38(28):4675-4687. doi:10.1016/j.atmosenv.2004.05.041.

19. Sklavounos S, Rigas F. Simulation of Coyote series trials—Part I: Chem. Eng. Sci. 2006;61(5):1434-1443. doi:10.1016/j.ces.2005.08.042.

20. ANSYS FLUENT 12.0 User Guide. www.users.ugent.be/. ANSYS, Inc, Apr. 2009. Web. 1 Jan. 2015. <http://users.ugent.be/~mvbelleg/flug-12-0.pdf>.

21. Hanna S, Hansen O, Dharmavaram S. FLACS CFD air quality model performance evaluation with Kit Fox, MUST, Prairie Grass, and EMU observations. Atmos. Environ. 2004;38(28):4675-4687. doi:10.1016/j.atmosenv.2004.05.041.

22. Pyros S, Rigas F. Simulation of Coyote series trials—Part I: CFD estimation of non -isothermal LNG releases and comparison with box-models predictions. Chem. Eng. Sci. 2006;61(5):1434-1443. doi:10.1016/j.ces.2005.08.042.

23. Giannissi S, Venetsanos G, Markatos N, Bartzis J. Numerical simulation of LNG dispersion under two-phase release conditions. J. Loss Prev. Process Ind. 2013;26(1):245-254. doi:10.1016/j.jlp.2012.11.010.

24. Sklavounos S, Rigas F. Validation of turbulence models in heavy gas dispersion over obstacles. J. Hazard. Mater. 2004;108(1-2):9-20. doi:10.1016/j.jhazmat.2004.01.005.

25. Gavelli F, Bullister E, Kytomaa H. Application of CFD (Fluent) to LNG spills into geometrically complex environments. J. Hazard. Mater. 2008;159(1, SI):158-168. doi:10.1016/j.jhazmat.2008.02.037.

26. Tauseef S, Rashtchian D, Abbasi S. CFD-based simulation of dense gas dispersion in presence of obstacles. J. Loss Prev. Process Ind. 2011;24(4):371-376. doi:10.1016/j.jlp.2011.01.014.

27. Alinot C, Masson C. k-ε Model for the Atmospheric Boundary Layer Under Various Thermal Stratifications. J. Sol. Energy Eng. 2005;127(4):438. doi:10.1115/1.2035704.

28. Richards P. Appropriate boundary conditions for computational wind engineering models using the k-E turbulence model u. 1993;47:145-153.

29. Parente A, Gorlé C, Van Beeck J, Benocci C. Improved k–ε model and wall function formulation for the RANS simulation of ABL flows. J. Wind Eng. Ind. Aerodyn. 2011;99(4):267-278. doi:10.1016/j.jweia.2010.12.017.

30. Pieterse J, Harms T. CFD investigation of the atmospheric boundary layer under different thermal stability conditions. J. Wind Eng. Ind. Aerodyn. 2013;121:82-97. doi:10.1016/j.jweia.2013.07.014.

31. Gavelli F, Bullister E, Kytomaa H. Application of CFD (Fluent) to LNG spills into geometrically complex environments. J. Hazard. Mater. 2008;159(1, SI):158-168. doi:10.1016/j.jhazmat.2008.02.037.

32. Sun B, Utikar R, Pareek V, Guo K. Computational fluid dynamics analysis of liquefied natural gas dispersion for risk assessment strategies. 2013;26. doi:10.1016/j.jlp.2012.10.002.

33. Pontiggia M, Derudi M, Busini V, Rota R. Hazardous gas dispersion: A CFD Model Accounting for Atmospheric Stability Classes. J. Hazard. Mater. 2009;171(1-3):739-47. doi:10.1016/j.jhazmat.2009.06.064.

34. John L. Woodward R. LNG Risk Based Safety Modeling and Consequence Analysis. New Jersey: WILEY; 2010:392.

35. Ivings M, Lea C, Webber D, Jagger S, Coldrick S. A Protocol for the Evaluation of LNG Vapour Dispersion Models. J. Loss Prev. Process Ind. 2013;26(1):153-163. doi:10.1016/j.jlp.2012.10.005.

36. Turbulence Modelling. Available at: http://www.ansys.com/staticassets/ANSYS/Conference/Confidence/San Jose/Downloads/turbulence-summary-4.pdf. Accessed October 6, 2014.

37. Blocken B, Stathopoulos T, Carmeliet J. CFD Simulation of the Atmospheric Boundary Layer: Wall Function Problems. Atmos. Environ. 2007;41(2):238-252. doi:10.1016/j.atmosenv.2006.08.019.

38. Barad M. Project Prairie Grass, a Field Program in Diffusion. 1958;I and II. Available at: http://scholar.google.com/scholar?hl=en&btnG=Search&q=intitle:Project+Prairie+Grass.+A+field+program+in+diffusion#0\nhttp://oai.dtic.mil/oai/oai?verb=getRecord&metadataPrefix=html&identifier=AD0152573.

APPENDIX

Turbulence Modeling

The velocity fluctuations are usually very small in scale and frequency. They are computationally very expensive to simulate so they may be time-averaged or filtered in order to remove small scale fluctuations.

Direct Numerical Simulations (DNS) solves the exact Navier-Stokes equations and does not require empirical formulas and approximations. It simulates the turbulence (small and large eddies). As a result, it needs enormous computational resources. Its application to engineering problems is not practical because of its requirements [20].

Large Eddy Simulation (LES) simulates only large eddies and models small eddies based on filtering approach. This model assumes that large eddies transport momentum, energy and other scalars and small eddies are usually isotropic. LES lies between DNS and RANS in terms of computational requirements (RANS and LES). Its use requires the use of supercomputers. However, its use for industrial complex problems is very demanding computationally and it is orders of magnitude higher than RANS models requirements. The use of LES for better results is mainly in the following areas: flows with large separation zones (airfoils/wings, flow past buildings, flows with swirls…) [16,20]. LES and DNS can perform transient simulations only.

The most used model for steady state simulations is RANS. In many applications, steady state simulations are preferred because they need shorter time and time averaged values are of interest for consequence modeling.

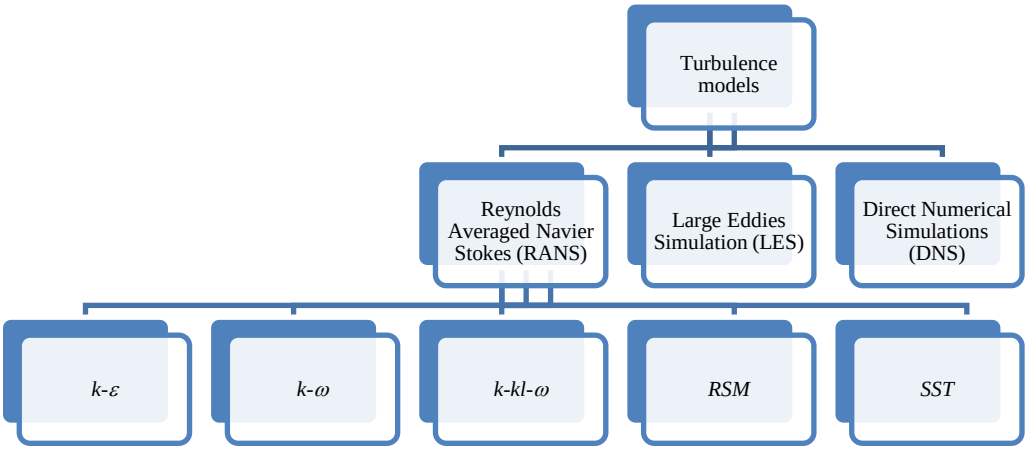

Figure 52: Classification of turbulence models used in CFD

Reynolds Averaged Navier Stokes (RANS) models

Reynolds Averaged Navier Stokes (RANS) equations describe the transport of flow quantities and model turbulence which reduces significantly the computational requirements. The RANS equations have the same form as instantaneous Navier-Stokes equations but the variables are time averaged and additional terms are added to account for turbulence effects [16].

For velocity components:

$$u_i = \overline{u_i} + u_i' \qquad \text{Equation 27}$$

For pressure and other scalars:

$$\phi = \bar{\phi} + \phi' \qquad \text{Equation 28}$$

These expressions are substituted in the instantaneous continuity and momentum equations of Navier Stokes. After that, they are time averaged to obtain the ensemble averaged momentum equations (Equation 36,

Equation 37) [20]:

$$\frac{\partial \rho}{\partial t} + \frac{\partial}{\partial x_i}(\rho u_i) = 0 \qquad \text{Equation 29}$$

$$\frac{\partial}{\partial t}(\rho u_i) + \frac{\partial}{\partial x_j}(\rho u_i u_j) = -\frac{\partial p}{\partial x_i} + \frac{\partial}{\partial x_j}[\mu(\frac{\partial u_i}{\partial x_j} + \frac{\partial u_j}{\partial x_i} - \frac{2}{3}\delta_{ij}\frac{\partial u_l}{\partial x_l})] + \frac{\partial}{\partial x_j}(-\rho\overline{u_i' u_j'}) \qquad \text{Equation 30}$$

In Equation 30, the term $-\rho\overline{u_i' u_j'}$ represents the Reynolds stresses. The Boussineq approximation is used in order to relate Reynolds stresses to mean velocity gradients:

$$-\rho\overline{u_i' u_j'} = \mu_t(\frac{\partial u_i}{\partial x_j} + \frac{\partial u_j}{\partial x_i}) - \frac{2}{3}(\rho k + \mu_t \frac{\partial u_k}{\partial x_k})\delta_{ij} \qquad \text{Equation 31}$$

This approach yields the turbulent viscosity μ_T (Equation 34) at a low computational cost. However, it assumes μ_T to be isotropic which is not accurate. On the other hand, the Reynolds Stress models (RSM) are founded on solving the transport equations including all Reynolds Stress components of Reynolds stress tensor and dissipation rate [20].

Standard k - ε Model

The $k-\varepsilon$ model involves two transport equations for turbulent kinetic energy k and turbulent dissipation rate ε as follows:

$$\frac{\partial(\rho k)}{\partial t}+\frac{\partial}{\partial x_i}\nabla\cdot(\rho k u_i)=\frac{\partial}{\partial x_j}[(\mu+\frac{\mu_T}{\sigma_k})\frac{\partial k}{\partial x_j}]+G_k+G_b-\rho\varepsilon-Y_M \qquad \text{Equation 32}$$

$$\frac{\partial(\rho\varepsilon)}{\partial t}+\frac{\partial}{\partial x_i}(\rho\varepsilon u_i)=\frac{\partial}{\partial x_j}[(\mu+\frac{\mu_T}{\sigma_\varepsilon})\frac{\partial\varepsilon}{\partial x_j}]+C_{\varepsilon 1}\frac{\varepsilon}{k}(G_k+C_{\varepsilon 3}G_b)-C_{\varepsilon 2}\rho\frac{\varepsilon^2}{k} \qquad \text{Equation 33}$$

The turbulent viscosity μ_T is calculated by combining k and ε as follows:

$$\mu_T=\rho C_\mu\frac{k^2}{\varepsilon} \qquad \text{Equation 34}$$

C_μ is an empirical constant defined in FLUENT as in Table 13:

Table 13: $k-\varepsilon$ - model constants

$C_{\varepsilon 1}$	$C_{\varepsilon 2}$	$C_{\varepsilon 3}$	σ_k	σ_ε	C_μ
1.44	1.92	1	1	1.3	0.09

$$G_k=-\rho\overline{u_i'u_j'}\frac{\partial u_j}{\partial x_i} \qquad \text{Equation 35}$$

$$G_b=\beta g_i\frac{\mu_T}{\mathrm{Pr}_t}\frac{\partial T}{\partial x_i} \qquad \text{Equation 36}$$

Realizable k-ε Model

The realizable k-ε model differs from the standard k-ε model in the following:

New eddy viscosity equation for Cμ (Equation 37).

Different equation for dissipation rate ε based on the dynamic equation of the mean square vorticity fluctuation.

$$C_{\mu} = \frac{1}{A_0 + A_s \frac{kU^*}{\varepsilon}}$$ Equation 37

$$\frac{\partial(\rho\varepsilon)}{\partial t} + \frac{\partial}{\partial x_i}(\rho\varepsilon u_i) = \frac{\partial}{\partial x_j}[(\mu + \frac{\mu_T}{\sigma_\varepsilon})\frac{\partial\varepsilon}{\partial x_j}] + \rho C_1 S\varepsilon - \rho C_2 \frac{\varepsilon^2}{k + \sqrt{\nu\varepsilon}} - C_{\varepsilon 1}\rho\frac{\varepsilon C_{3\varepsilon} G_b + S_\varepsilon}{k}$$ Equation 38

$$C_1 = \max[0.43, \frac{\eta}{\eta + 5}]$$ Equation 39

$$\eta = S\frac{k}{\varepsilon}$$ Equation 40

$$S = \sqrt{2S_{ij}S_{ij}}$$ Equation 41

Reynolds Stress Model (RSM)

The Reynolds stress model (RSM) solves the transport equations for the Reynolds stresses with a dissipation rate equation. The RSM model should yield better results for complex flows compared to two equation models because it accounts for effects of streamline curvature, rotation and change in strain rate. The Reynolds stresses transport equations are obtained by taking moments of the exact momentum equation.

The exact transport equation for the Reynolds stresses transport is as follows:

$$\underbrace{\frac{\partial}{\partial t}(\rho\overline{u_i'u_j'})}_{(1)} + \underbrace{\frac{\partial}{\partial x_k}(\rho u_k \overline{u_i'u_j'})}_{(2)} =$$
$$\underbrace{-\frac{\partial}{\partial x_k}[\rho u_i'u_j'\overline{u_k'} + \overline{p(\delta_{kj}u_i' + \delta_{ik}u_j'}]}_{(3)} +$$
$$\underbrace{\frac{\partial}{\partial x_k}[\mu\frac{\partial}{\partial x_k}(\overline{u_i'u_j'}]}_{(4)} -$$
$$\underbrace{\rho(u_i'u_k'\frac{\partial u_j}{\partial x_k} + \overline{u_j'u_k'}\frac{\partial u_i}{\partial x_k})}_{(5)} - \underbrace{\rho\beta(g_i\overline{u_j'\theta} + g_j\overline{u_i'\theta})}_{(6)} +$$
$$\underbrace{\overline{p(\frac{\partial u_i'}{\partial x_j} + \frac{\partial u_j'}{\partial x_i})}}_{(7)} - \underbrace{2\mu\overline{\frac{\partial u_i'}{\partial x_k}\frac{\partial u_j'}{\partial x_k}}}_{(8)}$$
$$\underbrace{-2\rho\Omega_k(u_j'u_m'\varepsilon_{jkm})}_{(9)} + \underbrace{S_{user}}_{(10)} \qquad \text{Equation 42}$$

Where:

(1): Local time derivative

(2): C_{ij} convection

(3): $D_{T,ij}$ Turbulent Diffusion

(4): $D_{L,ij}$ Molecular Diffusion

(5): P_{ij} Stress Production

(6): G_{ij} buoyancy production

(7): φ_{ij} Pressure Strain

(8): ε_{ij} Dissipation

(9): F_{ij} Production by system rotation

(10): S_{user} User defined source term

From these various terms, $D_{T,ij}$, $G_{i,j}$, ϕ_{ij}, and ε_{ij} require modeling to close the equations :

$$D_{T,ij} = \frac{\partial}{\partial x_k}\left(\frac{\mu_T}{\sigma_k}\frac{\partial \overline{u_i' u_j'}}{\partial x_k}\right)$$ Equation 43

$$\phi_{ij} = \phi_{ij,1} + \phi_{ij,2} + \phi_{ij,\omega}$$ Equation 44

$$\frac{\partial}{\partial t}(\rho k) + \frac{\partial}{\partial x_i}(\rho k u_i) = \frac{\partial}{\partial x_j}\left[(\mu + \frac{\mu_T}{\sigma_k})\frac{\partial k}{\partial x_j}\right] + \frac{1}{2}(P_{ii} + G_{ii}) - \rho\varepsilon(1 + M_t^2) + S_k$$ Equation 45

$$\frac{\partial}{\partial t}(\rho \varepsilon) + \frac{\partial}{\partial x_i}(\rho \varepsilon u_i) = \frac{\partial}{\partial x_j}\left[(\mu + \frac{\mu_T}{\sigma_k})\frac{\partial \varepsilon}{\partial x_j}\right] + \frac{1}{2}(P_{ii} + G_{ii}) - C_{\varepsilon 2}\rho\frac{\varepsilon^2}{k} S_\varepsilon$$ Equation 46

More details about each term calculation of these equations may be found in FLUENT Manual [20].

User Defined functions for CFD model simulations

PG-17 Model

```
#include "udf.h"
#define UMEAN 0.239
#define CMU 0.09
#define VKC 0.42
#define h 0.006
/*profile for kinetic energy*/
DEFINE_PROFILE(k_profile,thread,position)
{
real z, x[ND_ND],knw;
face_t f;
begin_f_loop(f,thread)
{
F_CENTROID(x,f,thread);
z = x[2];
F_PROFILE(f,thread,position)=pow(UMEAN,2.)/(sqrt(CMU));
}
end_f_loop(f,thread)
}
/* profile for dissipation rate */
DEFINE_PROFILE(dissip_profile,thread,position)
```

```
{
real z, x[ND_ND], kay;
face_t f;
begin_f_loop(f,thread);
{
F_CENTROID(x,f,thread);
z = x[2];
F_PROFILE(f,thread,position)=pow(UMEAN,3.)/(VKC*z);
}
end_f_loop(f,t)
}
DEFINE_PROFILE(x_velocity,thread,position)
{
real z, x[ND_ND];
face_t f;
begin_f_loop(f,thread);
{
F_CENTROID(x,f,thread);
z=x[2];
F_PROFILE(f,thread,position)=(UMEAN/VKC)*(double)log((double)(z/h));
}
end_f_loop(f,thread)
```

PG-13 Model

```
#include "udf.h"

#define UMEAN 0.0789

#define CMU 0.09

#define VKC 0.42

#define h 0.006

#define L 9.02

#define TW 293.18

#define g 9.81

#define CP 1005

#define TMEAN 0.0491

/*profile for kinetic energy*/

DEFINE_PROFILE(k_profile,thread,position)

{

real z, x[ND_ND];

face_t f;

begin_f_loop(f,thread)

{

F_CENTROID(x,f,thread);

z = x[2];

F_PROFILE(f,thread,position)=pow(UMEAN,2.)*(sqrt((1+(4.*z/L))/(1+(5.*z/L))))/(sqrt
(CMU));

}
```

```
end_f_loop(f,t)
}
/* profile for dissipation rate */
DEFINE_PROFILE(dissip_profile,thread,position)
{
real z, x[ND_ND];
face_t f;
begin_f_loop(f,thread);
{
F_CENTROID(x,f,thread);
z = x[2];
F_PROFILE(f,thread,position)=pow(UMEAN,3.)*(1+4.*z/L)/(VKC*z);
}
end_f_loop(f,t)
}
DEFINE_PROFILE(x_velocity,thread,position)
{
real z, x[ND_ND];
face_t f;
begin_f_loop(f,thread);
{
F_CENTROID(x,f,thread);
```

```
z=x[2];

F_PROFILE(f,thread,position)=(UMEAN/VKC)*((double)log((double)(z/h))+(5.*z/L));

}

end_f_loop(f,t)

}

DEFINE_PROFILE(inlet_x_temperature, thread, position)

{

real x[ND_ND];

real z;

face_t f;

begin_f_loop(f, thread)

{

F_CENTROID(x,f,thread);

z = x[2];

F_PROFILE(f, thread, position) = TW +
(TMEAN/VKC)*((double)log((double)(z/h))+(5.*z/L))-(g/CP)*(z-h);

}

end_f_loop(f,t)

}
```

PG-33 Model

```
#include "udf.h"

#define UMEAN 0.02084

#define CMU 0.09

#define VKC 0.42

#define h 0.006

#define L -81.021

#define TW 302.25

#define g 9.81

#define CP 1005

#define TMEAN -0.269

/*profile for kinetic energy*/

DEFINE_PROFILE(k_profile,thread,position)

{

real z, x[ND_ND];

face_t f;

begin_f_loop(f,thread)

{

F_CENTROID(x,f,thread);

z = x[2];

F_PROFILE(f,thread,position)=-0.0002*pow(z,2.)+0.0215*z+1.0051;

}
```

```
end_f_loop(f,t)
}
/* profile for dissipation rate */
DEFINE_PROFILE(dissip_profile,thread,position)
{
real z, x[ND_ND];
face_t f;
begin_f_loop(f,thread);
{
F_CENTROID(x,f,thread);
z = x[2];
F_PROFILE(f,thread,position)=0.4038*pow(z,-0.948);
}
end_f_loop(f,t)
}
DEFINE_PROFILE(inlet_x_temperature,thread,position)
{
real z,x[ND_ND];
face_t f;
begin_f_loop(f,thread)
{
F_CENTROID(x,f,thread);
```

```
z = x[2];
F_PROFILE(f,thread,position)= -0.558*(double)log((double)(z))+299.11;
}
end_f_loop(f,t)
}
DEFINE_PROFILE(x_velocity,thread,position)
{
real z, x[ND_ND];
face_t f;
begin_f_loop(f,thread);
{
F_CENTROID(x,f,thread);
z=x[2];
F_PROFILE(f,thread,position)=1.3549*(double)log((double)(z))+7.1161;
}
end_f_loop(f,t)
}
```

Residuals Graphs (convergence) for Prairie Grass & TP-5 simulations

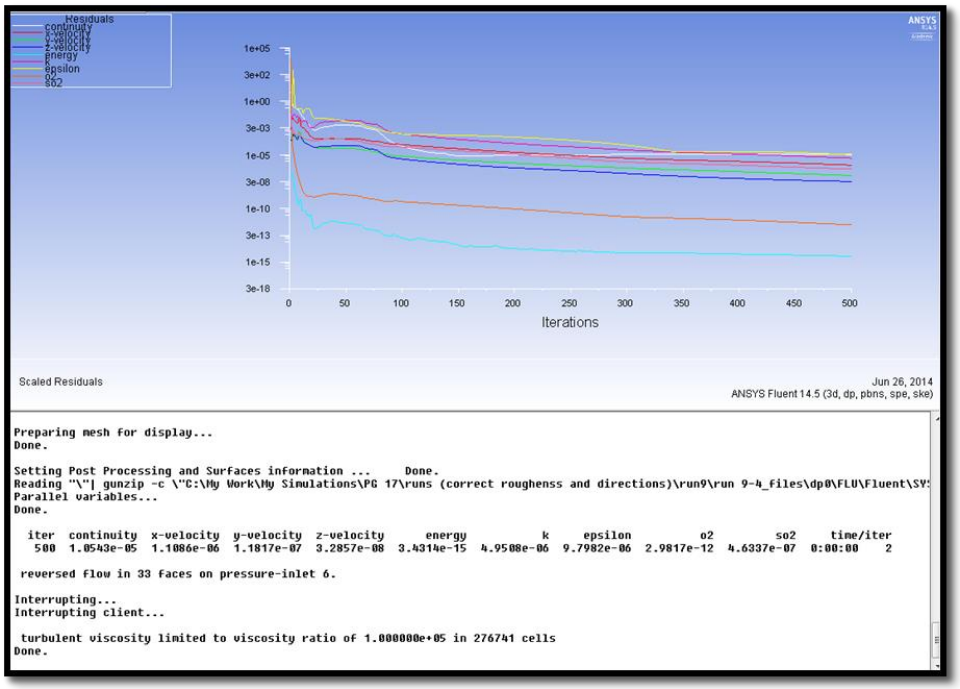

Figure 53: Residuals plot for PG-17 modelling using Standard k-ε model

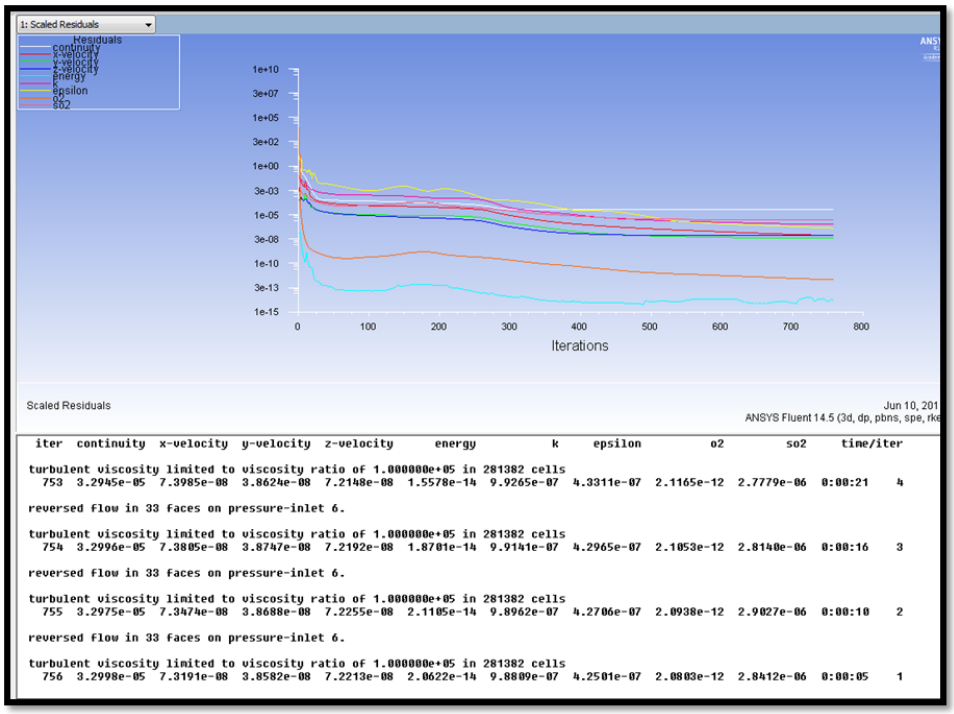


```
  iter  continuity  x-velocity  y-velocity  z-velocity      energy          k     epsilon          o2          so2     time/iter

turbulent viscosity limited to viscosity ratio of 1.000000e+05 in 281382 cells
   753  3.2945e-05  7.3985e-08  3.8624e-08  7.2148e-08  1.5578e-14  9.9265e-07  4.3311e-07  2.1165e-12  2.7779e-06  0:00:21    4

reversed flow in 33 faces on pressure-inlet 6.

turbulent viscosity limited to viscosity ratio of 1.000000e+05 in 281382 cells
   754  3.2996e-05  7.3805e-08  3.8747e-08  7.2192e-08  1.8701e-14  9.9141e-07  4.2965e-07  2.1053e-12  2.8140e-06  0:00:16    3

reversed flow in 33 faces on pressure-inlet 6.

turbulent viscosity limited to viscosity ratio of 1.000000e+05 in 281382 cells
   755  3.2975e-05  7.3474e-08  3.8688e-08  7.2255e-08  2.1105e-14  9.8962e-07  4.2706e-07  2.0938e-12  2.9027e-06  0:00:10    2

reversed flow in 33 faces on pressure-inlet 6.

turbulent viscosity limited to viscosity ratio of 1.000000e+05 in 281382 cells
   756  3.2998e-05  7.3191e-08  3.8582e-08  7.2213e-08  2.0622e-14  9.8809e-07  4.2501e-07  2.0803e-12  2.8412e-06  0:00:05    1
```

Figure 54: Residuals plot for PG-17 modelling using realizable k-ε model

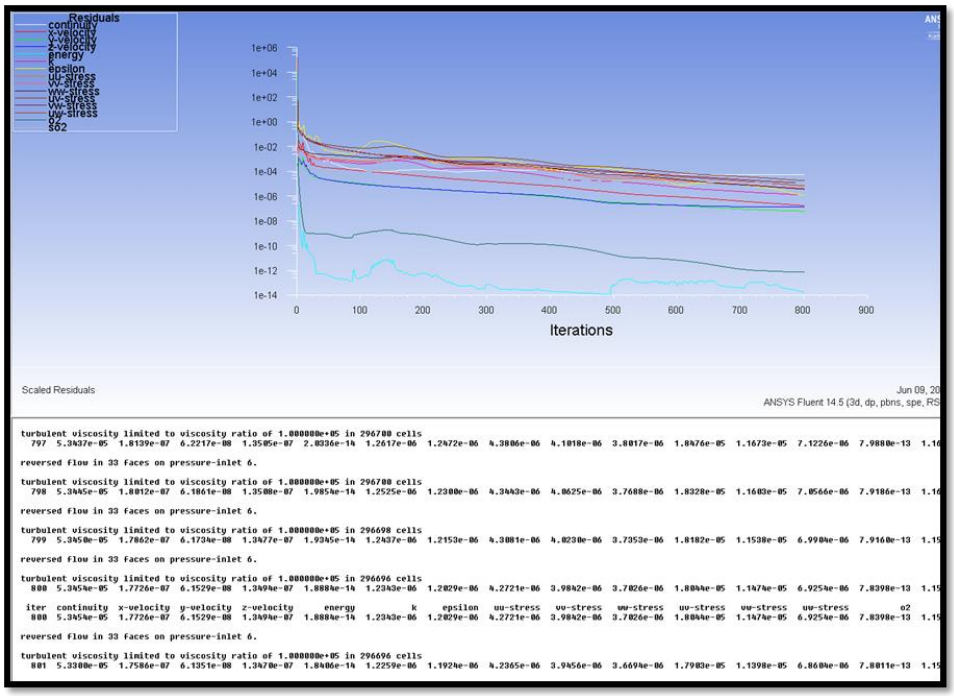


```
turbulent viscosity limited to viscosity ratio of 1.000000e+05 in 296700 cells
   797  5.3437e-05  1.8139e-07  6.2217e-08  1.3505e-07  2.0336e-14  1.2617e-06  1.2472e-06  4.3806e-06  4.1818e-06  3.8017e-06  1.8476e-05  1.1673e-05  7.1226e-06  7.9880e-13  1.16

reversed flow in 33 faces on pressure-inlet 6.

turbulent viscosity limited to viscosity ratio of 1.000000e+05 in 296700 cells
   798  5.3445e-05  1.8012e-07  6.1861e-08  1.3508e-07  1.9854e-14  1.2525e-06  1.2300e-06  4.3443e-06  4.0625e-06  3.7688e-06  1.8328e-05  1.1603e-05  7.0566e-06  7.9186e-13  1.16

reversed flow in 33 faces on pressure-inlet 6.

turbulent viscosity limited to viscosity ratio of 1.000000e+05 in 296698 cells
   799  5.3450e-05  1.7862e-07  6.1734e-08  1.3477e-07  1.9345e-14  1.2437e-06  1.2153e-06  4.3081e-06  4.0230e-06  3.7353e-06  1.8182e-05  1.1538e-05  6.9984e-06  7.9160e-13  1.15

reversed flow in 33 faces on pressure-inlet 6.

turbulent viscosity limited to viscosity ratio of 1.000000e+05 in 296696 cells
   800  5.3454e-05  1.7726e-07  6.1529e-08  1.3494e-07  1.8884e-14  1.2343e-06  1.2029e-06  4.2721e-06  3.9842e-06  3.7026e-06  1.8044e-05  1.1474e-05  6.9254e-06  7.8398e-13  1.15

 iter  continuity  x-velocity  y-velocity  z-velocity      energy          k     epsilon    uu-stress    vv-stress    ww-stress    uv-stress    vw-stress    uw-stress          o2
   800  5.3454e-05  1.7726e-07  6.1529e-08  1.3494e-07  1.8884e-14  1.2343e-06  1.2029e-06  4.2721e-06  3.9842e-06  3.7026e-06  1.8044e-05  1.1474e-05  6.9254e-06  7.8398e-13  1.15

reversed flow in 33 faces on pressure-inlet 6.

turbulent viscosity limited to viscosity ratio of 1.000000e+05 in 296696 cells
   801  5.3380e-05  1.7586e-07  6.1351e-08  1.3470e-07  1.8406e-14  1.2259e-06  1.1924e-06  4.2365e-06  3.9456e-06  3.6694e-06  1.7983e-05  1.1398e-05  6.8684e-06  7.8011e-13  1.15
```

Figure 55: Residuals plot for PG-17 modelling using RSM model

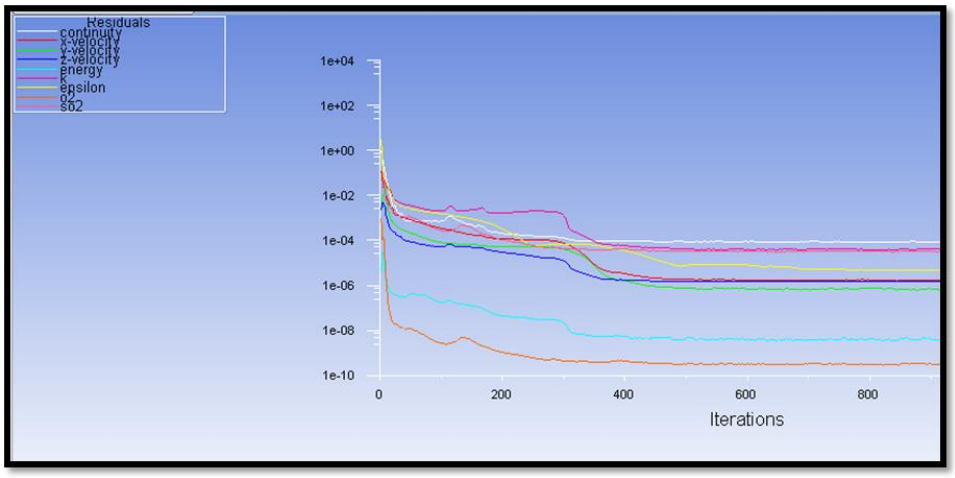

Figure 56: Residuals plot for PG-13 modelling using Standard k-ε model

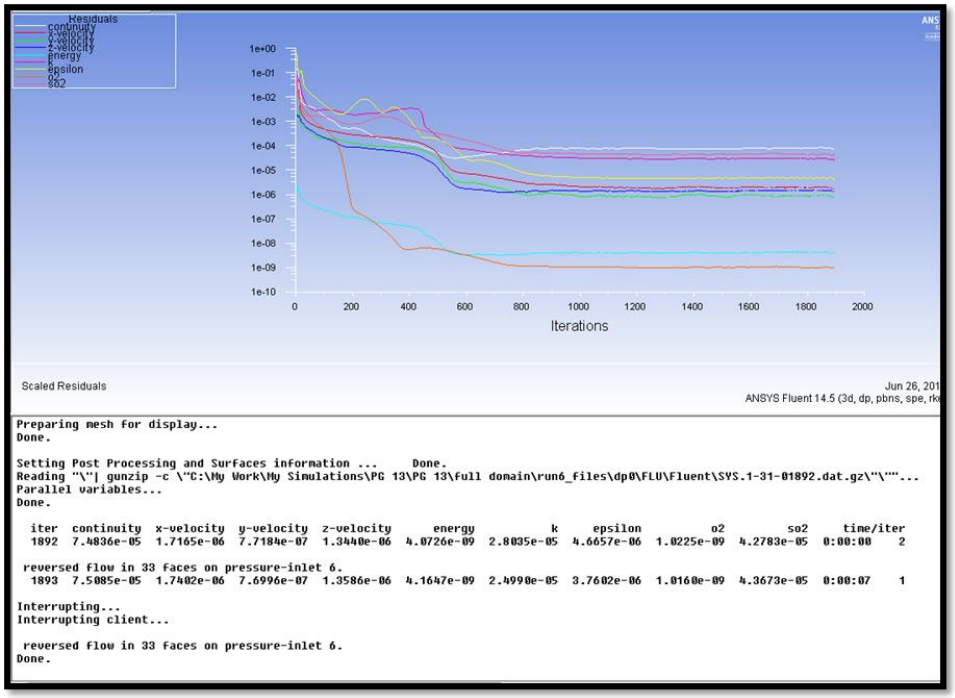

Figure 57: Residuals plot for PG-13 simulation using realizable k-ε model

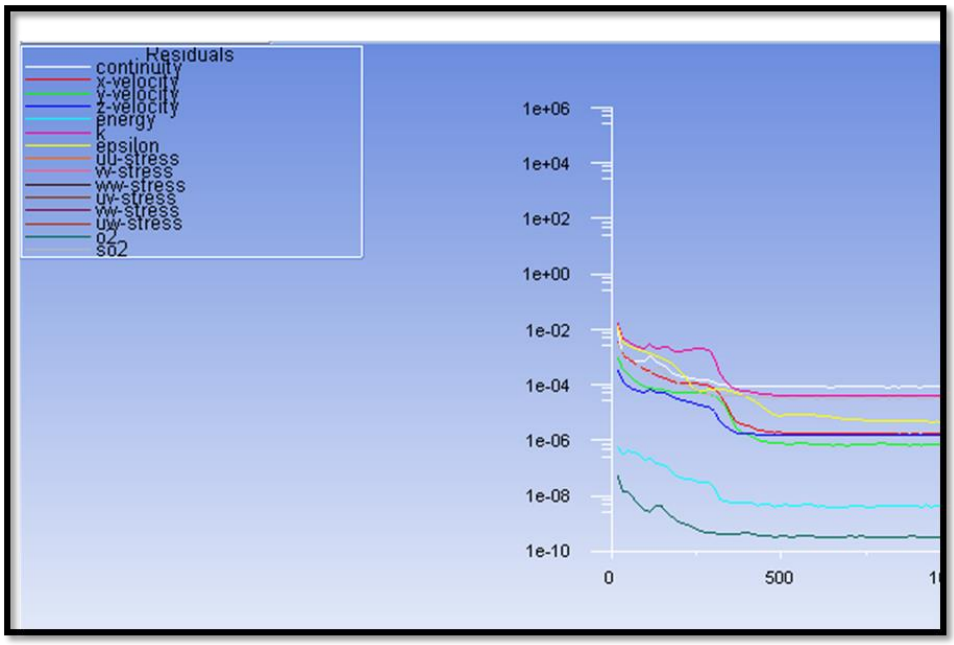

Figure 58: Residuals plot for PG-13 simulation using RSM model

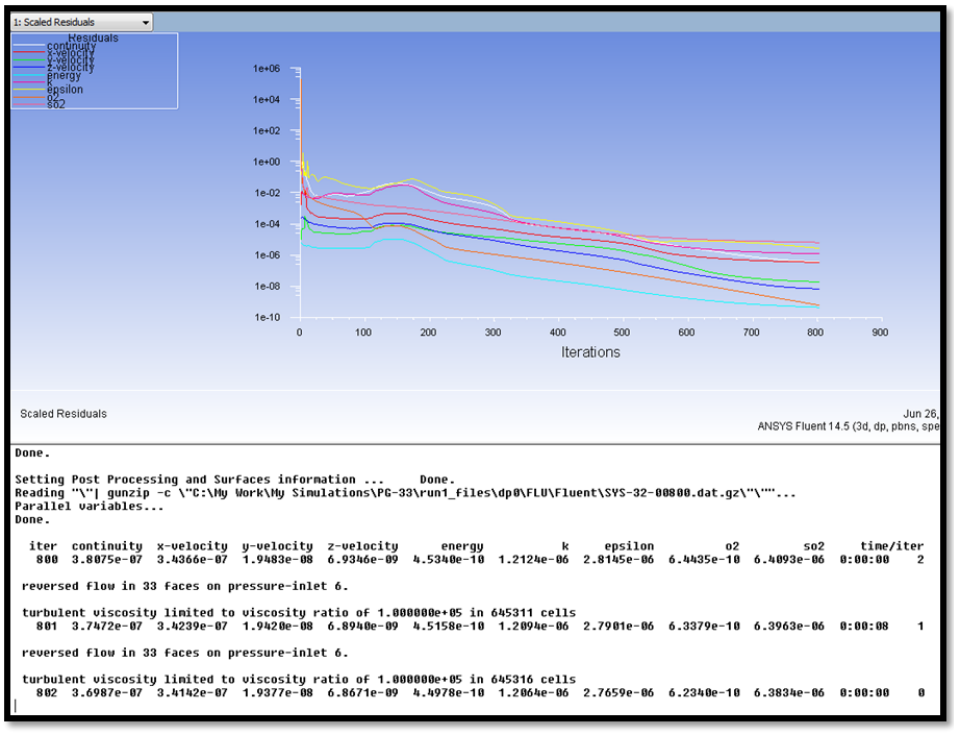

Figure 59: Residuals plot for PG-33 simulation using standard k-ε model

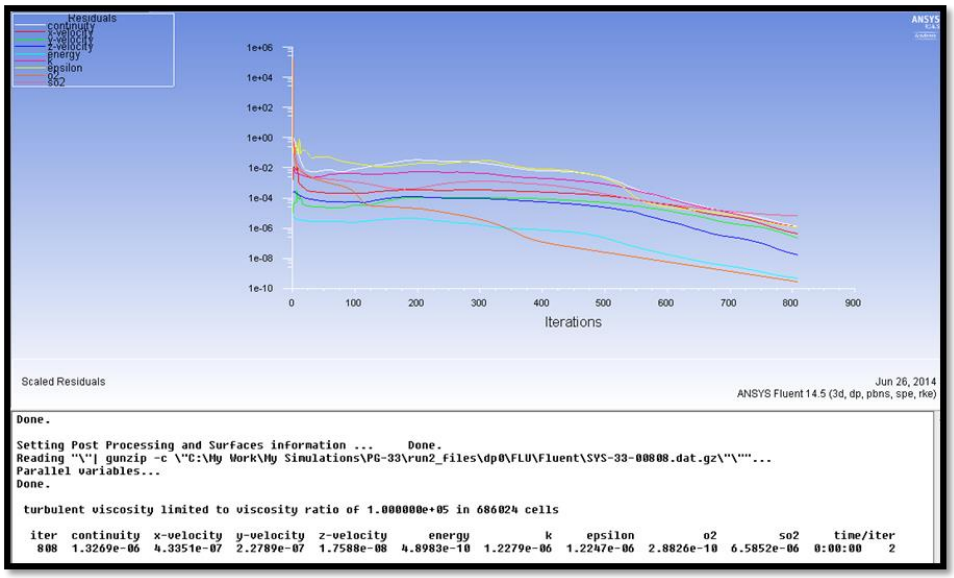

Figure 60: Residuals for PG-33 using realizable k-ε model

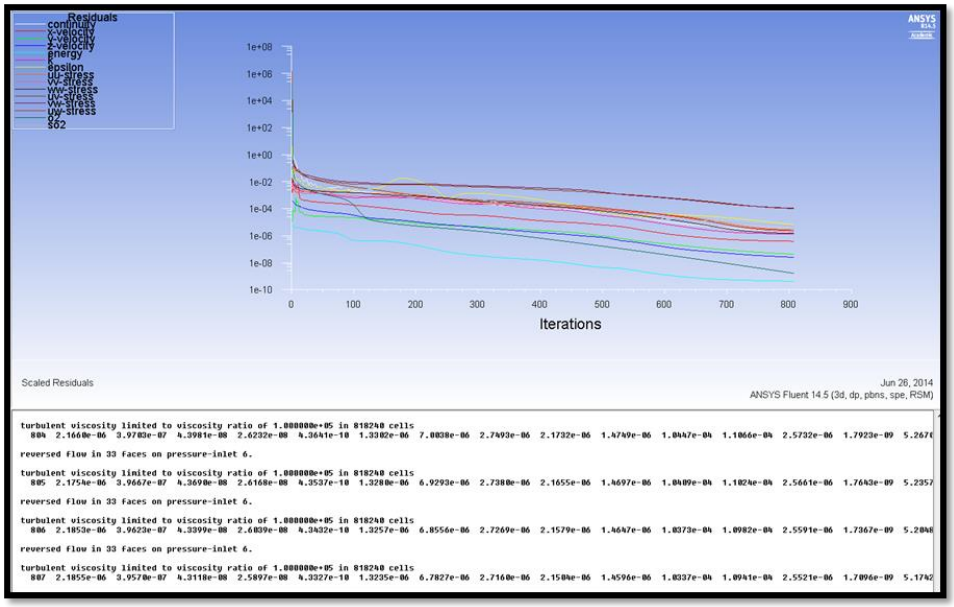

Figure 61: Residuals for PG-33 using RSM model

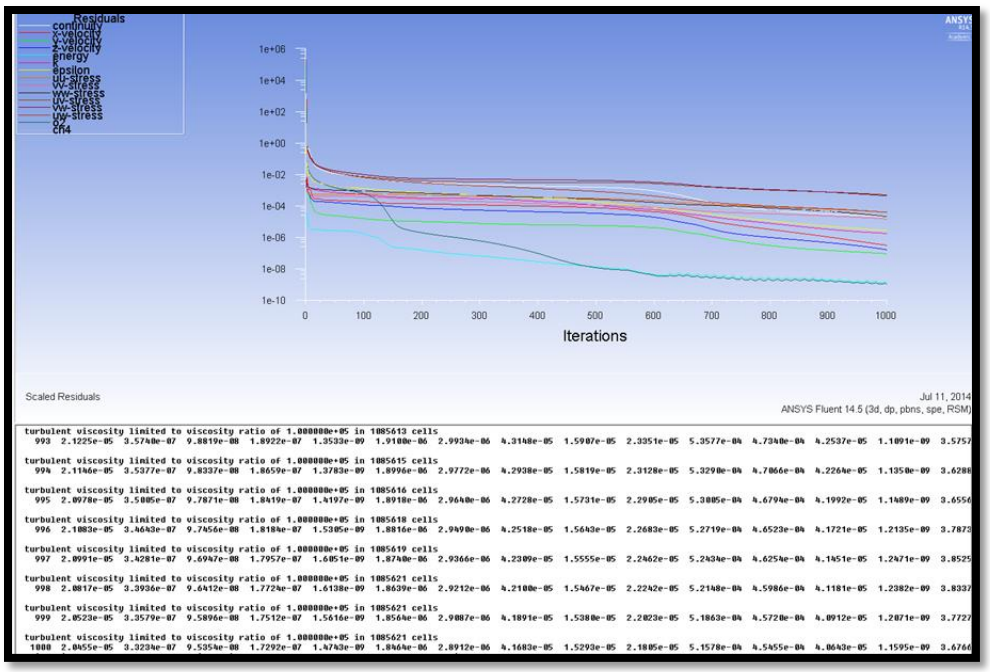

Figure 62: Residuals plot for TP-5 modeling